University of Alberta

The function of the mobile nuclear pore complex protein, Nup2p, in nucleocytoplasmic transport and the organisation of chromatin in the budding yeast, *Saccharomyces cerevisiae.*

by

David John Russell Dilworth ©

A thesis submitted to the Faculty of Graduate Studies and Research in partial fulfillment of the requirements for the degree of Doctor of Philosophy

Department of Cell Biology

Edmonton, Alberta
Spring 2006

Library and
Archives Canada

Published Heritage
Branch

395 Wellington Street
Ottawa ON K1A 0N4
Canada

Bibliothèque et
Archives Canada

Direction du
Patrimoine de l'édition

395, rue Wellington
Ottawa ON K1A 0N4
Canada

Your file Votre référence
ISBN: 0-494-13962-5
Our file Notre référence
ISBN: 0-494-13962-5

NOTICE:
The author has granted a non-exclusive license allowing Library and Archives Canada to reproduce, publish, archive, preserve, conserve, communicate to the public by telecommunication or on the Internet, loan, distribute and sell theses worldwide, for commercial or non-commercial purposes, in microform, paper, electronic and/or any other formats.

The author retains copyright ownership and moral rights in this thesis. Neither the thesis nor substantial extracts from it may be printed or otherwise reproduced without the author's permission.

AVIS:
L'auteur a accordé une licence non exclusive permettant à la Bibliothèque et Archives Canada de reproduire, publier, archiver, sauvegarder, conserver, transmettre au public par télécommunication ou par l'Internet, prêter, distribuer et vendre des thèses partout dans le monde, à des fins commerciales ou autres, sur support microforme, papier, électronique et/ou autres formats.

L'auteur conserve la propriété du droit d'auteur et des droits moraux qui protège cette thèse. Ni la thèse ni des extraits substantiels de celle-ci ne doivent être imprimés ou autrement reproduits sans son autorisation.

In compliance with the Canadian Privacy Act some supporting forms may have been removed from this thesis.

While these forms may be included in the document page count, their removal does not represent any loss of content from the thesis.

Conformément à la loi canadienne sur la protection de la vie privée, quelques formulaires secondaires ont été enlevés de cette thèse.

Bien que ces formulaires aient inclus dans la pagination, il n'y aura aucun contenu manquant.

Canada

Abstract

Nucleocytoplasmic transport is mediated by the interplay between soluble transport factors and nucleoporins resident within nuclear pore complexes (NPCs). Understanding this process demands knowledge of components of both the soluble and stationary phases and their interactions. Here, we provide evidence that Nup2p, previously considered a typical yeast nucleoporin, dynamically associates with the NPC and import- and export-bound karyopherins in a Ran-facilitated manner. While bound to the NPC, Nup2p associates with the nuclear basket and cytoplasmic fibril structures. On the nucleoplasmic face, where Ran-GTP levels are high, Nup2p binds to Nup60p. Deletion of *NUP60* renders Nup2p nucleoplasmic and compromises Nup2p-mediated Kap60p/Srp1p recycling. In a *Δnup60* strain, Ran-GTP depletion, *in vivo* by metabolic poisoning or disruption of the Ran cycle, or *in vitro* by cell lysis, results in a shift of Nup2p to the cytoplasmic face of the NPC. Nup2p mobility was detected *in vivo* using heterokaryons where, unlike nucleoporins, Nup2p was observed to move from one nucleus to the other. Taken together, our data support a model in which Nup2p movement facilitates the transition between the import and export phases of nucleocytoplasmic transport.

In addition to their role in nucleocytoplasmic transport, NPCs serve as key positional markers within the nucleus and several proteins associated with yeast NPCs have been implicated in the epigenetic control of gene expression. Among these, Nup2p is unique as it transiently associates with NPCs and, when artificially tethered to DNA, can prevent the spread of transcriptional activation or repression between flanking genes, a function termed boundary activity. To understand this function, we investigated the interactions of Nup2p with other proteins and with DNA using immunopurifications coupled with mass spectrometry and microarray analyses. These data combined with functional assays of boundary activity and epigenetic variegation suggest that Nup2p and the Ran guanylyl-nucleotide exchange factor, Prp20p, interact at specific chromatin regions. This interaction enables the NPC to play an active role in chromatin organization by facilitating the transition of chromatin between activity states. As a whole, these data provide an important link between the role of NPC in nucleocytoplasmic transport and its function in chromatin organization.

Acknowledgements

First and foremost, I would like to thank my supervisor, John Aitchison, not only for the steadfast dedication and scientific insight but also for his seemingly endless capacity to put up with mes hautes et mes bas. You have been a compass in the laboratory and an anchor in my personal life. Many others would have given up long ago and for that I owe you my sincerest gratitude. My thanks go out also to Richard Rachubinski and David Stuart for their time, effort and direction as members of my supervisory committee, and Michael Schultz and Michael Matunis, for agreeing to sit on my examination committee.

I wish to acknowledge the many individuals with whom I have collaborated during my thesis research, both those who were included as co-authors in publications and, more importantly, those whose efforts went unrewarded in this regard. In this first group: Adisetyantari Suprapto, a member of the Rout laboratory for her immunoelectron microscopy work that is presented in Figure 2-2 and published in Dilworth *et al.* JCB 2001; two members of Brian Chait's group: Julio Padovan, who was essential to the mass spectrometric identification of proteins in the shown in Figure 2-5 and published in Dilworth *et al.* JCB 2001, and Alan Tackett, who analyzed histone modification patterns in Prp20p-associated nucleosomes, which is shown in Figure 3-1 and discussed in section 3.2.2. and also in Dilworth *et al.* JCB 2005 (in press); Eugene Yi at the Institute for Systems Biology Proteomics facility for accurate and timely mass spectrometric identification of the protein interactions shown in Table 2-1 and Figure 3-1, a portion of which was published in Dilworth *et al.* JCB 2005 (in press); members of the Aitchison lab: Richard Rogers, Rowan Christmas and Jennifer Smith for their assistance with *in vitro* binding studies (Figure 3-1b, *lower*), microarray data analysis (Figure 3-4) and genome localisation (ChIP-CHIP) studies (Figure 3-5), respectively, all of which were included in Dilworth *et al.* JCB 2005 (in press).

Those whose efforts did not result in co-authorship, but were nonetheless essential to the progress of my research, include Helen Shio (Rockefeller University Electron Microscopy Facility) for her help with immunoelectron microscopy, Vera

Chlumecky (University of Alberta Confocal Microscopy Facility) for her assistance with confocal microscopy, Dwayne Weber (Aitchison lab technician) for general help in the laboratory, Marcello Marelli (Aitchison lab post-doc) for always lending an ear and, in particular, Bruz Marzolf and Michael Johnson (Institute for Systems Biology Microarray Facility), who provided essential, expert assistance with microarray experiments.

I wish to thank the following researchers for their generous gifts of strains, plasmids and other reagents, described in detail in the materials and methods found in Section 5: Nataliya Shulga, Laura Davis, Kenneth Belanger, Susan Wente, Charles Cole, Ulrich Laemmli, Hiroyuki Araki, Charles Boone, Michael Rexach, George Sprague and James Young.

Finally, a heartfelt thanks to the Canadian Institutes of Health Research (CIHR) [formerly the Medical Research Council of Canada (MRC)], the Natural Sciences and Engineering Research Council of Canada (NSERC), the Alberta Heritage Foundation for Medical Research (AHFMR) and the University of Alberta, who so generously footed the bill of my education for all these years with the exception of the bitter, bitter end.

Table of Contents

pg.

1. *Introduction* *1*

1.1. **Compartmentalisation in eukaryotic cells** **1**

1.2. **The nucleocytoplasmic transport machinery** **2**

1.2.1. The stationary phase - NPCs 3
1.2.2. The soluble phase - karyopherins 6
1.2.3. The regulators - Ran and its effectors 8

1.3. **Models of movement through the NPC** **9**

1.3.1. Gating by entropic exclusion – 'Brownian affinity gate' model 11
1.3.2. Hydrophobic phase partitioning and 'Oily spaghetti' models 12
1.3.3. Sequential binding and release – the 'FG affinity gradient' model 12

1.4. **Broad spectrum of NPC involvement in cellular functions** **14**

1.4.1. NPC mutants affect gross nuclear morphology 14
1.4.2. Components of the NPC are involved in cell cycle control 14
1.4.3. NPCs function in the organisation of chromatin in the nucleus 15
1.4.4. NPC-mediated transcriptional insulation (boundary activity) 17

1.5. **Focus of thesis research** **17**

2. ***The role of Nup2p in nucleocytoplasmic transport*** ***19***

2.1. **Overview - Nup2p is not a *bona fide* nucleoporin** **19**

2.2. **Results** **21**

2.2.1. The localisation of Nup2p in the NPC 21
2.2.2. Nup2p is mobile 23
2.2.3. Nup60p anchors Nup2p to the nuclear face of the NPC 27
2.2.4. Nup2p exhibits Ran-dependent association with NPCs 31
2.2.5. Nup2p and Nup60p aid in Kap60p recycling 33
2.2.6. A role for Nup2p in other kap transport pathways 36

2.3. **Discussion** **38**

2.3.1. Nup2p lies at the boundary between the classical division of nuclear transport components into stationary and soluble phases 38
2.3.2. Nup2p as a scaffold for transport reactions 41
2.3.3. The cytoplasmic function of Nup2p 43
2.3.4. Nup2p in higher eukaryotes? 43
2.3.5. Subsequent corroborating evidence 43
2.3.6. Extending transport past NPCs - intranuclear targeting 44

3. Nup2p and the epigenetic maintenance of transcription states *45*

3.1. Overview - Nup2p possesses boundary activity **45**

3.2. Results **45**

3.2.1. Prp20p is a potential chromatin anchor for Nup2p 45
3.2.2. Prp20p associates with atypically modified histones and proteins involved in chromatin remodeling 48
3.2.3. Genetic interactions support a link between *NUP2*, *NUP60*, *PRP20* and *HTZ1* 49
3.2.4. Prp20p harbours boundary activity that is affected but not absent in cells lacking Nup2p, Nup60p or the Mlp proteins 50
3.2.5. Cells lacking Nup2p exhibit transcriptional activation of ORFs encoded in subtelomeric regions 53
3.2.6. Nup2p and Prp20p bind to subtelomeric regions of chromatin 54
3.2.7. *Δnup2* and *Δnup60* cells exhibit defects in the ability to maintain subtelomerically encoded reporters in the silenced state 58

3.3. Discussion **62**

3.3.1. The convergence of nuclear functions at the NPC 62
3.3.2. Endogenous Nup2p-mediated boundary function 62
3.3.3. The chromatin connection 65

4. Conclusions and Perspectives *67*

4.1. Integrating the roles of Nup2p in nuclear transport and BA **67**

4.2. Formal proof for a dynamic model – chromosome tattooing **68**

4.3. Extrapolation to higher eukaryotes **69**

5. Materials and Methods *71*

5.1. Stocks and growth conditions **71**

5.1.1. Yeast strains 71
5.1.2. Bacterial strains 76
5.1.3. Plasmids 77
5.1.4. Oligonucleotides 78
5.1.5. Growth media 81

5.2. General laboratory procedures **82**

5.2.1. Mating, sporulation and tetrad dissection 82
5.2.2. Agarose gel electrophoresis 84
5.2.3. SDS-polyacrylamide gel electrophoresis 85
5.2.4. PCR amplification of DNA 85
5.2.5. Transformation of DNA into yeast and bacteria 86

5.2.6. Yeast protein extract preparation 87
5.2.7. Yeast genomic DNA isolation 88
5.2.8. Gene tagging, deletion and marker swapping 89
5.2.9. Immunoblotting and antibodies 91

5.3. Protein interaction studies 93

5.3.1. GST fusion protein expression and purification 93
5.3.2. *In vitro* GST binding studies 94
5.3.3. Yeast whole cell lysate immunopurifications 95
5.3.4. Prp20p-nucleosome complex formation with Nup2p 97
5.3.5. Prp20p-nucleosome complex histone modification analysis 98

5.4. Genetic interaction studies 98

5.4.1. *NUP2-NUP60* interactions 98
5.4.2. *NUP60-KAP60* interactions 99
5.4.3. *NUP2-NUP60-PRP20-HTZ1* interactions 99

5.5. Fluorescence microscopy 100

5.5.1. Microscopy and growth conditions 100
5.5.2. Heterokaryon mobility assay 100
5.5.3. Photobleach-recovery protein turnover assay 101
5.5.4. Galactose induction of Nup60p 101
5.5.5. Quantitation of fluorescent intensity along nuclear bisects 101
5.5.6. Metabolic poisoning 102
5.5.7. *prp20-7* temperature shift 102

5.6. DNA microarray experiments 102

5.6.1. mRNA expression microarrays 102
5.6.2. Genome localisation microarrays (ChIP-CHIP) 104
5.6.3. Microarray hybridisation and washing conditions, scanning parameters and data analysis pipeline 108
5.6.4. Post-pipeline analyses 110

5.7. Other methods 111

5.7.1. Immunoelectron microscopic localisation of protein A tags 111
5.7.2. Quantitation of nup expression by analytical flow cytometry 111
5.7.3. Boundary trap assay 112
5.7.4. Single cell telomeric silencing assay 112

6. References 115

7. Appendices 127

7.1. Digital data available on DVD-ROM:

7.1.1. Laboratory notebook images in jpeg format 127

7.1.2. Copy of thesis in Word format 127
7.1.3. Copy of figures in jpeg format 127
7.1.4. Copy of references in EndNote library 127
7.1.5. Copy of assembled thesis in pdf format 127
7.1.6. Copy of thesis defense presentation in PowerPoint format 127
7.1.7. MIAME compliant microarray data in tiff and txt format 127
7.1.8. Microarray data and analysis in Excel format 127
7.1.9. LC-MS/MS immunopurification eluate data in Excel format 127
7.1.10. Dilworth *et al.* J. Cell Biol. 2001 in pdf format 127
7.1.11. Dilworth *et al.* J. Cell Biol. 2005 accepted version in pdf format 127

8. Curriculum Vitae 129

List of Tables

pg.

Table 1-1 The yeast nucleoporins and their mammalian orthologues 5

Table 1-2 The yeast karyopherins, their known cargoes and mammalian orthologues 7

Table 2-1 MS/MS protein identifications supporting a role for Nup2p in additional kap transport pathways 37

Table 5-1 Yeast Strains 75

Table 5-2 Plasmids 77

Table 5-3 Oligonucleotides 78

Table 5-4 Primary and secondary antibodies 92

List of Figures

pg.

Figure 1-1 Molecular trafficking in the compartmentalised eukaryotic cell 2

Figure 1-2 The yeast nuclear pore complex 4

Figure 1-3 The Ran gradient and its effects on nuclear transport reactions 10

Figure 1-4 The boundary trap assay 16

Figure 2-1 Nup2p does not enrich with NPCs 20

Figure 2-2 Nup2p exhibits variable localisation in the NPC 22

Figure 2-3 Heterokaryon mobility assay reveals that Nup2p does not stably associate with NPCs 24

Figure 2-4 The steady-state levels and rate of turnover of Nup2p are similar to those of *bona fide* nups 26

Figure 2-5 Nup2p co-immunoprecipitates with stoichiometric levels of Kap60p, Kap95p and Nup60p 28

Figure 2-6 Nup60p anchors Nup2p to the nuclear face of the NPC 30

Figure 2-7 *NUP2* and *NUP60* genetically interact 31

Figure 2-8 The Ran-binding domain of Nup2p is required for its efficient steady state localisation at the NPC 32

Figure 2-9 Alterations in the Ran cycle affect the localisation of Nup2p 34

Figure 2-10 Deletion of *NUP2* or *NUP60* disrupts the ability of Kap60p to bind NPCs and inhibits its recycling to the cytoplasm 35

Figure 2-11 *NUP60* and *KAP60* genetically interact 35

Figure 2-12 Nup2p binds directly to Kap104p *in vitro* 36

Figure 2-13 Model of the role of Nup2p in nucleocytoplasmic transport events inside the nucleus 42

Figure 3-1 Prp20p and Nup2p associate with each other and immunopurify with chromatin remodeling factors........46-47

Figure 3-2 Genetic interactions between *NUP2*, *NUP60*, *PRP20* and *HTZ1*.....50

Figure 3-3 The ability of Nup2p to transiently associate with Nup60p at the nuclear face of the NPC is important for BA........51

Figure 3-4 Prp20p exerts BA that exhibits partially penetrant defects upon loss of Nup2p, Nup60p or both of the Mlp proteins........52

Figure 3-5 ORFs induced in *Δnup2* cells are biased to subtelomeric regions......54

Figure 3-6 Chromatin regions bound by Nup2p and Prp20p are enriched in subtelomeric regions........56-57

Figure 3-7 *ΔNUP2* and *ΔNUP60* cells exhibit defects in the maintenance of expression states of subtelomerically encoded reporters........60-61

Figure 3-8 Dynamic model of Nup2p-dependent boundary function........64

Figure 5-1 Strain generation by mating, sporulation and tetrad dissection........83

Figure 5-2 Generation of null strains and strains expressing endogenously encoded fusion proteins........90-91

List of Abbreviations and Symbols

5-FOA	5'-fluoroorotic acid
A	amp
A_{xxx}	absorbance at XXX nm
BA	boundary activity
bp	base pairs
BSA	bovine serum albumin
βMe	2-mercaptoethanol
cNLS	classical NLS
ChIP-CHIP	chromatin immunoprecipitation genome localisation microarray
CSM	complete synthetic media
Da	Dalton (g/mol)
DEPC	diethylpyrocarbonate
DNA	deoxyribonucleic acid
DNAse	deoxyribonuclease
DMSO	dimethylsulfoxide
dNTP	deoxyribonucleotide triphosphates (dATP, dCTP, dGTP, dTTP)
ECL	enhanced chemiluminescence
DTT	dithiothreitol
ER	endoplasmic reticulum
EDTA	ethylenediaminetetraacetic acid
FRET	fluorescence resonance energy transfer
g	gram
g	gravitational force
gDNA	genomic DNA
GAP	GTPase activating protein
Gbd	Gal4p DNA binding domain
GDP	guanosine diphosphate
GEF	guanylyl nucleotide exchange factor
GFP	green fluorescent protein
GST	glutathione S-transferase
GTP	guanosine triphosphate
GTPase	guanosine triphosphatase
HRP	horseradish peroxidase
IEM	immunoelecron microscopy
IgG	immunoglobulin G
k	kilo (10^3)
kap	karyopherin
kb	kilobases (10^3 bp)
L	liter
leuNES	leucine-rich NES
m	milli (10^{-3})
M	molarity (mol/L)
mol	mole (6.022 X 10^{23} molecules)
mRNA	messenger RNA

MS	mass spectrometry
MS/MS	tandem mass spectrometry
n	nano (10^{-9})
NE	nuclear envelope
NES	nuclear export signal
NLS	nuclear localisation signal
NPC	nuclear pore complex
nup	nucleoporin
OD_{600}	optical density at 600 nm
O/N	overnight
ORF	open reading frame
PAGE	polyacrylamide gel electrophoresis
PCR	polymerase chain reaction
p	pico (10^{-12})
PrA	protein A
pH	$-\log[H^+]$
poly(A)+	polyadenylated RNA
RBD	Ran-binding domain
rgNLS	arginine/glycine-rich NLS
RNA	ribonucleic acid
RNAse	ribonuclease
RT	room temperature
SDS	sodium dodecyl sulphate
TCA	trichloroacetic acid
ts	temperature sensitive
tRNA	transfer RNA
U	standardised units
U snRNA	uracil-rich small nuclear ribonucleoprotein
UTR	untranslated region
UV	ultraviolet light
v	volume
v/v	volume per volume
V	volt
w/v	weight per volume
w/w	weight per weight
WCL	whole cell lysate
WT	wild-type
~	approximately
<	less than
>	greater than
≤	less than or equal to
≥	greater than or equal to
°	degree
Δ	deletion
μ	micro (10^{-6})
Ψ	pounds per square inch

1. INTRODUCTION

1.1. Compartmentalisation in eukaryotic cells

The defining feature of eukaryotic cells is the presence of multiple, membrane-bound organelles that allow metabolic activities to be contained within functionally dedicated compartments (Figure 1-1a). This high-degree of subcellular organisation imparts eukaryotes with several innate advantages over their simpler prokaryotic cousins. These advantages include, but are by no means limited to, the ability to sequester potentially harmful cellular functions, exemplified by the lysosome and the peroxisome organelles, and the ability to exert a much higher degree of control over cellular activities, the archetypal example of which is the physical and temporal separation of mRNA transcription from protein translation.

In prokaryotes, transcription and translation occur simultaneously in the same compartment, which allows protein synthesis to initiate before the completion of nascent mRNA production; in contrast, eukaryotes possess a double-membrane lipid bilayer, termed the nuclear envelope (NE) that defines the nucleus and encapsulates the genetic material, thereby uncoupling nuclear transcription from cytoplasmic translation. Gained is the ability to regulate gene expression at the level of mRNA, for example, by controlling mRNA maturation, export or degradation. There is a cost associated with this increased control: the barrier presented by the NE necessitates a mechanism to transport molecules across it, including proteins, mRNA, tRNA and metabolites, in order to perform normal, essential cellular functions. Consider DNA replication. This process requires a host of proteins that arise from translation in the cytoplasm and, therefore, must be transported to the nucleus to where DNA synthesis occurs. Furthermore, the mRNAs coding for these proteins were transported to the cytoplasm prior to their translation into protein. Translation itself requires tRNAs, which are synthesised in the nucleus and then transported to the cytoplasm, and ribosomes, which have an extremely complex maturation sequence involving several nucleocytoplasmic exchange events.

It is clear that nucleocytoplasmic transport encompasses the movement of a wide variety of cargoes (Figure 1-1b), but to date the only known aqueous means of transfer is through the central channel of one of the several hundred nuclear pore complexes (NPCs) that are embedded in the NE. Although NPCs appear to have roles in a variety of cellular processes, the most studied and well characterised function of these massive protein structures is their participation in bidirectional nucleocytoplasmic exchange.

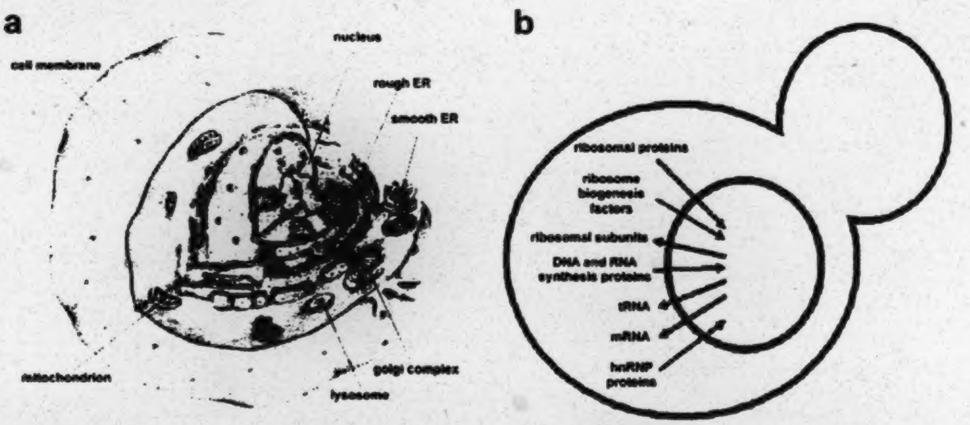

Figure 1-1. Molecular trafficking in the compartmentalised eukaryotic cell. (a) Eukaryotic cells employ lipid bilayers to physically separate various organelles from one another, including the nucleus, the endoplasmic reticulum (ER), the golgi apparatus, the peroxisome, the mitochondrion and the lysosome. Many molecular trafficking mechanisms evolved to allow communication between these compartments. Adapted from http://web.mit.edu/esgbio/www/cb/ org/animal.gif. (b) In the case of the separation of the nucleus and the cytoplasm by the nuclear envelope, the transport mechanism must be capable of bidirectional movement of an array of cargoes involved in fundamental cellular processes.

1.2. The nucleocytoplasmic transport machinery

Cells have developed a transport machinery capable of selectively gating cargo through NPCs and a considerable amount of effort has been dedicated to identifying the components of NPCs and the soluble factors that, together, comprise the nucleocytoplasmic transport machinery (reviewed in 1,9-12). The molecular composition of this machinery has been conserved through evolution, which implies that insights into the mechanism of nucleocytoplasmic transport in one organism are applicable to others. Given its genetic tractability, the budding yeast, *Saccharomyces cerevisiae*, serves as an excellent model organism to study nucleocytoplasmic transport. Indeed, much of what we understand about nucleocytoplasmic transport has been derived from studies in this organism. The yeast nucleocytoplasmic transport machinery can be said to be comprised of three components: (1) a stationary phase, the NPC, that provides channels through the NE allowing physical communication between the nucleus and cytoplasm, (2) a mobile phase that recognises and mediates the transport of cargo across the NE and (3) a family of factors that regulates the interaction between the mobile and stationary phases to elicit compartment-specific cargo deposition.

1.2.1. The stationary phase – NPCs

The structure of the NPC has been highly conserved through evolution. It exhibits eightfold symmetry in the plane perpendicular to the NE and twofold pseudo-symmetry in the plane parallel to the NE (Figure 1-2a). At the heart of the NPC lies the central transporter, which is held in place by a spoke-ring structure. Passage through the central transporter is achieved by transiting an ~10 nm wide aqueous central channel[13], a diameter that permits the passive diffusion of ions, metabolites, and small polypeptides of less than 50 kDa but presents an impassable barrier to larger molecules, that is, unless they harbour cis-acting transport signals that mark them for energy-dependent translocation. Emanating from the symmetrical core and extending outwards are two morphologically distinct and peripherally associated structures – the nuclear fibrils, which connect at their distal ends to form the nuclear basket and the cytoplasmic fibrils, which extend into the cytoplasm but are free at their distal ends[1,12,17-20].

The yeast and mammalian NPCs are comprised of ~30 protein components (listed in Table 1-1) that are collectively termed nucleoporins or nups, each present in multiple copies per NPC, thereby accounting for the large molecular mass of these structures (~50 X 10^6 Da in yeast and ~125 X 10^6 Da in higher eukaryotes)[4,21-23]. In yeast, the majority of nups are present within the core region of the NPC and are symmetrically distributed on the nuclear and cytoplasmic faces (Figure 1-2b)[4,24]. In addition, a small number of nups appear to be biased to one side of the NPC but are nonetheless present on both faces. On the other hand, some nups are localised specifically on one side of the NE. For example, Nup1p and Nup60p localise solely to the distal nucleoplasmic face of the NPC and likely form the nuclear basket. Similarly, three nups are found only on the cytoplasmic face: Nup159p, Nup42p and Nup82p and, together, these likely constitute the cytoplasmic fibrils.

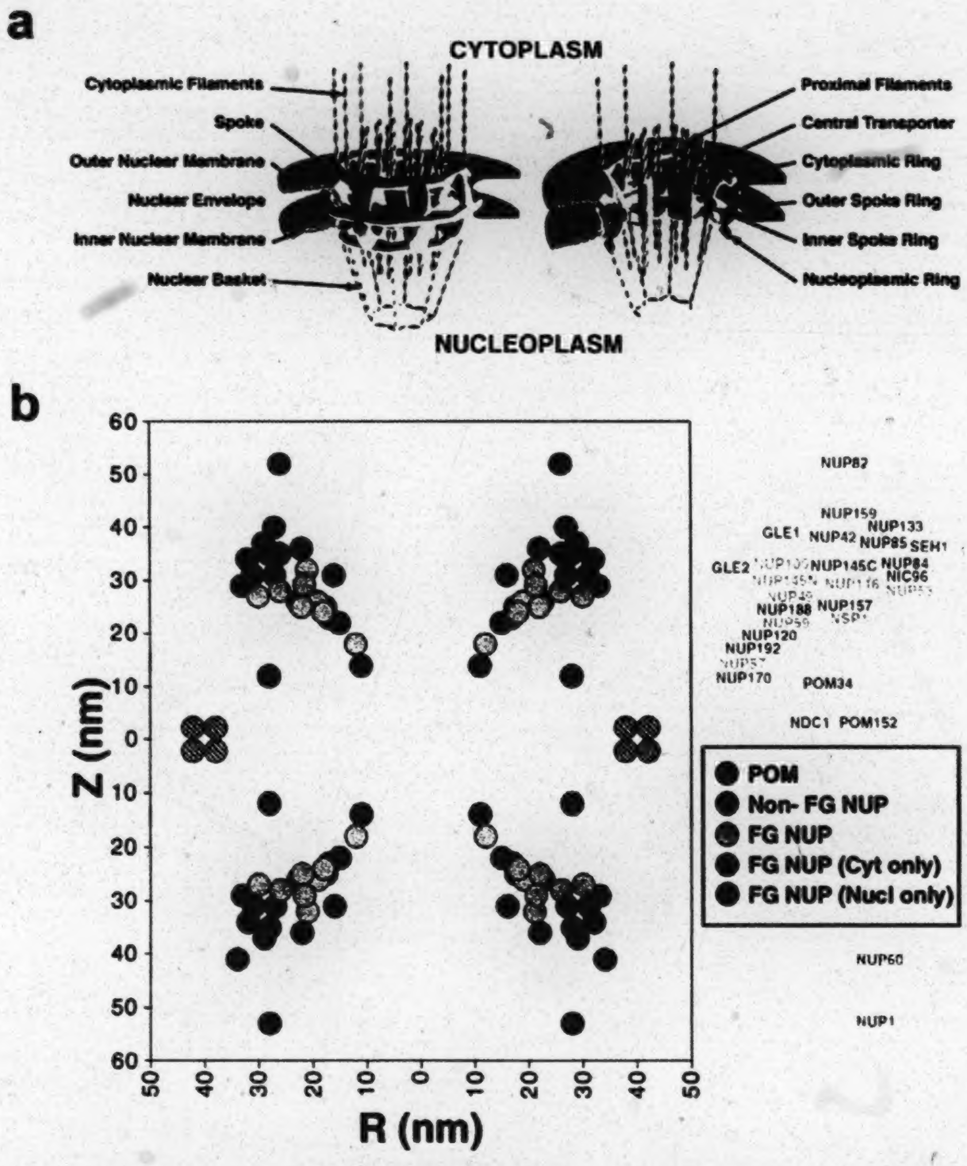
a
CYTOPLASM
Cytoplasmic Filaments
Spoke
Outer Nuclear Membrane
Nuclear Envelope
Inner Nuclear Membrane
Nuclear Basket
Proximal Filaments
Central Transporter
Cytoplasmic Ring
Outer Spoke Ring
Inner Spoke Ring
Nucleoplasmic Ring
NUCLEOPLASM
b
60
50
40
30
20
10
0
10
20
30
40
50
60
Z (nm)
50
40
30
20
10
0
10
20
30
40
50
R (nm)
NUP82
NUP159
NUP133
GLE1
NUP42
NUP85
SEH1
GLE2
NUP100
NUP145C
NUP84
NIC96
NUP145N
NUP116
NUP53
NUP49
NUP188
NUP157
NUP59
NSP1
NUP120
NUP192
NUP57
NUP170
POM34
NDC1
POM152
POM
Non- FG NUP
FG NUP
FG NUP (Cyt only)
FG NUP (Nucl only)

Figure 1-2. The yeast nuclear pore complex. (a) Diagram of the overall architecture of the yeast NPC showing the major physical features. Most of these substructures have been visualised by electron microscopy and the remainder are inferred structures based on indirect evidence. (b) The localisation of the yeast nucleoporins in the NPC. Each stably associated NPC component was C-terminally tagged with an immunoreactive protein tag (*Staphylococcus aureus* protein A, PrA) and its localisation within the NPC was determined by thin section immunoelectron microscopy. Five classes of nups were identified: FG-nups found on the cytoplasmic face of the NPC only (fuchsia), FG-nups found on the nuclear face of the NPC only (blue), FG-nups (green) and non FG-nups (grey) found on both faces of the NPC and membrane-associated nups (purple). Note that, in the latter group, only Pom34p was localised; thus, the shown localisations of Pom152p and Ndc1p (hatched purple) are inferred. Adapted from (1).

Table 1-1 **The yeast nucleoporins and their mammalian orthologues**

Yeast Nup	Vertebrate Nup	Null Viable?[a]	Localisation[a]	Motifs
Nup1p (114)	Nup153[b]	Y[c]	Nuclear	FXFG
Nsp1p (87)	Nup62	N	Symmetric	FG, FXFG
Nup2p[b,d] (78)	Nup50[b]	Y	Nuclear-biased	FXFG
Nup42p	NLP1/hCG1 (45)	Y	Cytoplasmic	FG
Nup49p	Nup58, Nup45	N	Symmetric	GLFG[y], FG[v]
Nup53p	Nup35	Y	Symmetric	
Nup59p	Nup35	Y	Symmetric	
Nup57p	Nup54	N	Symmetric	GLFG[y], FG[v]
Nup82p	Nup88	N	Cytoplasmic	
Nup84p	Nup107	Y (ts)	Symmetric	
Nup85p	Nup75/Nup85	Y (ts)	Symmetric	
Nic96p	Nup93	N	Symmetric	
Nup100p	Nup98[b]	Y	Cytoplasmic-biased	GLFG
Nup116p	Nup98[b]	Y (ts)	Cytoplasmic-biased	FG, GLFG
Nup145p-N (60)	Nup98[b]	Y	Nuclear-biased	GLFG
Nup120p	Nup160	Y (ts)	Symmetric	
Nup133p	Nup133	Y (ts)	Symmetric	
Nup145p-C (85)	Nup96	N	Symmetric	
Nup157p	Nup155	Y	Symmetric	
Nup170p	Nup155	Y	Symmetric	
Nup159p	Nup214/CAN	N	Cytoplasmic	FG
Nup188p	Nup188	Y	Symmetric	
Nup192p	Nup205	N	Symmetric	
Gle1p (62)	hGle1[b,d] (85)	N	Cytoplasmic-biased	
Gle2p (41)	Rae1/Gle2[b] (41)	Y (ts)	Symmetric	WD
Seh1p (39)	Seh1 (40)	Y	Symmetric	WD
Nup60p	–	Y	Nuclear	FXF
Ndc1p (74)	–	N	Pore membrane	TM
Pom34p	–	Y	Pore membrane	TM
Pom152p	–	Y	Pore membrane	TM
–	Pom121		Pore membrane	FG, TM
–	Gp210		Pore membrane	TM
–	Nup358/RanBP2		Cytoplasmic	FXFG
–	ALADIN (60)		?	WD
–	Nup37		?	WD
–	Nup43		?	WD

This table and the following text was adapted from (33) and is based on data presented or reviewed in (4,21,34-38). General nup nomenclature includes numerical designation reflecting the predicted mass in kDa. For a subset in which this is not the case, the predicted mass is in parentheses. A nup currently having two different names is indicated by "/". Yeast null mutant phenotypes be found at http://genome-www.stanford.edu/Saccharomyces/.
[a] in yeast; [b] dynamic nup; [c] initially identified as essential; [d] no coenrichment with NPCs; [y] yeast; [v] vertebrate

Nucleoporins can be subdivided into two groups: those that contain degenerate phenylalanine–glycine repeats (FG-nups) and those that do not. For one FG-nup, these repeats have been shown directly to form filaments *in vitro*[25]. Numerous other FG-nups have been localised to filamentous NPC structures[1,12,24,26] and, overall, FG-nups are predicted to lack structure, exhibiting a high degree of disorder[27,28]. The FG-repeats are important binding sites for transport factors as they traverse the NPC[16,29,30], and they are present at a high concentration throughout the NPC, extending from the cytoplasmic filaments (Nup159p and Nup42p) to the nuclear basket (Nup1p and Nup60p)[1,12,24]. Because of the high concentration of FG-repeat binding sites throughout the NPC, the interactions between these nups and soluble transport factors are thought to be fundamental to the mechanism of transport through NPCs. Proteins within the second group of nups, those that do not contain FG-repeats, contain no recognisable consensus motif. In general, non-FG-repeat nups are thought to form a structural framework upon which the FG-nups are strategically arranged[1,4,31,32], but that is not to say that they do not play important, possibly direct roles in transport. For example, they may contribute to the overall density of filaments in the central channel, which is relevant to several models put forth to explain the selective nature of birdirectional transport through NPCs (discussed in section 1.2).

1.2.2. The soluble phase - karyopherins

The soluble, or mobile, phase consists of transporters that associate with components of the NPC and also bind to either nuclear localisation signals (NLSs)[39] or nuclear export sequences (NESs)[40,41] encoded within cargoes. Most of these transporters are members of the structurally related β-karyopherin or kap family (also known as importins or exportins) of which there are 14 paralogues in yeast (Table 1-2). Until recently, individual kaps were thought to function exclusively in either import or export, but this is not in fact the case. Kap142p/Msn5p imports the trimeric replication protein A (RPA) into the nucleus but also exports Pho4p, Mig1p, and Far1p to the cytoplasm[42-44].

It is likely that the large variety of kaps evolved to accommodate the diversity of cargoes that must be transported into or out of the nucleus. Indeed, at least in some cases, specific kaps appear to be responsible for transporting specific classes of cargoes[10,85,95]. For example, in yeast, Kap123p has been shown to mediate the import of ribosomal proteins[56,58,59] prior to their assembly in the nucleus into mature ribosomes, and Kap104p recycles the mRNA binding proteins Nab2p and Hrp1p back into the nucleus by virtue of their encoded arginine/lysine-rich NLSs (rgNLS), where they are again incorporated into hnRNP complexes prior to the export of mature mRNA to the cytopalsm[51,96]. Likewise, Kap124p (Crm1p/Xpo1p) exports a class of proteins containing a 10 residue, leucine-rich NES (leuNES) like that initially found in the HIV-Rev protein[61,63,70,97]. Similarly, the export of tRNA is mediated by

Los1p[80,81,98] and U snRNA (and associated proteins) by Crm1p[55,61]. On the other hand, the kap, Cse1p (CAS in higher eukaryotes), appears to be dedicated to the nuclear export of Kap60p/Kapα, recycling it to the cytoplasm for another round of cNLS import[64,99].

Table 1-2 **The yeast karyopherins, their known cargoes and mammalian orthologues**

Yeast	Systematic & Aliases	Null viable?[a]	Function/Cargo[a]	Vertebrate
Kap60p	YNL189W Srp1p	N	Import of basic cNLS bearing proteins	Kapα
Kap95p	YLR347C Rsl1p	N	Import of Kap60p	Kapβ1 Impβ
Kap104p	YBR017C	Y[b]	Import of rgNLS bearing proteins functioning in mRNA export including Nab2p and Hrp1p	Kapβ2 Trn1 Impβ2
Kap108p	YDR395W Sxm1p	Y	Lhp1p and ribosomal proteins	
Kap109p	YGL238W Cse1p	N	Export of Kap60p	CAS
Kap111p	YOR160W Mtr10p	N	Import of proteins involved in mRNA export including Npl3p	
Kap114p	YGL241W	Y	Import of TBP, Spt15p, histones H2A and H2B, and Nap1p	
Kap119p	YJR132W Nmd5	Y	Import of Hog1p, Crz1p, TFIIS and ribosomal proteins	
Kap120p	YPL125W	Y	Unknown – functions in the assembly or export of 60S ribosomal subunits	
Kap121p	YMR308C Pse1p	N	Import of Yap1p, Ste12p and Aft1p, Pho4p and ribosomal proteins	Kapβ3 Pse1
Kap122p	YGL016W Pdr6p	Y	Import of the Toa1p-Toa2p complex	
Kap123p	YER110C Yrb4p	N	Import of ribosomal proteins and histones H3 and H4	
Kap124p	YGR218W Crm1p Xpo1p	N	Export of leuNLS bearing proteins and complexes including Ssb1p, Ace2p, Yap1p, Hog1p, RNA and ribosomal subunits.	Crm1 Xpo1
Kap127p	YKL205W Los1p	Y	Export of tRNA	Xpo-t
Kap142p	YDR335W Msn5p	Y	Import of RPA and Swi6p, Far1p, Mig1p and Pho4p export	Xpo5

This table was adapted from (45) and (46) and contains data presented or reviewed in (42,43,47-94). General kap nomenclature includes numerical designation reflecting the predicted mass in kDa. Phenotypes of yeast null mutants are catalogued at http://genome-www.stanford.edu/Saccharomyces/. [a] in yeast; [b] very slow growth

Despite this apparent dedication to specific classes of cargoes, kaps have been shown also to be somewhat promiscuous in that, in the absence of their primary kap, certain cargoes can be transported by a different kap to compensate for the loss. For example, Kap121p can facilitate the import of the ribosomal protein rpL25, in the absence of its normal transporter, Kap123p[56,59]. Likewise, a double deletion of *KAP121* and *KAP123* can be functionally complemented by an additional copy of a gene encoding a third kap, *KAP108/SXM1*[60]. Furthermore, Kap121p and Kap104p can each bind to the rgNLS encoded in Nop1p and either can mediate the nuclear import of this protein[100]. This functional overlap may provide for a flexible transport system that is able to accommodate the changing demands of the cell by providing additional receptors that can respond to increased transport burdens. In addition, because kaps have overlapping sets of cargoes, the cell could potentially regulate the transport of groups of proteins by regulating a specific kap, without mislocalising *all* of the cargoes transported by that kap[56,100].

Although most kaps bind to their cargoes and FG-nups directly[10,46], the first nuclear transport pathway to be characterised proved to be an exception to this generality. In this case, cargo proteins harbouring a classical NLS (cNLS) are recognised by the Kapα/β heterodimer (Kap60p/Kap95p in yeast). The Kap60p (or Srp1p) subunit acts as an adaptor by binding to Kap95p and to cNLS, thereby forming a stable trimeric Kap60p/Kap95p/cNLS import complex[16,101,102]. Kap95p in turn interacts with FG-nups to mediate translocation across the NPC[16,51].

In general, each kap has the ability to interact with numerous FG-nups (for review, see 10,34,46,103), suggesting that translocation is mediated by a series of binding and release steps spanning the length of the NPC[16]; however, each kap appears to bind to a unique subset of FG-nups, such that they likely traverse the NPC by overlapping, but distinct, routes[51,56,104-106]. In addition to the ability to bind FG-repeats, some kaps bind with high affinity to other sites within specific nups. Given that these high affinity sites are often found exclusively on the cytoplasmic or nucleoplasmic portion of the NPC, they likely impart directionality to transport by drawing transport complexes to a specific face of the NPC - to the nuclear basket in the case of import[107,108] or the cytoplasmic fibrils in the case of export[108,109]; nonetheless, the major directional cues are thought to be conferred by the nucleotide bound state of the small GTPase, Ran (Gsp1p in yeast).

1.2.3. The regulators - Ran and its effectors

Ran can bind to either GDP or GTP, and these two forms have dramatically different effects on kap interactions with cargoes and with NPCs[16] (for review, see 11,110,111). The cytoplasmic localisation of the Ran GTPase activating protein (RanGAP, Rna1p in yeast)[112], and the nuclear sequestration of the Ran guanylyl-nucleotide exchange factor (RanGEF, Prp20p in yeast)[113] has long been thought, and more recently shown in *Xenopus* egg extracts, to establish a sharply declining gradient of Ran-GTP across the NE when moving from the nucleus to the cytoplasm[114]. Vectorial nucleocytoplasmic transport is a result of the different effects that Ran exerts on import and export complexes dependent on its guanylyl nucleotide bound state (Figure 1-3). The interaction between an import-bound kap and an NLS is stable in the cytoplasmic environment of Ran-GDP, but in the nucleus, Ran-GTP binds to the kap, causing it to release its cargo[18]. The opposite is true of export-bound kaps. In this case, the interaction of Ran-GTP with the kap promotes the cooperative binding of the NES[61], but upon transport to the cytoplasm, the GTP is hydrolyzed and the cargo is released (for review see 115). It has also been demonstrated that Ran-GTP stimulates the release of import-bound kaps from specific nucleoporins[16,116], whereas export-bound kaps interact with nucleoporins in the presence of Ran-GTP[109]. Thus, Ran is thought to impart directional cues, based on its guanine nucleotide-bound state, and also provide energy to maintain nucleocytoplasmic transport through the hydrolysis of GTP.

The constant removal of Ran-GTP from the nucleus and its subsequent hydrolysis into Ran-GDP creates a flux of Ran from the nucleus into the cytoplasm that, in order for the nucleocytoplasmic transport cycle to continue unhindered, necessitates a mechanism to replenish nuclear pools of Ran-GTP. This Ran gradient is maintained by the co-operative effort of Ntf2p and Prp20p. Cytoplasmic Ntf2p binds to Ran-GDP and mediates its translocation into the nucleus[117-119], at which point the complex is dissociated by the conversion of Ran to its GTP-bound form by Prp20p. Ntf2p, now free of Ran-GDP, returns to the cytoplasm to undergo another round of Ran-GDP import. Given that Ntf2p can bind to both karyopherins and components of the NPC, it is possible that Ntf2p transits the NPC of its own accord or as part of a larger macromolecular complex containing kaps, but recent data support the former scenario[120,121].

1.3. Models of movement through the NPC

Despite our detailed understanding of the factors that govern the flow of macromolecules between the nucleus and cytoplasm, the actual mechanism by which kap/cargo complexes access and transit the aqueous central channel of the NPC is

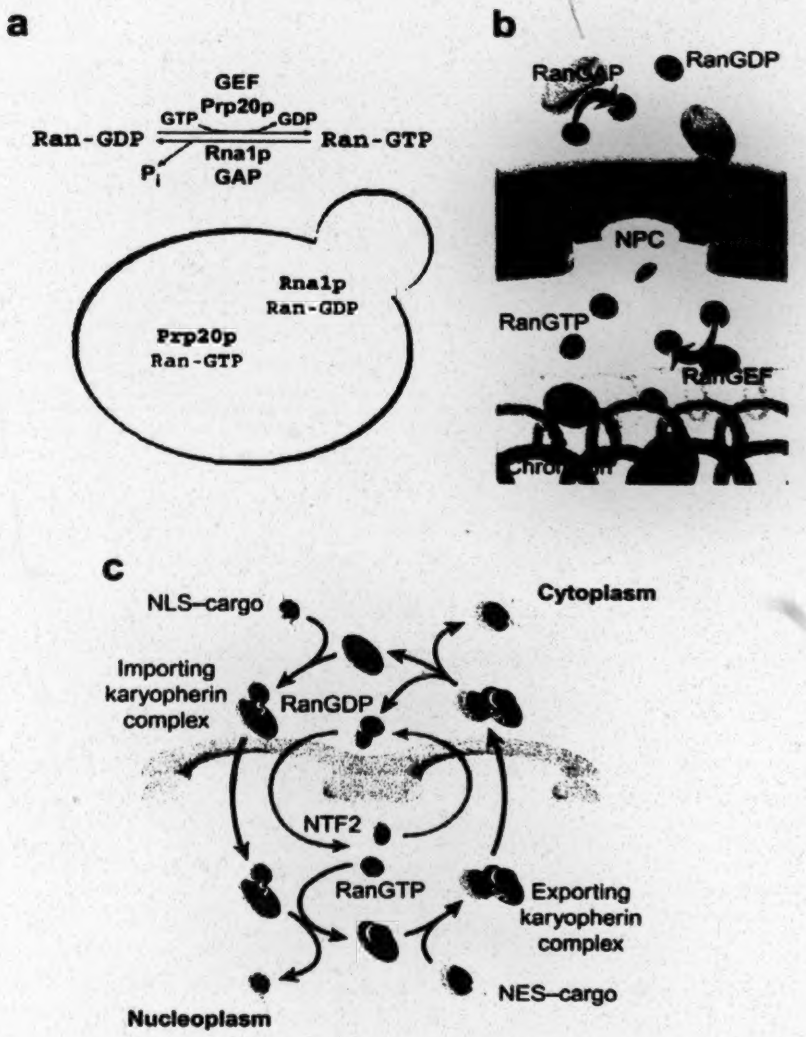
a
GEF
Prp20p
GTP
GDP
Ran-GDP
Ran-GTP
Rna1p
GAP
Pi
Rna1p
Ran-GDP
Prp20p
Ran-GTP
b
RanGAP
RanGDP
NPC
RanGTP
RanGEF
Chromatin
c
NLS–cargo
Cytoplasm
Importing
karyopherin
complex
RanGDP
NTF2
RanGTP
Exporting
karyopherin
complex
NES–cargo
Nucleoplasm

Figure 1-3. The Ran gradient and its effects on nuclear transport reactions. (a and b) The ras-like G-protein Ran (Gsp1p in yeast) converts between its guanylyl-nucleotide bound forms though the catalytic action of Prp20p and Rna1p, which promote the formation of Ran-GTP and Ran-GDP, respectively. The restricted subcellular localisations of Prp20p and Rna1p ensure that Ran is bound to GTP in the nucleus and GDP in the cytoplasm, which creates a gradient of Ran-GTP when moving across the NPC. (c) The Ran cycle. The constant removal of Ran-GTP from the nucleus as a vital component of nuclear export complexes and the subsequent Rna1p-catalyzed hydrolysis of Ran-GTP to form Ran-GDP in the cytoplasm necessitate a mechanism to replenish nuclear stores of Ran-GTP. In yeast, this function is performed by Ntf2p, a protein that recycles Ran-GDP to the nucleoplasm and promotes the Prp20p-dependent exchange of GDP for GTP. It is thought that the maintenance of this Ran cycle provides the energy required to drive nucleocytoplasmic transport. Adapted from (3).

far from clear. Several models, detailed below, have been to put forth to explain this activity.

1.3.1. Gating by entropic exclusion – Brownian affinity gate model

In this model, movement through the NPC can be envisioned as a process of facilitated effusion, in which the central channel of the NPC serves as a pin-hole, or more correctly a tube, of a dynamically variable diameter[1,3,4]. This alteration in central channel diameter is not thought to arise from a physical contraction or dilation (although NPC stretching during transport of large complexes has been observed[122,123]). Instead, the central channel presents each molecule with a unique 'apparent' diameter that determines each species' effusion rate - a molecule that 'sees' a large diameter easily transits the NPC, while a molecule to which the central channel appears very narrow will be much less likely to traverse the NPC and therefore sequestered in either the nucleus or the cytoplasm.

The ability of the NPC to virtually modulate its pore diameter is a consequence of two properties of FG-nups. First, FG-nups adopt highly flexible, filamentous conformations and, second, they have an affinity for karyopherins. On one hand, the filamentous, kinetically charged FG-nups induce a Brownian effect in the central channel and surrounding regions of the NPC that decreases the apparent diameter of the central channel (in effect contracting the pinhole), which results in the entropic exclusion of most molecules. This property agrees with observations that the molecular mass cut-off of the central channel for non-kap associated particles is lower than for those able to bind kapryopherins[124-126]. Thus, there is a very high overall avidity of kaps for the NPC due to its abundance of FG-binding sites, and this potential enthalpic binding energy is able to overcome entropic exclusion from the central channel of the NPC, akin to selectively dilating this virtual pin-hole. As a result, the NPC presents an impassable barrier to most soluble molecules, with the exception of kaps and their associated cargoes, which are virtually unhindered in their movement through the NPC. The ability of transport complexes to easily enter the nucleus and cytoplasm allows selective cargo deposition to occur dependent on the directional cues imposed primarily by the Ran gradient. In addition, this model proposes that the asymmetric distribution of certain FG-nups promotes the selective movement of cargo complexes to either the nuclear or cytoplasmic faces of the NPC, increasing the efficiency of transport and imparting directionality.

1.3.2. Hydrophobic phase partitioning and Oily spaghetti models

Two closely related models suggest that the hydrophobic nature of the FG-repeats and the overall lack of tertiary structure of the nups that contain these repeats create a hydrophobic barrier in the central channel of the NPC that separates the aqueous cytoplasmic and nuclear contents[127,128]. In the first model, the filamentous nups are envisioned to form a mesh that is held together by hydrophobic interactions between FG-repeats[127]. This mesh effectively prevents the passage of most macromolecules through the NPC, except those that are kap-associated, as the ability of kaps to bind to FG-repeats allows them and their cargoes to easily penetrate the otherwise impermeable barrier. Rather than form a phase barrier, the second model proposes that the hydrophobic, filamentous FG-nups provide an oily spaghetti-like coating to the surface of the central transporter of the NPC[128]. This coating has the effect of decreasing the diameter of the transport channel, thereby presenting an impassable barrier to all but very small macromolecules. Essentially using their affinity for FG-repeats for traction, kaps and their associated cargoes can 'squeeze' through the hydrophobic surface coating of the central transporter and thereby easily pass between the nucleus and cytoplasm. As with the Brownian affinity gate model, the Ran cycle imparts directionality to the process and provides the required energy.

1.3.3. Sequential binding and release – FG affinity gradient model[16]

One of the earliest proposed mechanisms of transport through the NPC, this model proposes that nups are strategically positioned within the NPC such that the FG-repeat and/or unique high-affinity binding sites for a given kap are arrayed along a gradient of increasing affinity. Thus, each kap and its associated cargo can translocate the central channel by stochastic movement from one kap binding site to another until a terminal, high-affinity binding site is reached, after which the complex can permanently dissociate. Directionality is determined by the affinity gradient itself in addition to the Ran cycle, which, in some versions of this model, is also proposed to catalyze the association and dissociation reactions involved in the step-wise movement of kap/cargo complexes across the NPC. Despite the fact that support for this model has diminished, it is important to note that several of its principles have been incorporated into the more modern models discussed previously, most notably the idea that high-affinity binding sites for kaps within the NPC can aid in determining the directionality of transport.

Interestingly, all the models discussed above have been founded on different interpretations of the role of the FG-repeats coded within many nups. In fact, the Brownian affinity gate, hydrophobic phase partition and oily spaghetti models are quite similar to one another in principle, with the major difference being the interpretation of the 'excitement state' of the filamentous FG-nups. That is, in the Brownian affinity gate model FG-nups are presented in an excited 'gas-like' state in which each nup's movement is independent of other nups. In contrast, the phase partition model suggests a less kinetically charged liquid-like cohesiveness between FG-nups that creates a hydrophobic matrix. Taking the idea even further, the oily spaghetti model suggests FG-nups form a semi-solid coating on the surface of the central channel.

While it is widely accepted that FG-nups are key to NPC function, it was recently shown that eliminating over half of these repeats has little effect on cell viability and only certain deletion combinations manifest detectable decreases in the rate of nucleocytoplasmic transport[106]. In general, the FG-regions of the asymmetrically disposed nups were not required. While seemingly contradictory to models incorporating a high-affinity binding site mechanism of vectorial movement through the NPC, it is important to note that only the FG regions in these nups were omitted. That is, given that the established high-affinity binding sites for Kap95p and Kap121p on Nup1p and Nup53p, respectively, are not located within FG-repeat regions[14,129], it is possible that many such high-affinity kap binding sites remain intact in the ΔFG mutant strains analyzed. Another *caveat* of this line of experimentation is that the elimination the FG-repeats decreases their overall concentration in the NPC; thus, in addition to decreasing the overall affinity of kaps for the NPC, deletion of FG-repeats could give rise to secondary effects, including increasing the apparent pore size of the central channel. Such secondary effects confound analyses as they could mask effects on transport rates related to the loss of kap affinity for the NPC.

1.4. Broad spectrum of NPC involvement in cellular functions

Far from simply serving to encapsulate the genetic material, the nucleus is a highly organised and compartmentalised organelle and NPCs appear to aid in its organisation[130]. Processes such as DNA replication, RNA transcription and ribosome assembly are coordinated spatially and temporally within the nucleus, which links NPCs, at least indirectly, to these functions. However, as detailed below, an increasing body of evidence points towards a more direct role for NPCs and other nucleocytoplasmic transport components in many nuclear activities. Taken together, these data underscore the idea that the function of the NPC goes far beyond that as a mediator of exchange between the cytoplasm and the nucleoplasm.

1.4.1. NPC mutants affect gross nuclear morphology

Early evidence of a role for NPCs in nuclear organisation came from the analysis of the effects of nup mutations on the distribution of NPCs within the NE. Mutations in the genes encoding many yeast nups, including *NUP145, NUP133, NUP159, NUP120, NUP84, NUP85* and *GLE2*[131-141], were shown to induce clustering of NPCs to discrete foci within the NE. These results indicate that the distribution of NPCs in the NE is at least partially dependent on NPCs themselves. More importantly, that these clusters reproducibly manifest opposite the nucleolus implies a link between NPCs and this nuclear subcompartment[131]. In addition to NPC clustering, other alterations in components of the yeast NPC have been shown to elicit gross morphological changes in nuclear structure. For example, when Nup53p is overexpressed in yeast, it induces the formation of multi-membraned structures at the nuclear periphery that appear to be *de novo* synthesised NE, indicating a link between the NPC and NE proliferation[132].

1.4.2. Components of the NPC are involved in cell cycle control

Analysis of the interaction of Kap121p with the NPC led to the discovery that a molecular switch within the NPC allows nucleocytoplasmic transport to be controlled in a cell cycle-dependent manner[142]. Like many kaps, Kap121p can interact with multiple

FG-nups and can also bind with high affinity to specific nups[104,129]. In the case of Kap121p, the high-affinity binding site is encoded within Nup53p, a central component of the NPC but, surprisingly, this binding site is not normally available to Kap121p because it is masked by the interaction between Nup53p and Nup170p. The M-phase specific phosphorylation of Nup53p induces Nup53p to shift from Nup170p to an alternate nup binding partner, Nic96p, and this rearrangement frees the high-affinity Kap121p binding site from steric constraint[142]. The effect of this unmasking is the sequestration of Kap121p, which results in the swift cessation of Kap121p-mediated nuclear import but leaves other transport pathways unperturbed. The fidelity of this inhibitory pathway is required for normal progression through M phase, which emphasises the complex relationships between the nucleocytoplasmic transport machinery and nuclear functions.

1.4.3. NPCs function in the organisation of chromatin in the nucleus

NPCs have long been proposed to aid in the organisation of chromatin within the nucleus, a function that enables cells to regionally control gene expression[143]. In the interphase nucleus, DNA is divided into actively transcribed euchromatin and silenced heterochromatin and, while heterochromatin predominates at the nuclear periphery, early electron microscopy studies revealed that euchromatic channels extend from NPCs into the nuclear interior[144]. These data provided evidence of NPC function in the structural organisation of chromatin states and placed NPCs at the interface between active and silenced chromatin. *S. cerevisiae* provides an excellent model to elucidate cellular mechanisms of genome organisation as, although it lacks observable heterochromatin, it possesses several heterochromatin-like silenced regions, including subtelomeric regions[145,146], the repressed *HML* and *HMR* mating type loci[147], and the tandem rDNA repeats[148].

The study of telomeres in diploid yeast has revealed that the 64 telomeres localise to less than 10 foci at the nuclear periphery[149], and this subcellular localisation correlates with their silenced state[150]. Moreover, this effect appears to be a result of localisation to the nuclear periphery, as reporter genes artificially tethered to the NE are silenced[151]. The precise mechanism for this position-based silencing is not known, but a protein network beneath the nuclear envelope comprised of Mlp1p and Mlp2p has been implicated in the organisation of functional nuclear subcompartments, telomere localisation and chromatin silencing[8,152]. Yeast that lack both Mlp proteins or certain nups exhibit aberrant telomere localisation and transcriptional activation of subtelomerically encoded reporter genes, suggesting that NPCs are, at least indirectly, important for these functions[8,152]. However, *mlp* mutants exhibit defects in both NE morphology and nucleocytoplasmic transport[153], and contradictory results regarding their role in telomeric anchoring have been reported[154,155]. Thus, this model remains somewhat controversial.

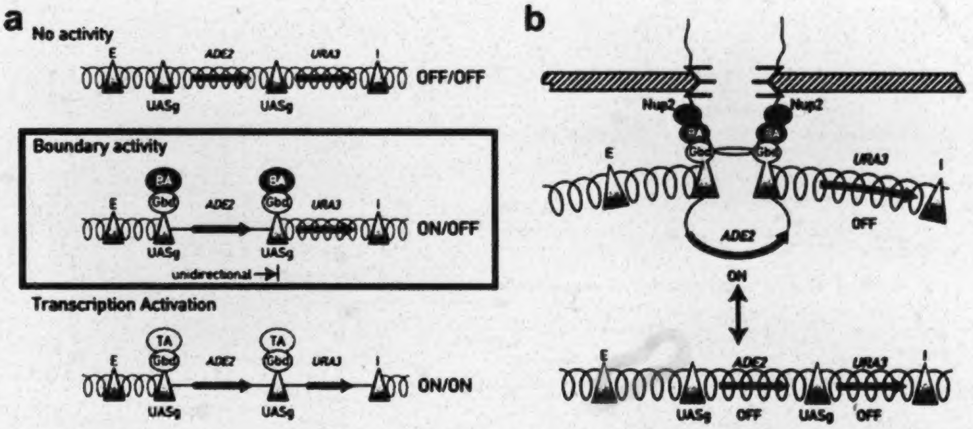

Figure 1-4. The boundary trap assay. (a) Construction of the boundary trap strain. The *HMLα1* and *HMLα2* genes are encoded between the E and I silencers within the silenced *HML* locus in the subtelomeric region of chromosome IIIL. In a strain in which the I silencer contains a partial deactivating mutation, the *HMLα1* and *HMLα2* genes were replaced by tandemly encoded *ADE2* and *URA3* reporter genes each with an upstream UASg binding site, which binds to the DNA-binding region of the Gal4p protein. The UASg binding sites allowed proteins fused to the Gal4p DNA-binding domain (Gbd) to be physically tethered to the upstream regions of these reporter genes. Under normal conditions and conditions wherein only Gbd is expressed, the entire region was silenced, resulting in the *ADE2/URA3* OFF/OFF phenotype (top). When fusions between Gbd and proteins that are transcriptional activators were expressed, the region adopted *ADE2/URA3* ON/ON expression state (bottom). Importantly, if a protein able to form DNA boundaries was expressed as a fusion to Gbd, then the UASg flanked *ADE2* gene was protected from the silencing effects of the E and I silencers and strains expressing these fusions were able to obtain an *ADE2/URA3* ON/OFF expression state – such proteins were said to harbour boundary activity (BA). Yeast proteins possessing BA were identified by screening yeast Gbd-fusion libraries for transformants able to grow on media lacking adenine and containing 5-FOA, a growth condition that selects for the *ADE2/URA3* ON/OFF expression state. When Ishii *et al.* performed these experiments they identified an abundance of nuclear transport factors which led them to propose the model of NPC-dependent boundary activity shown in (b). Adapted from 2,6.

1.4.4. NPC-mediated transcriptional insulation (boundary activity)

Another novel function of NPCs in nuclear organisation is their ability to interrupt the spread of transcriptional cues along chromatin by physically interacting with DNA. Active or silenced DNA is partitioned along chromosomes by insulators or boundary elements, which are operationally defined by their ability to buffer the spread of transcriptional activation and repression between flanking chromatin regions[156,157]. In yeast, these elements have been identified in subtelomeric regions[146] and the silenced mating type loci[158,159]; however, it is likely that as yet unidentified boundaries exist throughout the genome that aid in organising chromatin[160]. Ishii *et al.* have shown that when artificially tethered to specific DNA sequences, NPCs transcriptionally insulate adjacent DNA regions from one another, a hallmark of boundary activity (BA)[2]. Although this artificial system, detailed in Figure 1-4, revealed a potentially exciting new function of NPCs, several questions were unanswered, including whether or not these data reflect an endogenous mechanism of NPC-mediated BA and, if so, what provides the physical link between NPCs and DNA.

1.5. Focus of thesis research

My research is centered on Nup2p, one of the earliest identified yeast NPC components[161]. Nup2p is a 720 amino acid protein that can be divided into three distinct domains. The amino terminal 172 amino acids are responsible for interaction with both Kap60p and the NPC[162,163]. The central domain (aa 182–546) contains several FXFG repeats typical of domains found in other nucleoporins that bind to members of the karyopherin superfamily. The carboxy terminus (aa residues 556 to 720) contains a Ran binding domain (RBD), homologous to the RBD of the shuttling protein, Ran Binding Protein 1 (RanBP1, Yrb1p in yeast)[15,164,165], the yeast nuclear protein Yrb2p and the cytoplasmically disposed mammalian nucleoporin Nup358[166]. All previous studies suggested that Nup2p is a typical nup that functions in Cse1p-mediated recycling of Kap60p from the nucleus to the cytoplasm[162,163,167,168] but my investigations into its function(s) revealed that this is not the case. Nup2p is, in fact, a unique nucleoporin. My work can be divided into two projects, or aims, detailed in sections 2 and 3. In the first, I analyzed the association of Nup2 with the

NPC, which revealed that Nup2p transiently associates with this structure. Furthermore, I examined the relevance of this activity to the function of Nup2p in cNLS import, Kap60p recycling and other nucleocytoplasmic transport pathways. The second project was aimed at understanding a novel function of Nup2p. Using the boundary trap assay, Ishii *et al.* revealed that Nup2p is an important player in NPC-mediated BA, as Nup2p is required for the BA of all transport factors shown to harbour this activity and also possessed its own BA[2]. Our contribution was to identify and characterise the endogenous mechanism of Nup2p-dependent BA. Finally, section 4 discusses the importance of resolving the functions of Nup2p in nucleocytoplasmic transport and chromatin organisation into a single model, possible applications to higher eukaryotes, as well as directions for future work in this area.

2. THE ROLE OF NUP2P IN NUCLEOCYTOPLASMIC TRANSPORT

2.1. Overview - Nup2p is not a *bona fide* nucleoporin

The start of my studies in the Aitchison group coincided with the conclusion of a collaborative effort aimed at identifying all of the yeast nucleoporins and determining their locations and relative stoichiometric ratios within the NPC. The starting point of this proteomics-based approach was the development of a fractionation procedure able to yield extracts highly enriched in NPCs. From the proteome of this sample, a list of candidate nups was compiled, and the true nups within this list were identified using a series of diagnostic assays. One of the required characteristics to be considered a *bona fide* nucleoporin was co-enrichment with NPCs during the various stages of the NPC purification procedure and, despite its previous classification as a nup, Nup2p did not meet this criterion. Surprisingly, Nup2p was significantly distributed in cytoplasmic and nucleoplasmic fractions in addition to the NPC-enriched fraction, thereby indicating that Nup2p does not stably associate with the NPC (Figure 2-1). In fact, the fractionation pattern of Nup2p is more characteristic of karyopherins and, on these grounds, Nup2p was eliminated from the list of candidate nups. In support of this exclusion, immunopurification of Kap95p was shown to yield significant amounts of Nup2p when captured from yeast cytosols, yet these cytosols contain no other nups, as NPCs are not disrupted during cytosol preparation[51,56]. Interestingly, when the same experiment was performed using yeast whole cell extracts, the preparation of which disrupts NPCs, Nup1p was detected, in addition to Nup2p, at Coomassie blue observable levels in these eluates (data not shown, see also Table 2-1). The specific presence of Nup2p in Kap95p cytosol eluates argues for a weak, perhaps transient, interaction between Nup2p and the NPC or that a distinct cytoplasmic population of Nup2p exists. In light of these data, a project aimed at testing the hypothesis that Nup2p is an atypical nucleoporin that transiently associates with the NPC was initiated, with the further goal of elucidating the mechanism(s) controlling this interaction and its relevance to nucleocytoplasmic transport.

In the series of experiments detailed in the following section, an abundance of evidence supporting this hypothesis is presented. Nup2p is indeed transiently associated with the NPC, and this association is modulated by Ran. We identified the nucleoporin, Nup60p, as the major Nup2p binding site on the nuclear face of the NPC by *in vitro* binding and *in vivo* fluorescence and, like Nup2p, we show that Nup60p is required for efficient recycling of Kap60p from the nucleus to the cytoplasm. These data led us to propose a model in which Nup2p facilitates the transition between the import and export phases of the Kap60p-Kap95p transport pathway. Finally, we present preliminary unpublished data exhibiting that Nup2p binds to a variety of other kaps, which suggests that Nup2p functions in other kap pathways.

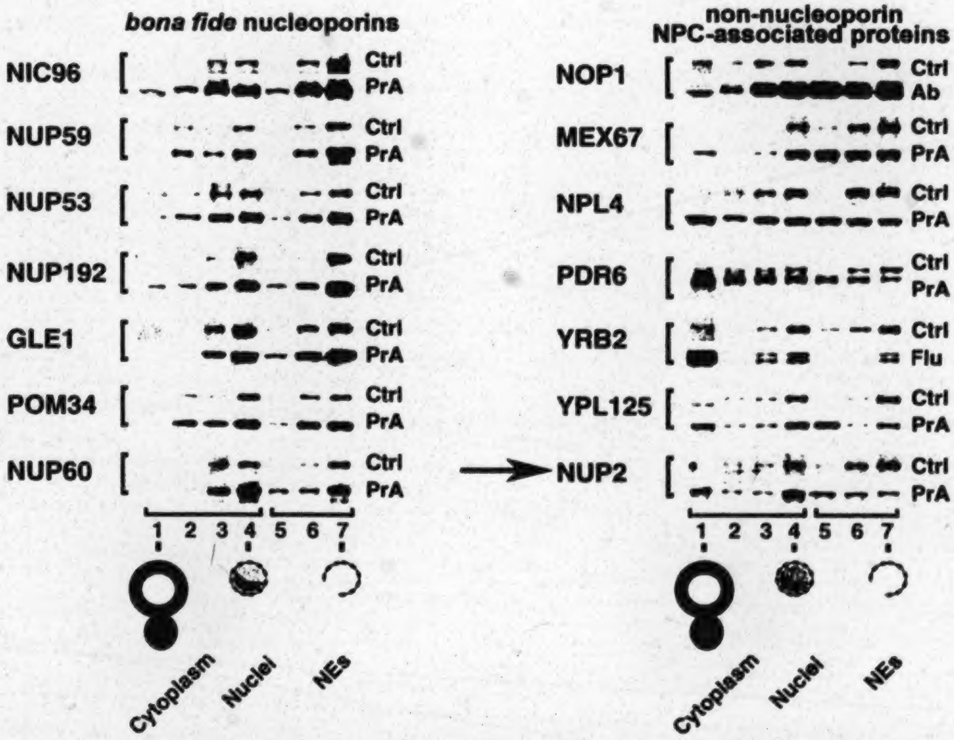

bona fide nucleoporins
non-nucleoporin NPC-associated proteins
NIC96
NUP59
NUP53
NUP192
GLE1
POM34
NUP60
NOP1
MEX67
NPL4
PDR6
YRB2
YPL125
NUP2
Ctrl
PrA
Ab
Flu
1 2 3 4 5 6 7
Cytoplasm
Nuclei
NEs

Figure 2-1. Nup2p does not enrich with NPCs. Candidate NPC proteins were tagged with proteinA and whole cell lysates from these strains were subjected to a two-step subcellular fractionation procedure. The lanes numbered 1 through 4 are fractions from the first purification step that separated cytoplasmic components (lane 1) from intact nuclei (lane 4). Lanes 5 through 7 are fractions from the second purification step in which soluble nuclear contents (lane 5) were separated from NEs (lane 7). Comparison of the enrichment profile of each tagged protein to the control profile, obtained using a specific antibody to Pom152p, allows the distinction between stably (left) and transiently (right) NPC-associated proteins. The profile obtained for Nup2p (black arrow) indicates that is does not stably associate with NPCs because a detectable amount of Nup2p is detected in cytosols (lane 1) and the soluble nuclear contents (lane 5), which is a pattern more consistent with that of a kap than a nup. Adapted from (4).

2.2. Results

2.2.1. The localisation of Nup2p in the NPC

Nup2p encodes FG-repeat motifs, is structurally disordered and exhibits a punctate pattern around the nuclear envelope when examined by fluorescence microscopy, all of which are typical of nucleoporins. Since only a portion of NPC-associated Nup2p ultimately copurified with nuclear envelopes during subcellular fractionation, we hypothesised that Nup2p binds to multiple sites within the NPC with differing affinities. Thus, the fraction of Nup2p released during the purification of NEs from intact nuclei is derived from low-affinity interactions with the NPC and that which remained NE-associated is bound to high-affinity sites. If so, we would expect the localisation of Nup2p in the NPC to be different in purified nuclear envelopes compared to intact nuclei, as binding at low-affinity sites would be lost during NE preparations. To this end, a genomically encoded fusion of the gene encoding *Staphylococcus aureus* Protein A (PrA) at the 3' end of the *NUP2* coding region was constructed, such that Nup2p-PrA was expressed under the control of its endogenous promoter. The Nup2p-PrA chimera was localised in nuclei and NEs by pre-embedding labeling and immunoelectron microscopy (IEM)[119,169]. In nuclear envelopes, Nup2p-PrA was present solely at the distal nuclear face of the NPC (Figure 2-2a), significantly further from the mid-plane of the NPC than all other nups[4]. In contrast, when this procedure was repeated using isolated nuclei, Nup2p-PrA was found on both the nuclear and cytoplasmic sides of the NPC (Figure 2-2b). Thus, because the isolation of nuclei precedes the partial solubilisation of Nup2p from the NE fraction, we have potentially revealed a separate specific location for that fraction of Nup2p liberated upon the isolation of NEs. These data suggest that there are at least two distinct sites on either side of the NPC to which Nup2p can bind. As controls, we also determined the positions of Nup159p-PrA and Nup1p-PrA. The relative positions of these two nucleoporins with respect to each other and the nuclear portion of Nup2p-PrA were similar in both purified NEs and intact nuclei (Figure 2-2c), confirming that the dual localisation of Nup2p is not due to gross alteration of NPC morphology between preparations. It should be noted that in each case, however, the tags appeared closer to the midplane of the NPCs in the

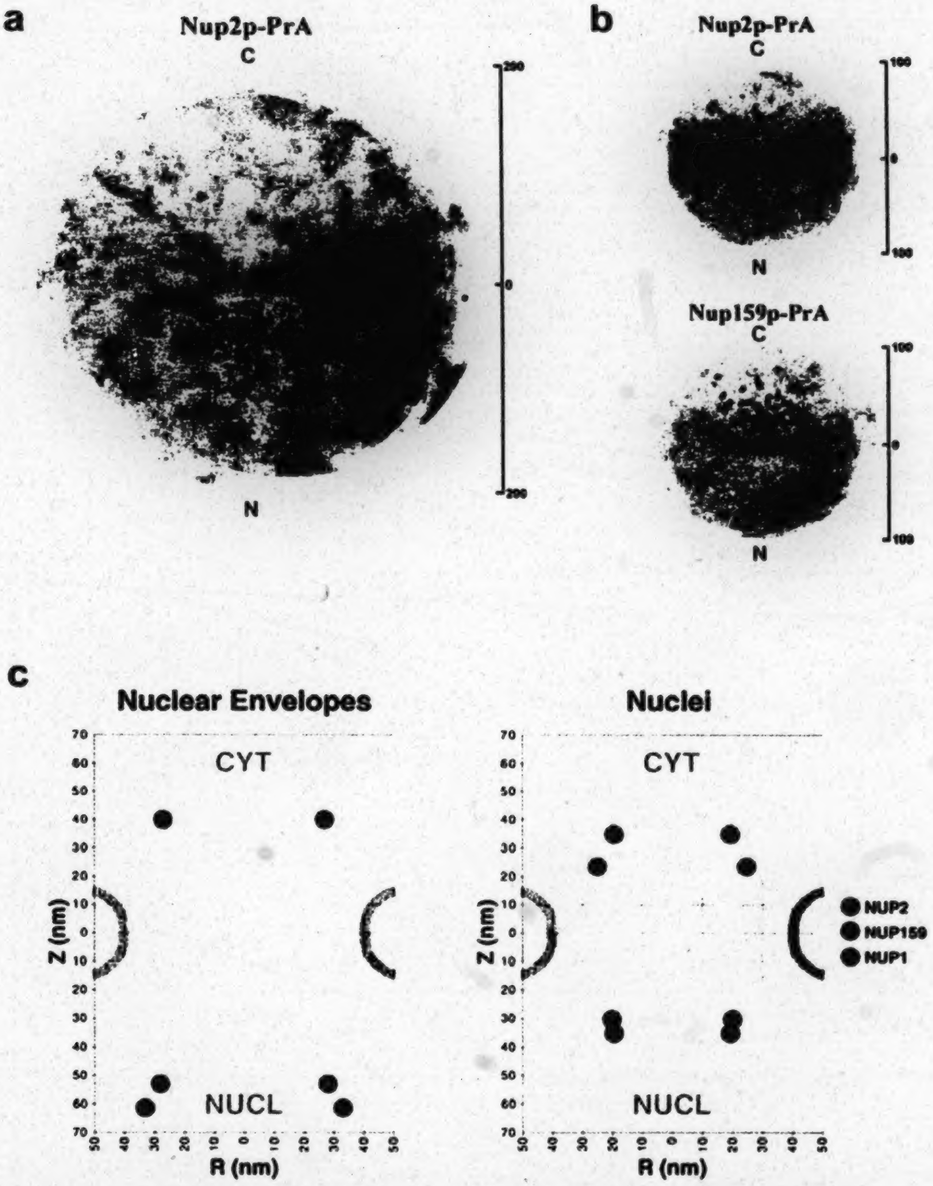
a
Nup2p-PrA
C
N
200
0
200
b
Nup2p-PrA
C
N
100
0
100
Nup159p-PrA
C
N
100
0
100
c
Nuclear Envelopes
Nuclei
CYT
NUCL
Z (nm)
R (nm)
70 60 50 40 30 20 10 0 10 20 30 40 50 60 70
50 40 30 20 10 0 10 20 30 40 50
NUP2
NUP159
NUP1

Figure 2-2. Nup2p exhibits variable localisation in the NPC. Nup2p-PrA was localised in purified NEs (a) and nuclei (b) by immunoelectron microscopy using gold-conjugated antibodies. Montages of 20 NPCs were prepared with the cytoplasmic side of the NPCs oriented up (determined by the presence of ribosomes on the NE). Scale bars units are nm. In NEs, Nup2p-PrA localised solely to the nuclear face of the NPC ~ 63 nm from the midplane of the NPC. In intact nuclei, Nup2p-PrA was detected on both faces of the NPC ~36 nm from the midplane. For comparison, Nup159p-PrA and Nup1p-PrA (not shown) were also localised under these conditions, demonstrating that the relative localisation of Nup1p-PrA, Nup159p-PrA and nuclear Nup2p-PrA did not vary significantly between the different preparations. (c) The positions of Nup2p-PrA, Nup159p-PrA and Nup1p-PrA are summarised.

nuclei samples compared to the NEs, which is not surprising, since different IEM preparations can give different absolute localisations[170,171]. Regardless, these data show that Nup2p is preferentially retained at the nuclear face during the fractionation and, given that the localisation of Nup2p in whole cells is predominantly on the nucleoplasmic face of the NPC[163,168], these data provide strong support for our initial hypothesis that the association of Nup2p with the NPC is dynamic, which led us to assay for Nup2p mobility directly *in vivo*.

2.2.2. Nup2p is mobile

To test for Nup2p mobility, we generated yeast heterokaryons and assayed for the movement of Nup2p between two adjacent nuclei. In this assay, a strain containing a genomically integrated gene fusion encoding a GFP-tagged nucleoporin (donor) was mated with a *kar1-1* strain (recipient)[172] resulting in a binucleated intermediate because the *kar1-1* mutation prevents nuclear fusion during the mating response but does not affect cytoduction (cytoplasmic joining). That the two nuclei remain intact but share the same cytoplasm in this assay allowed the mobility of nups to be assessed by monitoring the Nup-GFP distribution in these cells, termed heterokaryons. Under these conditions, we predicted that a nucleoporin stably associated with the NPC would remain in the donor nucleus, whereas a protein that continuously cycles between NPC docking sites would enter the soluble phase and quickly appear at the NPC of the recipient nucleus. We monitored the GFP signal in heterokaryons derived from cells expressing Nup2p-GFP or the control nucleoporin Nup49p-GFP. In contrast to Nup49p-GFP, the Nup2p-GFP signal was not restricted to the donor nucleus and it was first detectable in some *kar1-1* nuclei within 15 min after cytoduction with an increasing number of mated cells exhibiting fluorescence signal over the following 30 min (Figure 2-3a). Quantitation of the data from this 30 min window reveals that while *bona fide* nups are stably associated with the donor nucleus, over 60 % of Nup2p-GFP expressing heterokaryons exhibited detectable fluorescence in the recipient nuclei (Figure 2-3b). Given that, to avoid the scoring of a dividing nucleus as mobile, the recipient nucleus must have been clearly discernable from the donor nucleus to be classified as mobile, 60 % is likely a conservative estimate for the proportion of cells that exhibit movement of Nup2p

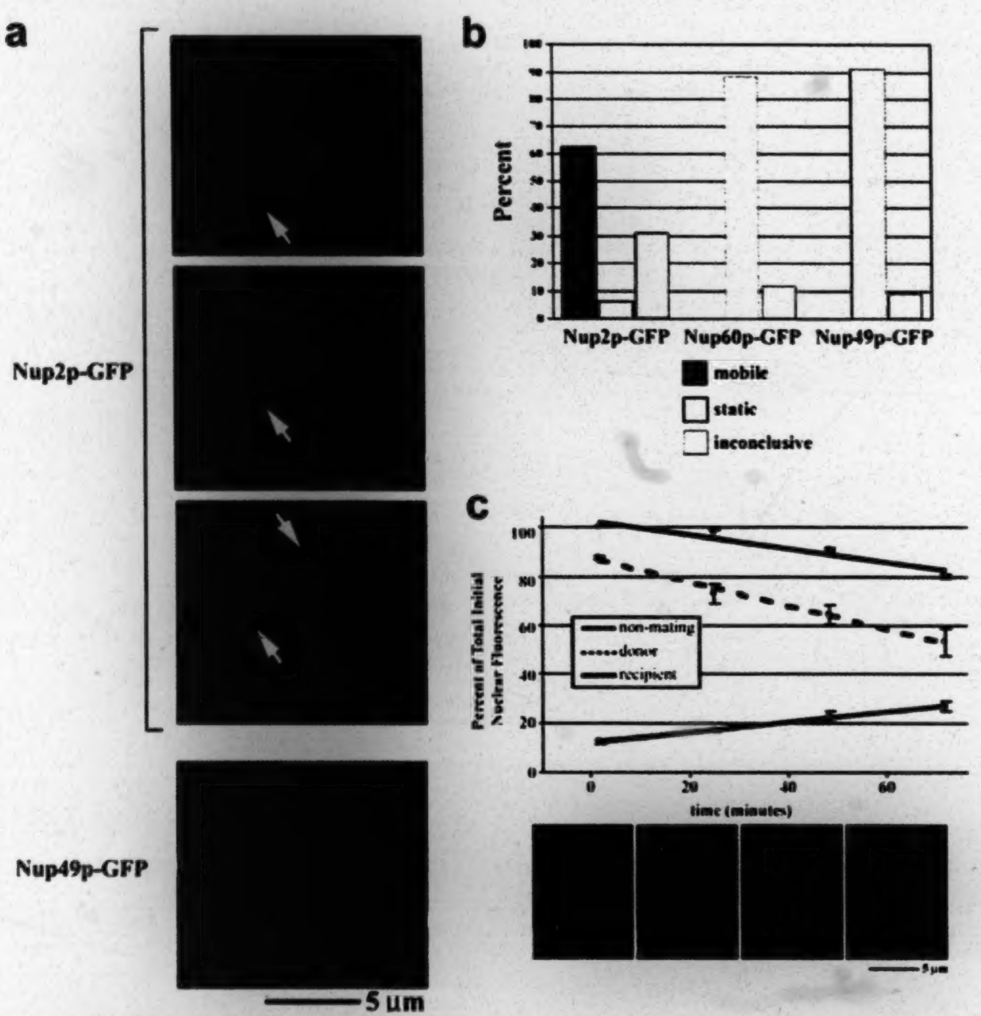

Figure 2-3. Heterokaryon mobility assay reveals that Nup2p does not stably associate with NPCs. (a) Confocal images of bright field and GFP fluorescence acquired 15 to 45 minutes after heterokaryon formation. Nup2p-GFP signal was detectable in the recipient *kar1-1* nucleus during this time (recipient nuclei are indicated by white arrows), whereas Nup49p-GFP remained in the donor nucleus. Other control nucleoporins, Nup60p and Nsp1p, were also detected only in the donor nucleus over these time courses (data not shown). (b) Summary of nucleoporin mobility assay results. Heterokaryons were scored as mobile if GFP signal was detected in two, well-separated nuclei, static, if only one fluorescing nucleus could be seen or inconclusive, in situations where it was difficult to distinguish between a dividing donor nucleus or adjacent donor/recipient nuclei. In the time interval tested, over 60% of Nup2p-GFP heterokaryons exhibited GFP signal in a clearly distinct recipient nucleus; whereas, we detected no movement in Nup60p-GFP and Nup49p-GFP heterokaryons over this time course. The percentage of inconclusive heterokaryons reported for Nup2p-GFP was significantly higher than that for control nucleoporins, which likely reflects the conservative nature of the classification. (c) Gain of signal in the recipient nucleus of Nup2p-GFP heterokaryons is concomitant with a loss of fluorescence in the donor nucleus. Nup2p-GFP heterokaryons were monitored for 1 hour from the point where the recipient nucleus could be visualised by GFP fluorescence and the percentage of the total initial nuclear fluorescence for the donor and recipient nuclei are plotted over time. Averages and error estimates were calculated with Excel (Microsoft) using data from two heterokaryons/cells. Shown below are representative image slices at each time point. The fluorescence of a non-mating Nup2p-GFP cell in the same field of view was also determined to show sample acquisition bleaching.

into the recipient nuclei. Importantly, Nup2p was the only nucleoporin assayed that exhibited movement in this time frame. Like Nup49p, neither Nsp1p-GFP nor Nup60p-GFP exhibited mobility (data not shown). Observation of heterokaryons at later time points revealed that Nup2p-GFP equilibrates between the donor and recipient nuclei between 60 and 120 min post cytoduction, a point at which there is only a modest signal detectable in a small percentage of Nup49p-GFP heterokaryons (data not shown). Importantly, the appearance of Nup49p-GFP signal in the recipient nucleus after this time period is consistent with reports of the assembly rate of new NPCs[173].

Several possibilities exist that would explain the observed mobility of Nup2p-GFP in this assay. That is, the appearance of Nup2p-GFP in recipient nuclei could be due to: (a) movement from one nucleus to another, which would indicate that Nup2p is indeed a mobile component of the NPC; (b) a significant cytoplasmic pool of Nup2p-GFP, undetected by visual observation of the fluorescence signal, that goes on to incorporate into the donor nuclei; or (c) a high Nup2p-GFP turnover rate relative to the control nups, which would imply that the GFP signal detected in recipient nuclei is due to newly synthesised protein rather that movement of pre-existing Nup2p-GFP. To distinguish among these possibilities, we first monitored the movement of Nup2p-GFP in heterokaryons from the point of cytoduction to signal equilibration. Through quantitation of the fluorescence signal in each nucleus, we established that the appearance of fluorescent signal in the recipient nucleus is coincident with a decrease in the donor nucleus signal (Figure 2-3c). This precursor/product relationship between the fluorescent intensity of the donor and recipient nuclei suggests that Nup2p-GFP signal appearing in the recipient nucleus is derived from the donor nucleus and that Nup2p is indeed mobile, being capable of moving from one nucleus to another. We detected no movement of Nup49p-GFP from the donor to the recipient nucleus during the time-frame of this assay (data not shown).

To further exclude the possibility that the observed mobility of Nup2p was the result of a significant cytoplasmic pool of Nup2p and/or a high turnover rate, we first established the expression level of Nup2p-GFP relative to control nucleoporins

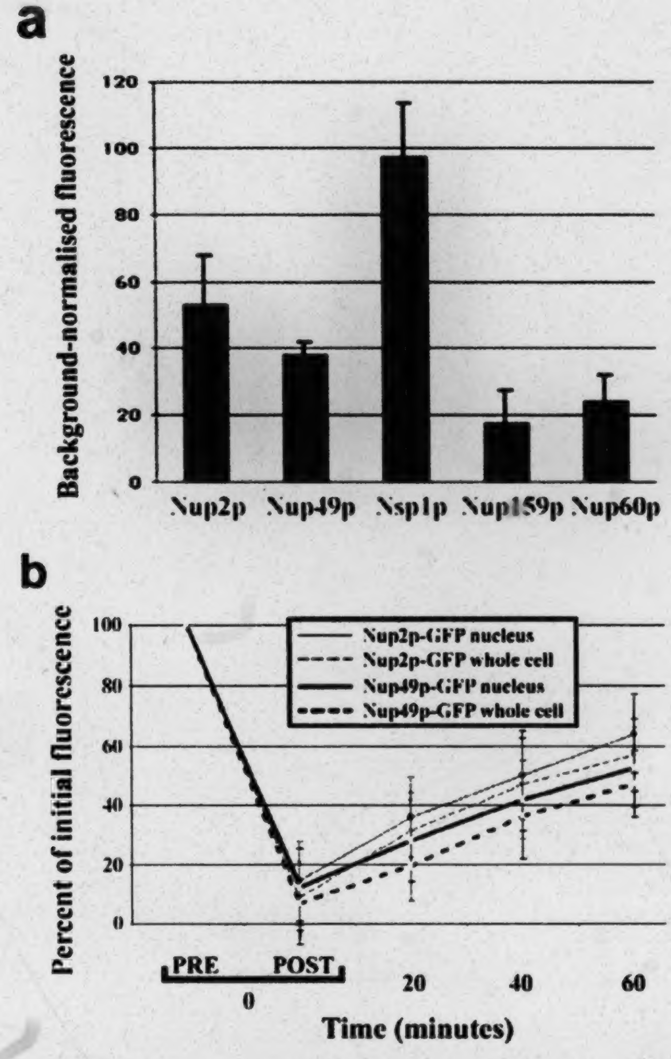

Figure 2-4. The steady-state levels and rate of turnover of Nup2p are similar to those of bona fide *nups.* (a) Nucleoporin levels quantified by analytical flow cytometry of GFP-tagged nucleoporins. Shown is a histogram of the mean, background-normalised fluorescent intensity observed for Nup2p-GFP, Nup49p-GFP, Nsp1p-GFP, Nup60p-GFP and Nup159p-GFP. These data confirmed that Nup2p-GFP and Nup49p-GFP are expressed at roughly equal levels with respect to other nucleoporins. Error bars represent the standard deviation over 4 independent experiments. (b) Quantitation of nucleoporin turnover rates using a photobleach/recovery assay. Nup2p-GFP or Nup49p-GFP expressing cells were photobleached in an area encompassing the nucleus or the entire cell and then imaged at 20, 40 and 60 minutes following the photobleach. The average nuclear fluorescent intensity of bleached cells as a percentage of the initial fluorescence over time was determined. Data points and error bars were calculated as the average and standard deviation of 5 cells. The recovery rate of Nup2p-GFP was equivalent to that of Nup49p-GFP and there was no significant difference between whole cell bleaching and bleaching of only the nuclear signal. Thus, the appearance of Nup2p-GFP in the recipient nucleus in heterokaryon experiments was due to movement of Nup2p-GFP rather than *de novo* protein synthesis or a cytoplasmic pool of Nup2p-GFP.

in vivo using analytical flow cytometry (Figure 2-4a). In this assay, fluorescence signal from Nup2p-GFP was approximately half of that of Nsp1p-GFP, twice that of Nup60p-GFP and Nup159p-GFP and equivalent to the signal from Nup49p-GFP. These data fit well with previous estimates of the abundance of nups by quantitative immunoblotting using PrA-tagged nucleoporins in isolated NEs[4] and suggest that Nup2p, like Nup49p, is present at approximately 16 copies per NPC.

Given that the abundance of Nup2p-GFP is similar to Nup49p-GFP, if the appearance of Nup2p in the recipient nucleus was due to high protein turnover, Nup2p would have to be synthesised (and degraded) at significantly higher rates than Nup49p. To test this possibility, we compared the turnover rates of these proteins by monitoring the GFP fluorescence recovery after photobleaching (FRAP) in real time. In this experiment, the GFP signal was photobleached in either the nuclear compartment or over the entire cell and the recovery of fluorescence was quantified. In this assay, the return of GFP signal at the NPC is likely due to the conversion of unoxidised, pre-fluorescent GFP to the mature fluorophore, but is nevertheless a direct measure of the synthesis rate of the GFP chimera. Not only did this assay provide an estimation of protein turnover rates, it also allowed us to further test for the existence of a significant cytoplasmic pool of Nup2p by comparing the recovery rates for cells that were entirely bleached to those where only the nucleus was bleached. If there is a significant cytoplasmic pool of Nup2p, capable of exchanging with NPC-associated Nup2p, we would predict that the fluorescent signal would recover at a faster rate in cells where only the nucleus was bleached than in cells subjected to whole cell bleaching. As shown in Figure 2-4b, the rate of fluorescence recovery for Nup2p-GFP was equivalent to that of Nup49p-GFP, irrespective of the bleached region. Taken together, these data lead us to conclude that the appearance of Nup2p-GFP in the recipient *kar1-1* nucleus in the heterokaryon experiments was due to the movement of Nup2p-GFP specifically from the donor nucleus, rather than from *de novo* synthesis or from a cytoplasmic pool.

2.2.3. Nup60p anchors Nup2p to the nuclear face of the NPC

To further characterise the interaction of Nup2p with the NPC, Nup2p-PrA was immunoisolated from whole cell lysates to identify any interacting proteins. Both

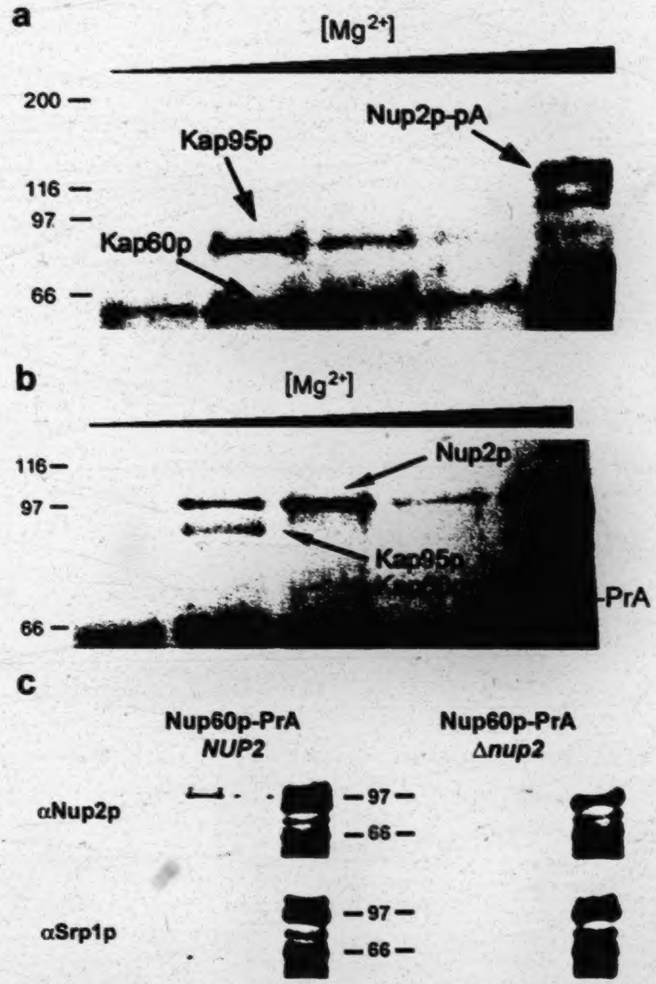

Figure 2-5. Nup2p co-immunoprecipitates with stoichiometric levels of Kap60p, Kap95p and Nup60p. (a) Nup2p-PrA from whole cell lysates was bound to IgG-Sepharose. Co-precipitating proteins were eluted with a $MgCl_2$ gradient, separated by SDS-PAGE and detected by Coomassie blue staining. Shown, from left to right, are relative molecular weight standards (kDa) followed by the fractions eluted by treatment with 0.2, 0.5, 1.0, 2.0 and 4.0 M $MgCl_2$. The two abundantly co-purifying proteins were identified by mass spectrometry as Kap60p and Kap95p. No co-purifying nucleoporins were detected. (b) Nup60p was immunoprecipitated from yeast whole cell lysates and analyzed as for Nup2p. Immunoprecipitation of Nup60p-PrA from whole cell lysates co-precipitated Kap60p, Kap95p and Nup2p suggesting that Nup60p is the nucleoporin that anchors Nup2p to the nuclear face of the NPC. We detected no co-precipitating proteins by Coomassie blue staining when the same immunoprecipitation was performed from a strain lacking Nup2p (not shown). (c) Immunoblot analysis of Nup60p-PrA immunopurifications in wild-type and *Δnup2* strains confirms the absence of both Nup2p and Kap60p in *Δnup2* cells. The 0.5, 1.0, 2.0 and 4.0 M $MgCl_2$ elution fractions from Nup60-PrA immunoprecipitations in wild-type and *Δnup2* strains were probed using anti-Kap60p (anti-Srp1p) and anti-Nup2p antibodies. The absence of Kap60p in the immunoprecipitation from strains lacking Nup2p indicates that Nup2p facilitates the interaction between Nup60p and Kap60p and suggests that the interaction between Nup2p and Nup60p is direct. The two closely migrating bands recognised by the anti-Nup2p antibody were specific to Nup2p, as neither band was present in strains lacking Nup2p. The signal observed in the 4.0 mM elution fraction represents Nup60-PrA and Nup60p-PrA breakdown products that bound to the rabbit polyclonal antibodies.

Kap60p and Kap95p co-purified with Nup2p-PrA, supporting a role for Nup2p in cNLS import; however, although NPCs were disrupted under these conditions[104], we identified no co-purifying nucleoporins (Figure 2-5a). Because the IEM data presented above suggested that Nup2p binds with a relatively high affinity to the nuclear face of the NPC and this interaction is stable to the disruption of nuclei, we attempted to immunopurify Nup2p in a complex with either Nup1p-PrA or Nup60p-PrA. These two proteins were chosen as candidate Nup2p binding partners because they are the only nucleoporins asymmetrically localised to the distal nuclear face of the NPC[4] and are thus in a position to provide a uniquely nuclear binding site for Nup2p. Immunopurification of Nup60p-PrA yielded three proteins, identified by mass spectrometry as Kap60p, Kap95p and Nup2p (Figure 2-5b). In contrast, immunopurification of Nup1p-PrA yielded Coomassie blue detectable levels of several proteins, including Kap95p and Kap60p but not Nup2p (data not shown), which suggests that Nup60p is the nuclear site to which Nup2p binds.

Nup2p interacts with both Kap60p and Kap95p in a trimeric complex. We therefore tested if Nup60p is capable of co-precipitating Kap60p and Kap95p without Nup2p by repeating the Nup60p-PrA immunopurification from lysate derived from a *nup2* null strain. In this case, we detected neither Kap60p nor Kap95p by Coomassie blue staining (data not shown), and a polyclonal antibody directed against Kap60p was also unable to detect this protein in these eluates (Figure 2-5c). These results suggest that, under these conditions, the interaction between Kap60p, Kap95p and Nup60p requires, or is facilitated by, Nup2p and, furthermore, that the Kap60p/Kap95p/Nup2p complex docks via Nup2p to Nup60p at the nucleoplasmic face of the NPC, possibly as a terminal step in cNLS import.

If Nup60p is at least partially responsible for the localisation of Nup2p to the NPC, then loss or alteration of Nup60p should measurably affect the subcellular distribution of Nup2p. We therefore observed the *in vivo* distribution of a Nup2p-GFP chimera in various genetic backgrounds by fluorescence microscopy (Figure 2-6). In a wild-type (WT) background, Nup2p-GFP chimeras display punctate staining at the nuclear periphery that is characteristic of nucleoporins and, like other nups, Nup2p-GFP clusters to one side of the NE in strains lacking Nup120p[4,131,136] (Figure 2-6a). In agreement with our immunopurification results, deletion of *NUP1*[167] had no effect on the localisation of Nup2p-GFP (Figure 2-6a). In contrast, deletion of *NUP60* caused Nup2p-GFP to accumulate in the nucleoplasm with a concomitant loss of signal at the nuclear rim, yet no effect on the localisation of control nucleoporins was observed (Figure 2-6b). Furthermore, restoration of *NUP60* expression using a galactose-inducible promoter returned Nup2p-GFP to its original location at the NPC (Figure 2-6c). Interestingly, there also appeared to be an increase in the cytoplasmic signal of Nup2p-GFP in the *nup60* null strain relative to the WT strain. In agreement with our immunopurification data, these fluorescence experiments suggest that Nup2p is tethered to the nuclear face of the NPC through its interaction with Nup60p.

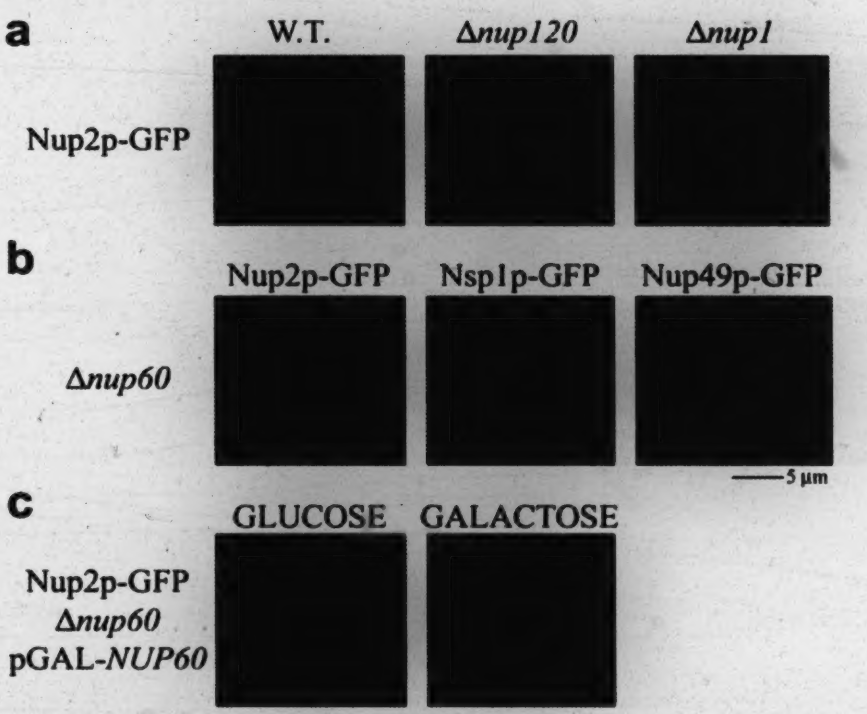

Figure 2-6. Nup60p anchors Nup2p to the nuclear face of the NPC. (a) Nup2p-GFP in wild-type backgrounds exhibited punctate peripheral nuclear rim staining characteristic of a nucleoporin. Like other nucleoporins, Nup2p-GFP clustered to one face of the nuclear rim in cells lacking Nup120p. Consistent with our *in vitro* binding data, deletion of *NUP1* did not affect the localisation of Nup2p-GFP. (b) Deletion of *NUP60* resulted in the nuclear accumulation of Nup2p-GFP, but had no effect on the localisation of the control nucleoporins, Nsp1p and Nup49p. (c) In strains lacking Nup60p, Nup2p-GFP signal returned to the nuclear rim upon expression of *NUP60* from a galactose-inducible

The above data are also supported by genetic data. Cells lacking Nup2p or Nup60p were viable and grew at rates comparable to WT cells, although *Δnup60* cells exhibited a modest, slow-growth phenotype; in contrast, deletion of both *NUP60* and *NUP2* rendered cells unable to grow without plasmid-based expression of *NUP2* (Figure 2-7a). This genetic interaction demonstrates that although Nup2p is mislocalised to the nucleoplasm in *Δnup60* cells, its function is only partially dependent on its ability to interact with Nup60p at the NPC.

2.2.4. Nup2p exhibits Ran-dependent association with NPCs

Although the RBD of Nup2p has been shown to bind Ran in a yeast 2-hybrid assay[15], no other function has yet been defined for this domain. We therefore investigated if the RBD of Nup2p is required to rescue the lethal phenotype observed in cells lacking both Nup2p and Nup60p. A plasmid allowing production of a truncated Nup2p mutant lacking the RBD (Nup2ΔRBD, aa1-546, pLDB690) was unable to fully compensate for the loss of Nup2p in the double null background (Figure 2-7b). Although viable at 30°C, *Δnup2/Δnup60* double mutant cells expressing Nup2ΔRBD failed to grow at 37°C. This result can be explained if the

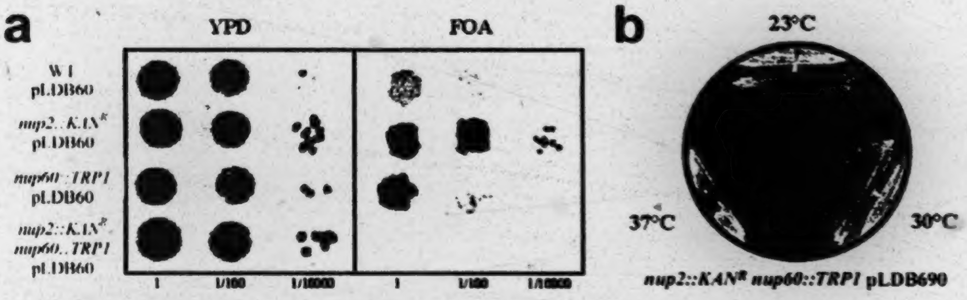

Figure 2-7. NUP2 *and* NUP60 *genetically interact.* (a) *Δnup2* and *Δnup60* strains were crossed and sporulated with the covering plasmid, pLDB60 (*NUP2 URA3 CEN*). Progeny of the indicated genotypes were assayed for the ability to grow without the *NUP2* covering plasmid by growth on FOA. As shown by serial dilution of logarithmically growing cultures, only the double mutant fails to grow on FOA, indicating that *NUP2* and *NUP60* are synthetically lethal. (b) Expression of a Nup2p mutant lacking the Ran binding domain of Nup2p rescues the genetic interaction observed between *NUP2* and *NUP60*, but conveys a temperature-sensitive phenotype. A plasmid encoding amino acid residues 1 through 546 of Nup2p (pLDB690) was able to partially rescue the genetic interaction observed between *NUP2* and *NUP60*. *Δnup2, Δnup60* cells carrying the pLDB690 plasmid grew slowly at 23 °C, normally at 30 °C but failed to grow at 37 °C. Thus, the RBD of Nup2p performs a function that becomes essential in strains lacking Nup60p.

function of the RBD of Nup2p overlaps with the ability of Nup60p to tether Nup2p to the NPC, a possibility that was investigated by fluorescence microscopy.

We constructed a genomic integration of Nup2ΔRBD-GFP (Nup2p residues 1 through 605 carrying a C-terminal fusion to GFP) and monitored the distribution of this chimera in an otherwise WT background. Indeed, although this mutant contains the minimal domain required for NPC association[163], confocal microscopy revealed that there was a substantial increase in the nuclear proportion of Nup2p in the absence of its RBD (Figure 2-8). These data support a model in which the RBD of Nup2p contributes to its interaction with the NPC, perhaps by modulating its ability to bind to either Nup60p at the nuclear face or another nucleoporin at the cytoplasmic face.

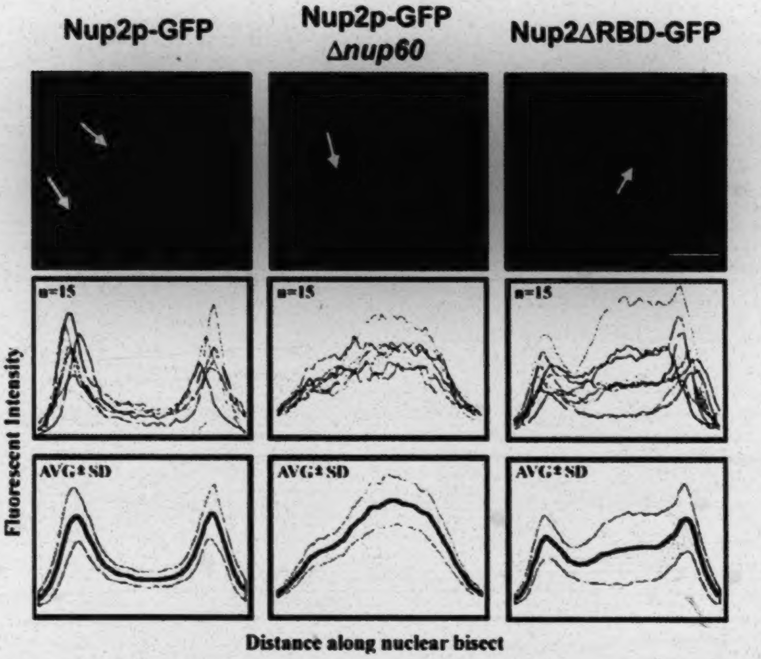

Figure 2-8. The Ran-binding domain of Nup2p is required for its efficient steady state localisation at the NPC. (upper panel) Images of Nup2p-GFP in wild-type and *Δnup60* cells as well as for Nup2ΔRBDp-GFP in an otherwise wild-type background. Representative, focused nuclei are indicated by white arrows. (middle panel) Plots of the fluorescent intensity across a nuclear bisect for fifteen cells each of the strains above. (lower panel) Plots of the mean (thick line) and standard deviation (shaded region) of data presented above. Comparison revealed an increased nuclear signal of Nup2ΔRBDp-GFP relative to Nup2p-GFP. However, relative to Nup2p-GFP in strains lacking Nup60p, there remained a significant portion of Nup2ΔRBDp-GFP present at the nuclear rim.

To further explore the role of Ran in the association of Nup2p with the NPC, we tested if perturbations in the Ran cycle could alter the distribution of Nup2p-GFP *in vivo* by two methods, the results of which are shown in Figure 2-9a. First, cells were metabolically poisoned by treatment with sodium azide and deoxyglucose. Azide/deoxyglucose treatment inhibits nuclear transport by decreasing ATP levels, which, in turn, reduces free GTP and results in a drop in available Ran-GTP[174,175]. In the second method, Ran-GTP pools were depleted by shifting strains harbouring a temperature-sensitive allele of the RanGEF, Prp20p (*prp20-7*)[113] to the non-permissive temperature. The inactivation of Prp20p should result in the breakdown of the Ran gradient due to the inability to efficiently replenish Ran-GTP pools in the nucleus. Interestingly, we observed no effect of these Ran perturbations on the localisation of Nup2p, nor control nups in WT cells; however, when Nup2p-GFP was monitored in a Δ*nup60* background, in which Nup2p is nuclear at steady-state, both conditions led to the return of Nup2p-GFP to the nuclear rim. Thus, it is likely that another site within the NPC serves to dock Nup2p under conditions where Ran-GTP levels are low and/or transport is inactive. Our IEM localisation data suggest that this alternative docking site is at the cytoplasmic face of the NPC and, indeed, when we determined the localisation of Nup2p by IEM in a Δ*nup60* background, Nup2p was found solely on the cytoplasmic face of the NPC (Figure 2-9b). In addition, this likely explains why the localisation Nup2p-GFP appeared unaffected by Ran perturbations in a WT background, as fluorescence microscopy would not detect a relocalisation of Nup2p-GFP from the nuclear to the cytoplasmic face of the NPC.

2.2.5. Nup2p and Nup60p aid in Kap60p recycling

In light of the established role for Nup2p in the efficient Cse1p-mediated export of Kap60p[162,163,168], we investigated a role for Nup60p in this process. The steady-state distribution of Kap60p-GFP was observed in WT cells and derivative strains lacking Nup60p, Nup2p or the control nup, Nup100p (Figure 2-10). As expected, Kap60p-GFP signal was concentrated at the nuclear rim in WT cells and in cells lacking Nup100p but also present in both the cytoplasm and nucleoplasm. On the other hand, Kap60p-GFP shifted to a predominantly nuclear distribution in strains

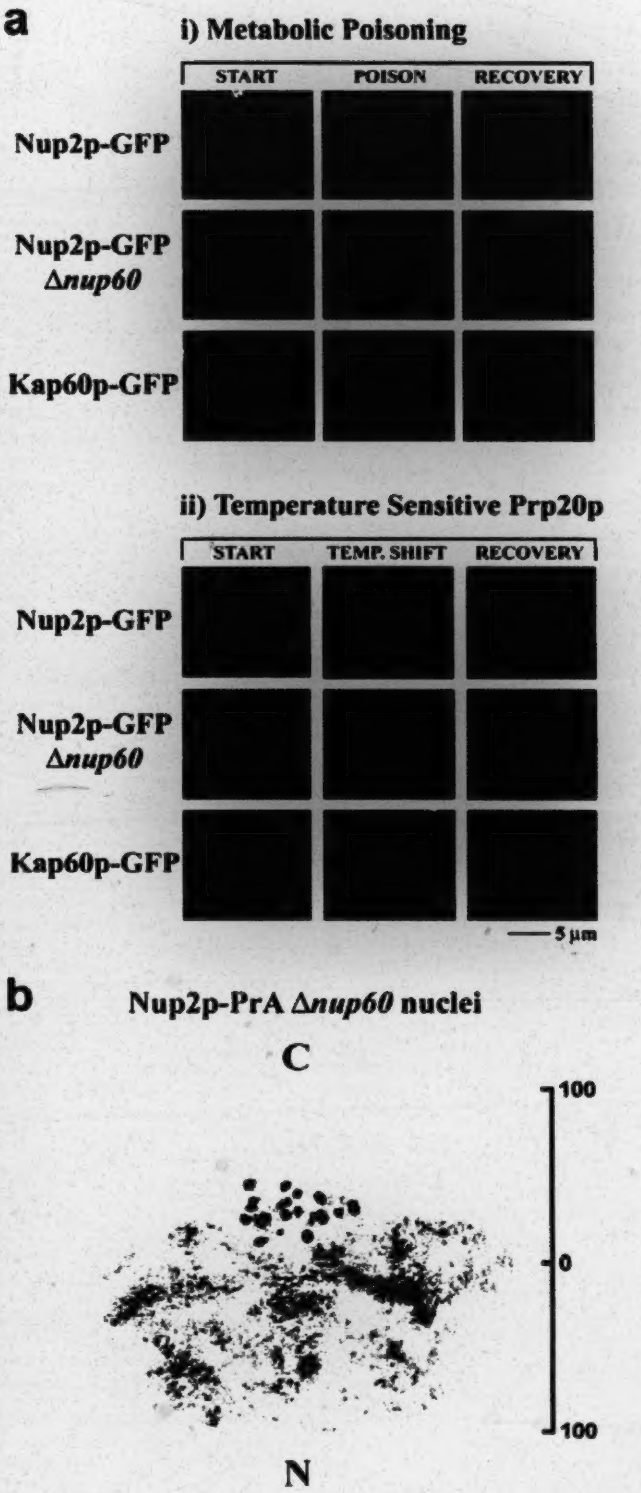
a
i) Metabolic Poisoning
START
POISON
RECOVERY
Nup2p-GFP
Nup2p-GFP
Δnup60
Kap60p-GFP
ii) Temperature Sensitive Prp20p
START
TEMP. SHIFT
RECOVERY
Nup2p-GFP
Nup2p-GFP
Δnup60
Kap60p-GFP
5 µm
b
Nup2p-PrA Δnup60 nuclei
C
100
0
100
N

Figure 2-9. Alterations in the Ran cycle affect the localisation of Nup2p. (a-i) After initial image acquisition (START), the indicated strains were metabolically poisoned by azide/deoxyglucose treatment (POISON). No change in the localisation of Nup2p-GFP was observed. In contrast, Nup2p-GFP accumulated at the nuclear rim in strains lacking Nup60p after a 45 minute poisoning treatment. The localisation of Kap60p-GFP similarly accumulated at the nuclear rim under these conditions. Furthermore, a 10-minute recovery period in glucose-containing media resulted in the return of Nup2p-GFP and Kap60p-GFP to their respective steady-state locales (RECOVERY). (a-ii) Inactivation of the Ran-GTP exchange factor, Prp20p, enhanced binding of Nup2p to alternative sites within the NPC. Nup2p-GFP was expressed in *Δnup60,prp20-7* cells, grown at 23 °C (START) and shifted to 37 °C for 90 minutes (TEMP. SHIFT) and then recovered at room temperature for 60 minutes (RECOVERY). Kap60p-GFP accumulated at the nuclear rim at the non-permissive temperature, indicating a block in nuclear transport. Neither Nup49p-GFP nor Nup2p-GFP in otherwise wild-type cells appeared affected by this treatment; however, Nup2p-GFP signal returned to the nuclear rim, and accumulated in the cytoplasm in a strain lacking Nup60p. This effect was reversible as growth at the permissive temperature partially restored the steady-state nuclear localisation of Nup2p-GFP in the *Δnup60* strain. (b) The alternative NPC docking site of Nup2p is likely at the cytoplasmic face of the NPC. Nup2p-PrA in cells lacking Nup60p was localised by immunoelectron microscopy of purified nuclei. As expected, no signal was detected on the nuclear face of the NPC; however, there remained a pool of Nup2p-PrA that was associated with the NPC on the cytoplasmic face.

lacking Nup2p or Nup60p. However, we do note that the Kap60p export defect in *Δnup60* cells was not as severe as that previously reported for *nup2* null cells[162] as evidenced by the lower nuclear GFP signal in *Δnup60* cells relative to *Δnup2* cells. These data suggest that Nup2p can support limited Kap60p export without interacting with Nup60p at the NPC since Kap60p export is compromised, but not completely abrogated, when Nup2p is unable to interact with Nup60p.

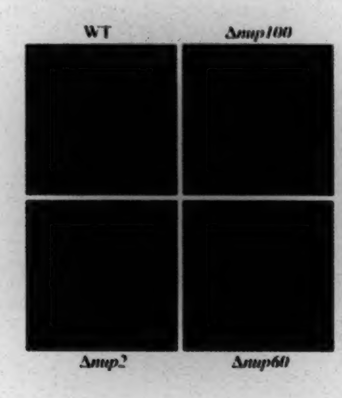

Figure 2-10. Deletion of NUP2 *or* NUP60 *disrupts the ability of Kap60p to bind NPCs and inhibits its recycling to the cytoplasm.* In agreement with previous reports, we observed a nuclear accumulation of Kap60p-GFP in cells lacking Nup2p. This defect was also observed, but was less severe, in strains lacking Nup60p, which suggests that Nup2p docking to Nup60p plays a role in Cse1p-mediated export of Kap60p. The localisation of Kap60p-GFP was unaffected by deletion of *NUP100* indicating that the redistribution observed in cells lacking Nup2p or Nup60p is specific.

Given that loss of *NUP2* has previously been shown to be synthetically lethal with a temperature-sensitive mutation of *KAP60*[162], we tested for a genetic interaction between *NUP60* and *KAP60* to corroborate our findings. In contrast to *Δnup2* cells, *Δnup60* cells were not synthetically lethal with *ts* mutations of *KAP60*, but the double mutant failed to grow at 30 °C, which indicates a genetic interaction (Figure 2-11). This result is in line with the observation that the Kap60p recycling defect was more severe in *Δnup2* cells than in *Δnup60* cells.

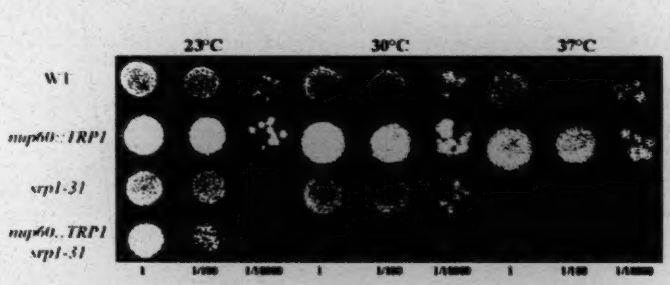

Figure 2-11. NUP60 *and* KAP60 *genetically interact.* To assess any genetic interaction between *NUP60* and *KAP60*, we mated a strain harbouring a temperature-sensitive *KAP60* allele, *srp1-31*, with a *nup60* null strain. Wild-type, single and double mutant spores were isolated and assayed for their ability to grow at 23 °C, 30 °C and 37 °C. At 30 °C, we detected an interaction between *KAP60* and *NUP60*.

2.2.6. A role for Nup2p in other kap transport pathways

We have, thus far, provided evidence that Nup2p transiently associates with the NPC at two distinct sites, the major anchor being Nup60p on the nuclear aspect of the NPC at steady state. Additionally, we have shown that Nup2p, Nup60p, Kap60p and Kap95p form a complex *in vitro* and that cells lacking Nup2p or Nup60p accumulate Kap60p in the nucleus. Together, these data implicate Nup60p and Nup2p in both Kap60p/Kap95p-mediated cNLS import and Cse1p-mediated export of Kap60p, the latter of which has already been shown for Nup2p[162]. These function need not be considered unique given the cyclical nature of nuclear transport reactions. But what about the myriad of other transport pathways? Does Nup2p play a role in these as well? Our initial *in vitro* binding data suggest this is indeed the case. Bacterially expressed and purified Kap104p binds directly to GT-resin coated with GST-Nup2p (Figure 2-12) and the data presented in Table 2-1 support interactions between Nup2p and Kap104p, Kap121p and Kap123p. Presumably, these kaps associate with the FG-repeats found in Nup2p, and this association, in addition to the ability of Nup2p to recruit Ran-GTP, would allow Nup2p to catalyze the termination of import reactions involving these kaps. Nup2p catalyzes the formation of a trimeric complex in the Kap60p recycling pathway (Cse1p, Kap60p and Ran-GTP), but the role that we propose for Nup2p in other transport pathways is only a second order reaction. Thus, it is not surprising that the Kap60p recycling pathway is the sole transport pathway yet shown to exhibit a steady state defect in *Δnup2* cells and further investigation into other transport pathways is merited.

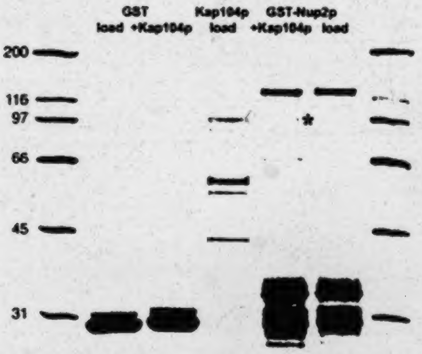

Figure 2-12. Nup2p binds directly to Kap104p in vitro. When challenged with bacterially expressed and purified Kap104p (lane 4), GST-Nup2p-coated glutathione beads captured a Coomassie blue detectable band (lane 5, denoted by *) that corresponded to full length Kap104p. This protein was absent from GST-Nup2p coated beads if Kap104p was not added (lane 6). The protein composition of GST coated glutathione beads remained unchanged before (lane 2) and after (lane 3) incubation with Kap104. Thus, the ability to interact with Kap104p is specific to Nup2p. Lanes 1 and 7 contain molecular weight standards.

Table 2-1 **MS/MS protein identifications supporting a role for Nup2p in additional kap transport pathways**

Nup1p-PrA

ID	P	#
KAP95	***1.00***	***29***
KAP60	***1.00***	***12***
TUB1	1.00	3
HTB1	1.00	2
HTA1	0.85	1
PTC2	1.00	1
RVB2	0.98	1

Nup2p-PrA

ID	P	#
NUP60	1.00	14
KAP60	***1.00***	***14***
KAP95	***1.00***	***9***
RVB2	1.00	8
CDC19	1.00	6
RVB1	1.00	5
KAP123	1.00	4
NUP1	1.00	4
TUB2	1.00	2
YDR071C	0.99	2
ACT1	0.99	1
CBF5	0.96	1
HTB1	0.51	1
RED1	0.59	1
UBIQ	0.99	1
YER139C	0.71	1

Nup49p-PrA

ID	P	#
NIC96	***1.00***	***4***
HTB1	1.00	3
SIK1	1.00	2
KAP60	1.00	2
NSP1	***1.00***	***1***
TUB2	0.84	1

Nup60p-PrA

ID	P	#
NUP2	***1.00***	***17***
KAP95	***1.00***	***16***
KAP60	***1.00***	***11***
HTB1	0.97	1
TPO3	0.87	1

Kap95p-PrA

ID	P	#
NUP2	***1.00***	***14***
KAP60	***1.00***	***13***
NUP1	***1.00***	***9***
NUP60	1.00	7
GSP1	***1.00***	***3***
ULP1	1.00	2
TUB2	0.51	1
YJL200C	0.63	1

Kap104p-PrA

ID	P	#
HRP1	***1.00***	***23***
ENP1	1.00	19
NAB2	***1.00***	***8***
DED1	0.99	1
NSR1	0.98	1
NUP2	0.99	1
RVB1	0.99	1
SNF1	0.99	1
TUB1	0.99	1

Kap121p-PrA

ID	P	#
NUP53	***1.00***	***15***
YGR081C	1.00	9
NUP2	1.00	6
ARX1	1.00	4
RVB1	1.00	4
RVB2	1.00	4
SCS2	1.00	4
ULP1	1.00	4
YDR071C	1.00	4
DBP9	1.00	3
NOP58	1.00	3
TUB1	1.00	3
DED1	0.95	2
KAP123	0.99	2
KAP60	0.99	2
TUB2	0.99	2
KAP95	0.97	1
NIC96	***0.99***	***1***
NSR1	0.99	1
NUP170	***0.99***	***1***
POM34	0.91	1

Kap123p-PrA

ID	P	#
NUP60	1.00	85
NUP2	1.00	47
RVB1	1.00	5
PRP20	1.00	5
KAP60	1.00	5
TUB1	1.00	4
CRP1	0.89	3
HHF1	0.99	3
RVB2	1.00	3
YDR071C	1.00	3
KAP95	0.99	2
DBP2	0.96	1
IST3	0.93	1
NSP1	0.89	1
NSR1	0.98	1
TUB4	0.73	1

Protein identification from direct MS/MS analysis of immunopurification eluates prepared from yeast lysates expressing PrA-tagged Nup1p, Nup2p, Nup49p, Nup60p, Kap95p, Kap104p, Kap121p or Kap123p. ID = protein match; P = probability of correct assignment as determined by ProteinProphet[176,177]); # = total number of peptide hits (includes duplicate hits); ***BOLD ITALICS*** = Coomassie blue observable protein bands; BOLD RED = nucleocytoplasmic transport factors present at levels below Coomassie blue threshold of detection.

2.3. Discussion

2.3.1. Nup2p lies at the boundary between the classical division of nuclear transport components into stationary and soluble phases

The yeast NPC, which comprises the stationary phase of the nucleocytoplasmic transport machinery, contains ~30 nucleoporins, defined by their stable contributions to the overall structure[4]. Nucleoporins, in turn, interact with numerous transport factors that dock transiently to the NPC to mediate the translocation of cargoes across the NE and these kaps, together with Ran and its effectors, constitute the soluble phase of the transport machinery. Based on our observations, Nup2p fits into neither of these categories. By most criteria, Nup2p resembles a typical nucleoporin: it contains FG repeats, exhibits punctate peripheral nuclear rim staining by fluorescence microscopy, genetically interacts with other nucleoporins and is present in biochemical fractions enriched in NPCs. These characteristics, though, are not limited to static components of the NPC and careful examination of the localisation and dynamics of proteins that harbour these attributes has led to novel insights into their functions. For example, because of its concentration at the NPC and its genetic interactions with nucleoporins, the cNLS receptor, Kap60p, was originally characterised as a NPC component[167]. Also Kap123p, a karyopherin responsible for importing ribosomal proteins, was identified as a major protein within the isolated highly enriched NPC fraction, and it too yields punctate peripheral NPC-like staining[56]. However, further characterisation of these and other transport factors has since demonstrated that members of this class of proteins are present in the cytoplasm and nucleoplasm and, thus, their staining patterns reflect an observed dynamic presence at the NPC. Furthermore, Yrb2p, like Nup2p, contains FG repeats and a RBD and was originally classified as a nucleoporin[119]. More detailed examination of Yrb2p determined that it is a soluble nuclear protein, and this information was used to establish a novel role for Yrb2p in NES-mediated export[178,179]. On the other hand, despite its original classification as a nucleoporin, Nup2p was excluded as a *bona fide* nucleoporin based on its failure to enrich with purified NEs and its partial presence in the nucleoplasm and cytosol[4,51,56]. In this study, we focused on answering two fundamental questions: is Nup2p a stable component of the NPC, and, if not, how is its dynamic connection to the NPC mediated?

To answer the first question, we exploited the *kar1-1* mutant to produce yeast heterokaryons and monitored the ability of GFP fusions of Nup2p and control nucleoporins to illuminate the unlabelled NPCs. In this assay, only Nup2p was capable of transferring rapidly to the second nucleus, demonstrating that it is indeed a mobile component of the NPC and is capable of entering the soluble phase of nucleocytoplasmic transport and moving from one NPC to another. Interestingly, however, in these experiments, Nup2p did not move as rapidly as the karyopherins, Kap60p or Cse1p (data not shown). This suggests that Nup2p did not freely equilibrate between the two nuclei in the heterokaryon experiments, rather that it escapes the vicinity of the NPC at a relatively low rate, at which time it is capable of diffusing through the cytoplasm and moving to the recipient NPC.

To address how Nup2p is tethered to the NPC, we immunopurified protein A chimeras and showed that Nup2p binds in a complex with Kap95p and Kap60p, which together interact at the nuclear face of NPC through Nup60p. In support of these *in vitro* binding studies, we showed that deletion of *NUP60* led to a shift of the steady-state localisation of Nup2p from the NPC primarily to the nucleoplasm, but also to a lesser extent to the cytoplasm. In addition, the absence of Nup60p led to a defect in Kap60p export. Others have recently provided evidence that Nup2p interacts directly with Kap60p and acts as a scaffold in the formation of a trimeric export complex between Cse1p, Kap60p and Ran-GTP[162,163,168]. Given the nature of the complex formed, it is likely these reactions occur at the nucleoplasmic side of the NPC. Our results support this model and demonstrate that the previously observed interaction between the amino-terminal region of Nup2p and the NPC[163] is through the nucleoplasmically disposed nucleoporin, Nup60p. Furthermore, genetic and fluorescence microscopy evidence presented here demonstrates that the interaction between Nup2p and Nup60p facilitates, but is not required for, efficient Kap60p export. In addition, because we were able to isolate a complex between Nup60p, Nup2p, Kap60p and Kap95p, it is likely that the Kap60p and NPC binding domains are distinct.

In addition to localising Nup2p to the nuclear side of the NPC and observing a strong interaction between Nup2p and Nup60p, we detected a significant fraction of Nup2p in the nucleoplasm and bound to the cytoplasmic face of the NPC. This observation supports the idea that Nup2p is mobile, shuttling between different sides of the NPC. Nevertheless, it appears that Nup2p binds most avidly to Nup60p in the normal cellular environment. This is based primarily on two pieces of data. First, deletion of *NUP60* causes the majority of Nup2p to lose its interaction with the NPC. Secondly, electron cryomicroscopy of whole fixed cells shows that the majority of Nup2p is localised to the distal nuclear regions of the NPC[163,168]. Therefore, to understand the movement of Nup2p, we asked what conditions promote the movement of Nup2p away from the nuclear face of the NPC.

In light of the central role that Ran plays in conferring the directional movement of transport factors, we deleted the RBD of Nup2p and altered the GTP-bound state of Ran in order to determine if these changes influenced the subcellular distribution of Nup2p. Deletion of the RBD from the carboxy-terminus of Nup2p shifted the equilibrium of Nup2p to the nucleoplasm. Secondly, when *NUP60* was deleted, Nup2p returned to the NPC when ATP or Ran-GTP concentrations were depleted by metabolic poisoning or by mutations of the Ran cycle, respectively. These data suggest that Ran-GTP strengthens the interaction between Nup2p and Nup60p. Furthermore they suggest that Nup2p moves in response to the absence of Ran-GTP, or in association with Ran-GDP, as domains homologous to the RBD of Nup2p bind both nucleotide-bound forms of Ran. This may explain why Nup2p was not found at the cytoplasmic side of the NPC by immunoelectron microscopy of whole cells. In wild type, actively growing cells, a high availability of Ran-GTP would favor Nup2p's interaction with Nup60p, whereas during the isolation of nuclei, Ran-GTP would be depleted, shifting Nup2p's equilibrium, serendipitously allowing us to visualise it at the cytoplasmic face. However, it appears that although the interaction between Nup60p and Nup2p is strengthened by Ran-GTP, Ran-GTP is not required for this binding, because we readily observe this complex by various means *in vitro*.

2.3.2. Nup2p as a scaffold for transport reactions

Nup2p, like many other components of the nucleocytoplasmic transport machinery, is not essential, but increases the efficiency of transport[161-163,168]. It has been previously suggested that nucleoporins asymmetrically positioned on one side of the NPC provide a high-affinity binding site for transport complexes, thereby enhancing the directionality of movement across the NPC[4]. Again, the binding sites provided by these nucleoporins are not essential but increase the efficiency of transport[167,180,181] In the case of the Kap95p/Kap60p/cNLS import complex we believe that the nucleoporin contributing to directional movement through the NPC is Nup1p. This is based on our observations that Nup1p is an asymmetric nuclear disposed nucleoporin[4] and is the most stably bound nucleoporin in Kap95p-PrA immunopurifications (data not shown). Nup2p also binds avidly to Kap95p-PrA, but does so within soluble subcellular fractions[51,56]. Taken together, we suggest that upon import, the Kap95p/Kap60p complex moves preferentially to Nup1p at the nuclear side of the NPC. Once bound to this site, efficient transport is maintained by transferring the complex to the mobile factor Nup2p, which can enter the nucleoplasm. The constant removal of Kap60p and Kap95p from Nup1p by Nup2p would enhance transport by removing the products of the transport reaction away from the NPC. Kap95p, and perhaps cargo, would be released from Nup2p by the transfer of Ran-GTP to Kap95p. This transfer may also be facilitated by the ability of Nup2p to interact simultaneously with both Kap95p and Ran-GTP. Kap60p would remain bound to Nup2p, and the Kap60p/Cse1p/Ran-GTP export complex would form on Nup2p, and this complex may then return to the NPC, perhaps by binding to Nup60p. In this way, in addition to relieving congestion at NPCs, Nup2p can further facilitate transport by catalyzing the formation of transport complexes.

It is also possible that the mobility of Nup2p plays a more direct role in the Ran cycle and transport. Although the asymmetric distribution of Ran-GTP and Ran-GDP is central to current models of transport, it remains unknown to what extent Ran is active in the NPC itself, and to what extent it modulates individual reactions between transport factors and individual nucleoporins. Recent results demonstrate that the mammalian orthologue of Prp20p, RCC1, while thought to be restricted to the nucleus, is also present on the cytoplasmic surface of the NPC[182]. Furthermore, Rna1p is not restricted to the cytoplasm, as it is observed in the nucleoplasm in yeast[183]. In addition, RanBP1, a protein proposed to augment Rna1p's Ran-GAP activity in the cytoplasm, also shuttles between the nucleus and cytoplasm[165]. Thus, although it is virtually certain that there exists a steep Ran-GDP versus Ran-GTP gradient across the NE, modifiers of the nucleotide-bound state of Ran exist on both sides of the NPC. Given that Nup2p exhibits genetic interactions with Prp20p[162], perhaps Nup2p is involved in the regulation of Ran in the vicinity of the NPC.

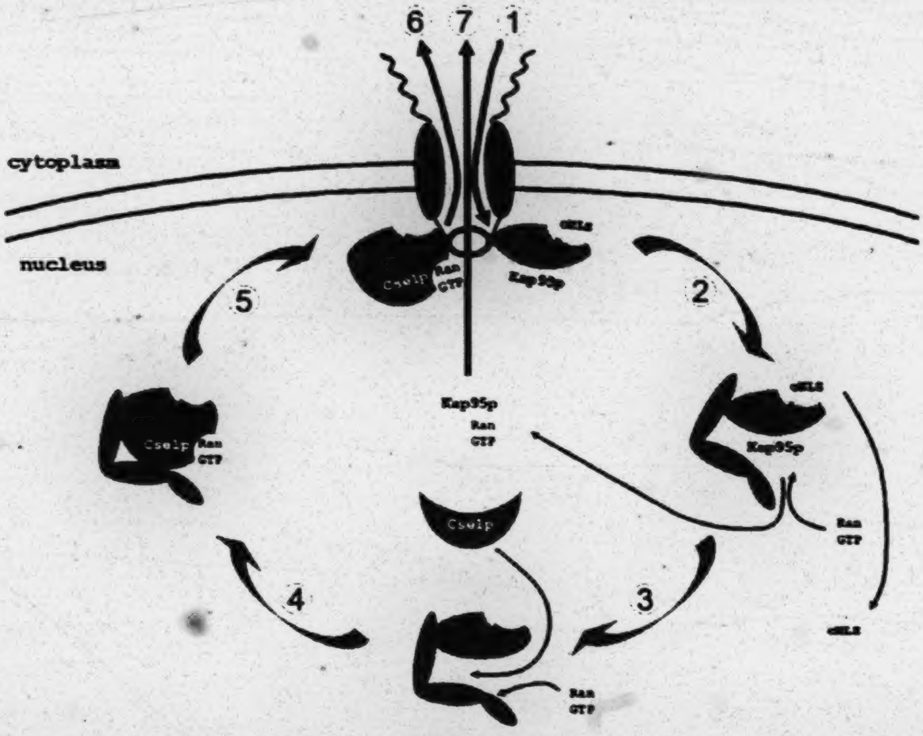

Figure 2-13. Model of the role of Nup2p in nucleocytoplasmic transport events inside the nucleus. Nup2p likely facilitates transport in two ways. First, by acting as a scaffold for the formation and dissociation of transport complexes, and, second, by performing these functions away from NPCs, thereby relieving congestion at these highly trafficked sites. ① A Kap95p/Kap60p/cNLS complex reaches the nuclear basket of the NPC likely through the association of Kap95p with a high-affinity binding site on Nup1p. ② The import complex dissociates into the nucleoplasm on the mobile scaffold provided by Nup2p. ③ The Nup2p RBD recruits Ran-GTP, which terminally dissociates the import complex, releasing Kap95p/Ran-GTP and the cNLS cargo from Nup2p. ④ Nup2p then recruits Cse1p and Ran-GTP to the Nup2p/Kap60p complex to promote the formation of a Cse1p/Kap60p/Ran-GTP export complex. ⑤ The increase in the affinity of Nup2p for Nup60p by the presence of Ran-GTP promotes the movement of the Nup2p/Cse1p/Kap60p/Ran-GTP intermediate to the NPC. The Cse1p export complex is then able to leave the nucleus (⑥), completing the recycling of Kap60p, as is the Kap95p/Ran-GTP complex (⑦) that was released in step ③.

2.3.3. The cytoplasmic function of Nup2p

At this time, we have not elucidated a role for Nup2p in the cytoplasm. In mammalian cells, Ran binds to nucleoporins present on both the cytoplasmic and nucleoplasmic faces of the NPC. As none of the yeast nucleoporins contain RBDs, the cytoplasmically disposed Nup2p may perform functions analogous to the cytoplasmic mammalian nucleoporin, Nup358. Nup358 binds Ran-GDP and Ran-GTP through its multiple RBDs, whereas a separate Zn-finger motif binds to Ran-GDP[184]. Like Nup2p, Nup358 also contains FG repeats for binding to karyopherins and has been proposed to act at the cytoplasmic face as a molecular scaffold for the recycling of the Kap95p orthologue, Kapβ, by coordinating Ran-GTP hydrolysis with the termination and re-initiation of each transport cycle[185]. In support, we have detected a direct *in vitro* interaction between Nup2p and the Ran GTPase, Rna1p (data not shown).

2.3.4. Nup2p in higher eukaryotes?

Interestingly, a potential mammalian orthologue of Nup2p has recently been characterised. Nup50, originally termed Npap60, contains a Ran binding domain, FG repeats and localises to the nuclear face of the NPC[171,186,187]. The localisation of Nup50 to the region near Nup153 by IEM and *in vitro* binding data suggest that Nup153 may perform a function similar to the role of Nup60p in yeast by docking Nup50 at the NPC[187]. Like Nup2p, Nup50 exhibits many characteristics not typical of *bona fide* nucleoporins, such as fixation-dependent localisation by immunofluorescence and variable expression and localisation at different stages of the cell cycle and in different cell types[171,187]. It will be interesting to see if this potential Nup2p orthologue is also a mobile nucleoporin that cycles on and off the NPC in a Ran-dependent manner.

2.3.5. Subsequent corroborating evidence

The work described in this section provided key evidence of a novel class of transiently NPC-associated nups. In the time since these studies were performed, many of the conclusions drawn have been upheld, including the existence of this class of mobile nup[188], which includes Nup50. Indeed, Nup50p appears to be the mammalian orthologue of Nup2p, functioning in the these cells similar to Nup2p in yeast[35]. In addition, others have reported on the mobile characteristics of Nup2p[189], the identification of Nup60p as the steady-state NPC anchor for Nup2p[14], the presence of Nup2p at multiple sites within the NPC[189,190] and the ability of Nup2p to act as a scaffold to catalyze transport reactions[191,192].

2.3.6. Extending transport past NPCs – intranuclear targeting

It remains unclear to what extent Nup2p functions in the cytoplasm or in the nuclear interior. The ability of Nup2p to associate at multiple sites within NPCs through Kap60p/Kap95p complexes and also to enter the nucleoplasm and cytoplasm, together, provide evidence that Nup2p may chaperone import complexes, not only as they traverse NPCs but potentially to sites distant from these structures[14,190,193]. With respect to nuclear import, an attractive model is that Nup2p targets import complexes to regions of chromatin where it then catalyzes the release of cargo. Although speculative, this would allow cells to activate or repress specific regions of the genome through selective cargo deposition. One possible mechanism is through the RanGEF, Prp20p, which can bind to Nup2p, as detailed in the following section, is predominantly associated with chromatin and, where bound, exhibits an increase in its GEF activity[194-197]. Thus, the association of Nup2p with Prp20p on chromatin might act to enhance the ability of Nup2p to catalyze/scaffold transport reactions in these regions, due to the local production of Ran-GTP, thereby providing a means of targeted cargo release. Interestingly, the following section describes a novel function of Nup2p in the organisation of chromatin within the nucleus that may operate by a related mechanism that involves Prp20p.

3. NUP2P AND THE EPIGENETIC MAINTENANCE OF TRANSCRIPTION STATES

3.1. Overview - Nup2p possesses boundary activity

The boundary trap assay identified Nup2p as a key player in NPC-dependent boundary activity[2] but, given the data presented in the previous section indicating that Nup2p is a mobile nup[14,193], the original model of BA proposed by Ishii *et al.* must be revised. That is, because their model incorporates a static mechanism of DNA anchoring to the NPC (see Figure 1-4), it cannot be resolved with the transient nature of the association of Nup2p with the NPC. In fact, the observation that only Nup2p, among yeast nups, is capable of mediating BA suggests that BA is abrogated by stable NPC-association. Therefore, we set out to determine if there exists an endogenous mechanism of NPC-dependent BA in yeast and to uncover the role of Nup2p in this activity. To these ends, we carried out proteomic, transcriptomic and genetic analyses, the data from which implicate Nup2p in the maintenance of gene expression states and reveal that endogenous Nup2p-dependent BA is mediated by the interaction of Nup2p with chromatin-associated Prp20p. This protein interaction provides a mechanism to physically link NPCs with chromatin, possibly coupling this activity to nuclear transport reactions. Interestingly, the nucleoporin responsible for anchoring Nup2p to the nuclear face of the NPC, Nup60p, plays important roles in Nup2p-dependent BA. Given the mobile characteristics of Nup2p, we propose a dynamic mechanism of NPC-mediated boundary function whereby Nup2p facilitates the movement of chromatin to the NPC, which functions as a nexus between the transcriptionally active nuclear interior and the silenced periphery.

3.2. Results

3.2.1. Prp20p is a potential chromatin anchor for Nup2p

NPC-mediated BA is mediated by Nup2p or proteins that interact with Nup2p[2]. This implies that a physical connection exists between Nup2p (or Nup2p-associated proteins) and DNA. However, we find that Nup2p does not strongly bind to DNA when purified from yeast whole cell lysates (data not shown). Rather, we and others have reported that Nup2p interacts primarily with Nup60p and the karyopherins, Kap60p and Kap95p[14,193]. While these data emphasise the important function of Nup2p in cNLS import, and Kap60p recycling, and demonstrate that Nup2p binds to the NPC through Nup60p, they do not provide insight into the unique functions of Nup2p with respect to its BA. In Chapter 2, Nup2p was shown to be a mobile nup, suggesting that its function is not limited to the NPC. We, therefore, sought to identify additional interacting proteins that might shed light on these functions. An attractive candidate is the Ran-nucleotide exchange factor, Prp20p, because it has been reported to interact with Nup2p[14], binds avidly to nucleosomal DNA when immunopurified from whole cell lysates (Figure 3-1a) and is thought to be involved in the organisation of the nucleus[198]. Curiously, using similar *in vitro* methods

Figure 3-1. Prp20p and Nup2p associate with each other and immunopurify with chromatin remodeling factors. (a) Prp20p is nucleosome-associated. *left* Prp20p-PrA was immunopurified from yeast whole cell lysates and abundantly co-purifying proteins were identified by mass spectrometric analysis of excised gel slices. All the components of the histone octamer, H2A, H2B, H3 and H4, were present as well as the linker histone, H1 and Ran/Gsp1p. The presence of Mgm101p was likely due to a non-specific interaction, as this protein has been identified as a component of several other complexes by high-throughput methods[5]. *right* Prp20p-PrA eluates contain DNA. Eluates were resolved by agarose gel electrophoresis and visualised by ethidium bromide staining. Prp20p-PrA associated DNA is ~600 bp long due to chromatin shearing during the cell lysis procedures. This DNA underwent partial digestion when treated with micrococcal nuclease and complete digestion by treatment with DNAseI, indicative of nucleosome associated DNA. (b) The interaction between Nup2p and the Prp20p-nucleosome complex can be reconstituted *in vitro*. *upper* Bacterially expressed and purified Prp20p was incubated with GST or GST-Nup2p that was previously bound to glutathione resin, revealing a direct association between Nup2p and Prp20p. Bound and unbound Prp20p were visualised by Coomassie blue staining of SDS-PAGE resolved proteins. *middle* The Prp20p-nucleosome complex was bound to IgG-coated magnetic beads and then incubated with GST-CFP, GST-Nup2p-CFP or GST-Nup2p. Probing with αGST revealed that although GST alone could not bind to the Prp20p-nucleosome complex, chimeras containing Nup2p bound efficiently (asterisks). The arrows indicate non-specific αGST reactive proteins. *lower.* Glutathione resin coated with GST-Nup2p, but not GST alone, was able to capture Prp20p-PrA from yeast extracts, in which the majority of Prp20p is nucleosome-associated. (c) Diagram depicting interactions between the NPC and chromatin. Proteins present at Coomassie blue detectable levels in Nup2p, Nup60p and/or Prp20p immunopurifications are connected by solid black lines, while other known physical and yeast two-hybrid interactions are shown by dotted and dashed lines respectively[8,14-16]. To identify less abundant proteins, we performed high-coverage tandem mass spectrometry on unresolved immunopurification eluates for Nup2p, Prp20p and Nup60p, as well as Kap95p and Nup49p to determine specificity. The inset list (Eluate MS/MS) shows proteins present exclusively in Nup2p (*top*) or Prp20p (*bottom*) eluates and those present in both (*middle*). Three proteins present in both Nup2p and Prp20p eluates (Act1p, Rvb1p and Rvb2p) and several proteins specifically to Prp20p (Itc1p, Isw2p, Rsc8p, Htz1p and Spt16p) participate in chromatin remodeling functions. Gsp2p, a Ran variant that, like Nup2p, harbours boundary activity, was also found solely in Prp20p eluates. (d) Nucleosomes associated with Prp20p and Htz1p possess unique acetylation patterns suggestive of boundary chromatin. The acetylation levels of residues K5, K8, K12 and K16 of histone H4 were quantified by mass spectrometry for global (white), Prp20p-associated (dark grey) and Htz1p-associated (light grey) nucleosomes.

involving bacterially expressed and purified proteins, one group has reported that full length Nup2p and Prp20p bind directly to one another[14], while another reported they do not[168]. In both cases, the data were not shown. Thus, in order to clarify this potentially critical link between the NPC and chromatin, we examined this interaction using three experimental approaches that are summarised in Figure 3-1b. In the first, we used recombinant Prp20p and Nup2p in a solution binding assay, establishing that these proteins do indeed interact directly *in vitro*. In the second approach, we utilised Prp20p-PrA whole cell lysates to immobilise the Prp20p-nucleosome complex on beads then added bacterially expressed and purified Nup2p. The presence of Nup2p in the bound fractions suggests that Nup2p can

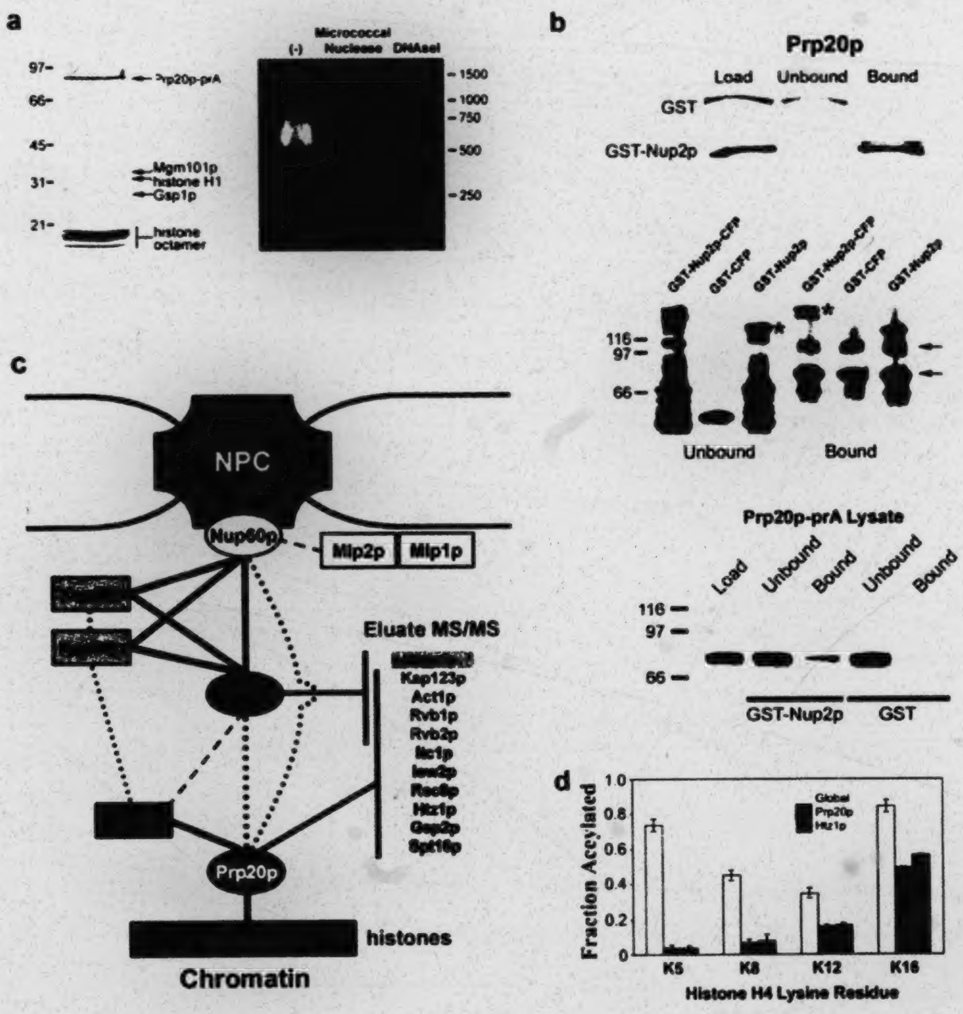

interact with Prp20p in the context of chromatin. Third, beads coated with GST-Nup2p, but not GST alone, were able to capture Prp20p-PrA from yeast whole cell extracts. When these data are combined with previously published physical and genetic interactions involving Nup2p, Nup60p and Prp20p[8,14-16], they suggest that the Nup2p-Prp20p interaction can provide the link between the NPC and chromatin (Figure 3-1c).

We performed high-coverage tandem mass spectrometry on trypsin-digested immunopurification eluates of Nup2p, Prp20p and Nup60p, as well as Kap95p and Nup49p to ensure specificity. This approach does not depend on Coomassie blue visualisation and is, therefore, capable of identifying proteins present at low (substoichiometric) levels. Relevant proteins found specifically in Nup2p eluates, Prp20p eluates or those present in both of these but absent in Nup60p, Kap95p and Nup49p eluates are shown in the inset in Figure 3-1c. The increase in sensitivity afforded by this technique is underscored by the identification of Nup1p in Nup2p eluates (see Table 2-1), although we did not detect Nup1p in these samples by Coomassie blue staining. Nup1p functions in cNLS import and, thus, might participate in some complexes involving Nup2p. In addition, two proteins, Dbp9p and Arx1p, were identified specifically in Kap121p eluates, and these proteins are Kap121p substrates (unpublished data). In support of the association of Nup2p and Prp20p with chromatin, both Prp20p and Nup2p baits yielded Rvb1p, Rvb2p and Act1p, which are components of several DNA remodeling complexes, including the recently identified SWR-C complex[199]. Several additional proteins involved in chromatin remodeling were detected specifically with Prp20p. Among these, the histone 2A variant, Htz1p, has been shown to be recruited to chromatin by the SWR-C complex and is believed to act as a boundary factor in yeast[200,201]. Prp20p also immunopurified with peptides corresponding to Gsp2p, the non-essential Ran homologue that has been implicated in boundary activity[2].

3.2.2. Prp20p associates with atypically modified histones and proteins involved in chromatin remodeling

Active and silent chromatin are associated with nucleosomes that exhibit unique acetylation and methylation patterns at key histone residues, and these can be quantified by mass spectrometry[202]. The data above suggest that Prp20p binds to chromatin regions subject to remodeling. Therefore, we investigated the histone modifications present in Prp20p-associated nucleosomes and also nucleosomes containing Htz1p as indicators of the chromatin environment bound by these proteins. Hypoacetylation at lysine residues on histone H4 (K5, K8, K12 and K16) correlate with silent DNA[203], as does hypomethylation at residue K79 on histone H3[204]. We immunopurified Htz1p and Prp20p from yeast whole cells extracts as above, except that the procedure was carried out in the presence of butyric acid to inhibit deacetylation. Relative to bulk histones, we found that nucleosomes associated with Prp20p were hypoacetylated on histone H4, suggestive of heterochromatin (Figure 3-1d). In contrast, we observed a high level of methylation at residue K79 on histone H3 (~80 % cumulative mono-, di- and tri-methylated at K79, data not shown), which is a marker of active DNA. This mixed phenotype, characteristic of neither silent nor active DNA, is consistent with Prp20p and Htz1p binding to DNA regions near chromosome boundaries. These data agree with the observed association of Prp20p with proteins known to be involved in chromatin remodeling and supports the premise that Htz1p and Prp20p bind to similar DNA regions. In addition, these results are highly similar to those obtained for Dpb4p[205], a protein involved in boundary maintenance[206], further supporting a role for Prp20p in providing the link between Nup2p and DNA boundary regions.

3.2.3. Genetic interactions support a link between ***NUP2*, *NUP60*, *PRP20*** and ***HTZ1***

NUP2 has previously been shown to interact genetically with *PRP20* and *NUP60*[162,193]. Given the physical links between Nup2p, Prp20p and Htz1p, we tested for genetic interactions between the genes that encode these proteins. The growth rates of strains harbouring single and double mutant combinations of *NUP2*, *NUP60*, *PRP20* and *HTZ1* at various temperatures were tested. *NUP53*, an unrelated nucleoporin that functions in Kap121p-mediated transport[104] was included in these studies as a negative control. As shown in Figure 3-2, the temperature-sensitive allele of *PRP20*, *prp20-7*, conferred increased sensitivity when combined with null mutations of *NUP2*, *NUP60* or *HTZ1*, as these double mutant strains, but not *NUP53* double mutants, grew poorly at 30 °C. In addition, we detected *HTZ1-NUP2* and *HTZ1-NUP60* genetic interactions, while again, no effect was observed for combinations involving deletion of *NUP53*, which functionally links Htz1p with components of Nup2p-dependant BA.

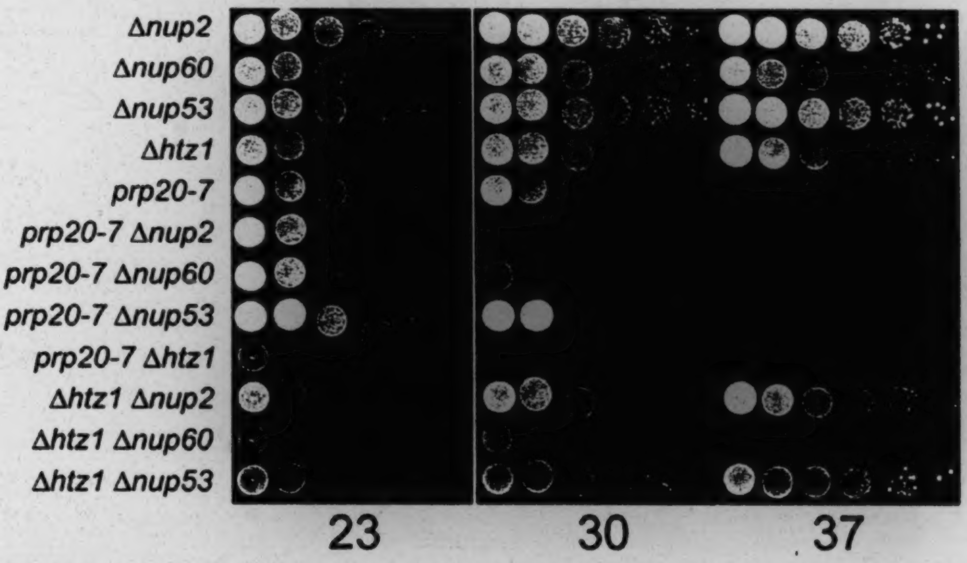

Figure 3-2. Genetic interactions between NUP2, NUP60, PRP20 *and* HTZ1. Growth rate analysis of *Δhtz1*, *Δnup2*, *Δnup60*, *Δnu*p53 and *prp20-7* single mutant and relevant double-mutant strains at 23 °C, 30 °C and 37 °C. Double mutant *Δhtz1 prp20-7*, *Δhtz1 Δnup2*, *Δhtz1 Δnup60*, *prp20-7 Δnup2* and *prp20-7 Δnup60* strains all exhibited more severe growth defects than those detected in their parental strains, while double mutant combinations involving deletion of *NUP53* revealed no genetic interactions.

3.2.4. Prp20p harbours boundary activity that is affected but not lost in cells lacking Nup2p, Nup60p or the Mlp proteins

The data above led us to hypothesise that Nup2p boundary activity is mediated by its interaction on the one hand with Nup60p at the NPC, and on the other hand with Prp20p on chromatin. To test this, we examined if Nup2p-mediated BA was dependent on NPC association, and whether Prp20p possesses its own boundary activity. As a formal test for boundary function, we used the boundary trap assay (kind gift of UK Laemmli)[2]. The results are summarised in Figure 3-3. In this assay, described in Figure 1-4, the *URA3* and *ADE2* genes are placed in a silenced region of DNA and *ADE2* is flanked by sequences that bind Gal4p. Boundary activity, such as that exhibited by the positive control *Drosophila* protein BEAF, is detected by the ability of chimaeras, consisting of the proteins of interest and the DNA binding domain of Gal4p (Gbd), to selectively activate the expression of the *ADE2* marker, while maintaining *URA3* in an OFF state[2]. We observed that the boundary activity of Nup2p (and Cse1p) was indeed dependent on its ability to bind to the NPC through Nup60p (Figure 3-3). As deletion of *NUP60* is not significantly deleterious to cell growth or nuclear transport, but does cause a misolocalisation of Nup2p to the nucleoplasm, these data are in agreement with the original model for Nup2p-mediated boundary activity proposed by Ishii *et al.*[2].

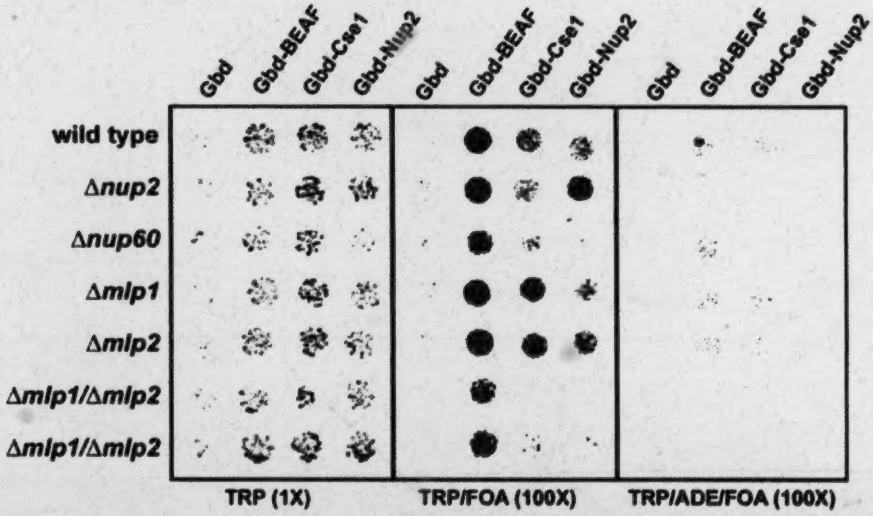

Figure 3-3. The ability of Nup2p to transiently associate with Nup60p at the nuclear face of the NPC is important for BA. The boundary trap strain, KIY54, and isogenic *Δnup2*, *Δnup60*, *Δmlp1*, *Δmlp2* and *Δmlp1*/*Δmlp2* derivatives expressing plasmids encoding the Gal4 DNA binding domain alone, Gbd (pGBC11) or fused to the C-terminal portion of the *Drosophila* BEAF protein, Gbd-BEAF (pGBC11-BEAF-C), a GFP-tagged portion of Cse1p, Gbd-Cse1p (pGBC11-CSE1[474-960]-GFP) or full-length Nup2p, Gbd-Nup2p (pGBC12-NUP2[1-720]) were serially spotted onto CSM-TRP (TRP), CSM-TRP+FOA (TRP/FOA) and CSM-TRP-ADE+FOA (TRP/ADE/FOA) to assess boundary function. Strains were serially spotted and representative dilutions are shown. The relative number of cells spotted for each media type is indicated by the multiplication factor; thus, a hundred-fold more cells were spotted on TRP/FOA and TRP/ADE/FOA relative to TRP. As expected, cells lacking Nup60p were defective in their ability to silence the *URA3* reporter, indicated by a reduced viability on media containing 5-FOA. This phenotype was also shared by two independently isolated double mutant strains lacking the both of the Mlp proteins, but the severity of the defect was variable in this strain background. Boundary activity was indicated by growth on media lacking adenine and containing 5-FOA (TRP/ADE/FOA) as only cells able to silence *URA3* while maintaining the expression of the adjacently encoded *ADE2* reporter were viable on this media. As expected, a plasmid encoding only Gbd failed to elicit BA and the positive control fusion, Gbd-BEAF, exhibited BA in all genotypes tested. The BA of Gbd-Cse1p was dependent on Nup2p, as previously published by Ishii *et al.* (2002) and we also observed complete loss of BA for both Gbd-Cse1p and Gbd-Nup2p in *Δnup60* mutants. Double mutant *Δmlp1*/*Δmlp2* strains exhibited reduced BA, but this defect was partially penetrant (not shown, see also Figure 3-4).

Prp20p also elicited BA at frequencies comparable to those of Gbd-Nup2p and Gbd-Cse1p (Figure 3-4a, compare to Figure 3-3; see also (232)). In addition, full activity required Nup2p (and Nup60p) suggesting that Prp20p boundary activity involves binding to Nup2p at the NPC. It should be noted, however, that a low amount of BA was still detected for Gbd-Prp20p in the absence of Nup2p, which we interpret as a reflection of the ability of Prp20p to bind to multiple components of the nucleocytoplasmic machinery, including Nup60p[14], Nup1p[207], Crm1p/Xpo1p/Kap124[179], Srp1p/Kap60p[168], Ran/Gsp1p[208] and Yrb1p[209], which offer alternative, albeit less efficient, means of association with the NPC. In further support of the pivotal role of Nup2p in BA reported by Ishii *et al.* and observed here, neither Nup60p nor Htz1p was active in the boundary trap assay (data not shown), indicating that the ability to bind to Prp20p is not sufficient to confer BA and confirming the observation that boundary activity is not a general feature of nups[2]

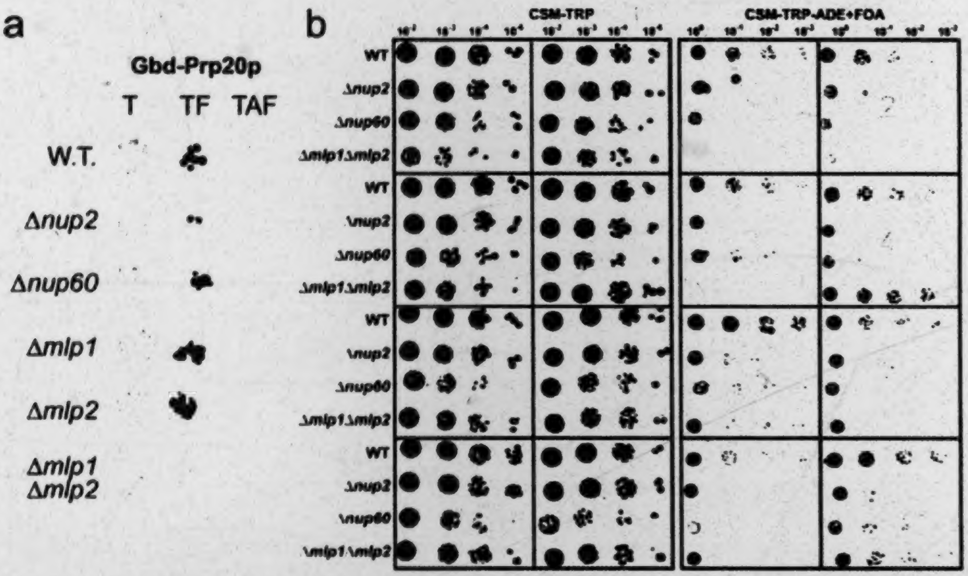

Figure 3-4. Prp20p exerts BA that exhibits partially penetrant defects upon loss of Nup2p, Nup60p or both of the Mlp proteins. (a) Gdb-Prp20p imparted BA in wild-type and single Mlp mutant strains at frequencies comparable to other transport factors (Figure 3-3 and (2)) but deletion of *NUP2* or *NUP60* or both *MLP1* and *MLP2* resulted in dramatically reduced Gbd-Prp20p boundary activity. (b) The defects observed in Gbd-Prp20p were partially penetrant as exhibited by replicate serial spotting experiments.

In light of the evidence linking Nup60p with Mlp-dependent silencing, we also investigated the requirement of Mlp1p and Mlp2p for boundary activity. While single *MLP1* or *MLP2* null mutants showed no effect on BA, we observed a significant decrease in the BA of Gbd-Cse1p, Gbd-Nup2p and Gbd-Prp20p in *mlp* double mutant strains (Figures 3-3 and 3-4), suggesting that while not essential for BA, as noted by Ishii *et al.*[2], the integrity of the Mlp structure associated with the distal regions of NPC is an important for full function. However, it must be noted that the *Δmlp1Δmlp2* defect was only partially penetrant, as these double mutant strains occasionally exhibited BA at near wild-type levels (Figure 3-4b).

3.2.5. Cells lacking Nup2p exhibit transcriptional activation of ORFs encoded in subtelomeric regions

The physical connections between Nup2p, Prp20p, chromatin modifying proteins and atypically modified nucleosomes suggest that Nup2p can act as an endogenous boundary factor. We therefore predicted that boundaries in *Δnup2* cells would not be stably maintained, and these cells would exhibit unique transcriptional profiles relative to their wild-type counterparts. To test this hypothesis, we determined the global steady-state mRNA levels in logarithmically growing wild-type and *nup2* null cells using DNA microarrays (representing 6,271 yeast ORFs)[210,211] and analyzed the chromosomal locations of the top 5 % (313) most significantly induced (123) or repressed (190) ORFs in *nup2* null cells. These experiments revealed a striking bias of *Δnup2* induced ORFs to subtelomeric regions, while repressed ORFs tended to be localised to intrachromosomal regions (Figure 3-5). This pattern suggests a steady-state alleviation of telomeric repression and an increase in repression at other chromatin regions in cells lacking Nup2p.

Interestingly, a similar telomeric bias was observed in cells lacking Htz1p[200,212], except that in *Δhtz1* cells, the pattern was reversed, with repressed genes enriching at telomeric regions. As Htz1p aids in the spread of activation along chromatin[201], these data suggest that Nup2p plays an opposite role, either by promoting repression or antagonising activation. The reciprocal nature of the transcriptional profiles of *Δnup2* and *Δhtz1* cells suggests that the bias of induced ORFs to telomeric regions is a consequence of a role for Nup2p in chromatin dynamics, rather than a manifestation of the known nucleocytoplasmic transport defects present in *Δnup2* cells[162,168]. We note that for the majority of ORFs that were significantly altered in their expression, the magnitude of change was often less than two-fold, which is expected if Nup2p is involved in boundary maintenance rather than required for the formation of boundaries. That is, if cells lacking Nup2p can form, but not efficiently maintain, chromatin boundaries, then we would predict that only a subset of cells in a given *Δnup2* population would experience a stochastic breakdown of boundaries in subtelomeric regions, leading to the slight overall increase in telomeric gene expression of the population as a whole.

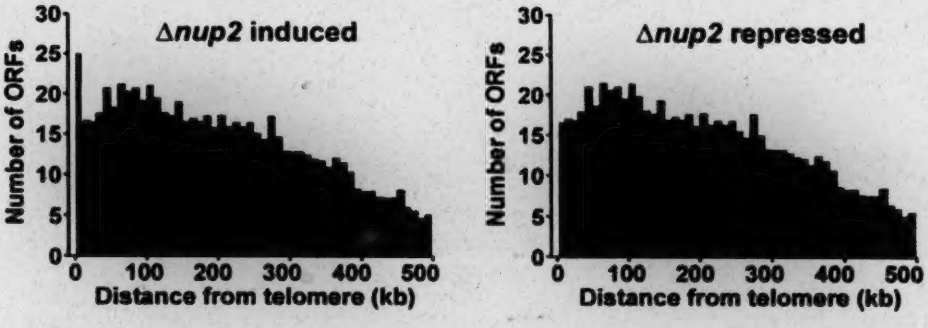

Figure 3-5. ORFs induced in Δnup2 *cells are biased to subtelomeric regions.* For the top 5 % of significant *Δnup2* induced or repressed ORFs, the distance from each ORF to the nearest telomere was determined. These distances were grouped into 10 kb bins and plotted as a function of telomeric distance (i.e. bin1 contains all ORFs between 1 and 10 kb from the nearest telomere, bin2 10 to 20 kb and so on). These plots revealed a striking enrichment of *Δnup2* induced ORFs at telomeric regions as 25 % of induced ORFs were found within 20 kb of a chromosome end, whereas repressed ORFs were internally situated, exhibiting only 1 % of significantly affected ORFs within this distance. For comparison, the red shaded histograms indicate the distribution of telomeric distances for all ORFs plotted at 1/8th scale on the y-axis. Statistical comparison of the *Δnup2* induced and repressed distributions to the profile for all ORFs using a two-sample Kolmogorov-Smirnov test confirmed that the induced profile was unique (p = 0.0000386) but the repressed profile was not (p = 0.287).

3.2.6. Nup2p and Prp20p bind to subtelomeric regions of chromatin

To further examine the role of Prp20p in endogenous NPC-mediated BA, we performed chromatin immunopurification microarray analyses (ChIP-CHIPs) using myc-epitope tagged Prp20p and microarrays containing 6,081 yeast intergenic regions[213]. These experiments allowed us to identify the DNA regions that are most highly associated with Prp20p in logarithmically growing cells. Like the telomeric bias of induced ORFs observed in expression microarrays of *Δnup2* cells, the top 5 % of Prp20p-enriched intergenic regions (304 targets) clustered together and enriched near telomeres (Figure 3-6a, compare to Figure 3-5). Because the "ChIP-

CHIP" procedure involves cross-linking proteins to DNA followed by PCR amplification of bait-associated DNA fragments, we were able to perform these experiments with myc-tagged Nup2p despite the inability of this protein to stably associate with DNA during standard immunopurification procedures (Nup2p-myc yielded ~50-fold less DNA than Prp20p-myc as determined by SyBr green fluorimetry, data not shown). Strikingly, we found that immunopurification of Nup2p, like Prp20p, significantly enriched for regions near telomeres (Figure 3-6a) but such a distribution was not observed with the numerous transcription factors we have investigated (data not shown).

When the Nup2p and Prp20p ChIP-CHIP data sets were compared, there was a 16 % exact match correlation (48 out of 304) for the top 5 % most significantly enriched intergenic regions. The probability of this overlap occurring by chance alone is 3.1 X 10^{-13} (calculated by hypergeometric distribution analysis)[210], which supports the data presented above indicating that Nup2p and Prp20p aid in defining boundaries and further suggests that as a complex these proteins share some chromatin binding sites. The lack of complete overlap between the two data sets is also expected because these proteins are not constitutively complexed.

To test for a correlation between *Δnup2* mRNA expression microarrays and results from ChIP-CHIP studies, we calculated the chromosomal distance between each Nup2p or Prp20p ChIP-CHIP enriched intergenic region and the closest *Δnup2* induced or repressed ORF. Relative to another laboratory member's ChIP-CHIP results using an unrelated control protein, Oaf1p, and randomised data sets, Nup2 and Prp20p ChIP-CHIP enriched intergenic sites lie in close proximity to *Δnup2* induced ORFs (Figure 3-6b), while comparisons made to *Δnup2* repressed ORFs did not reveal a bias towards close proximity (not shown). Indeed when the chromosomal location of significant data from the *Δnup2* expression and ChIP-CHIP microarrays were plotted (Figure 3-6c), there appeared to be data-rich regions of chromosomes that might represent chromatin boundaries.

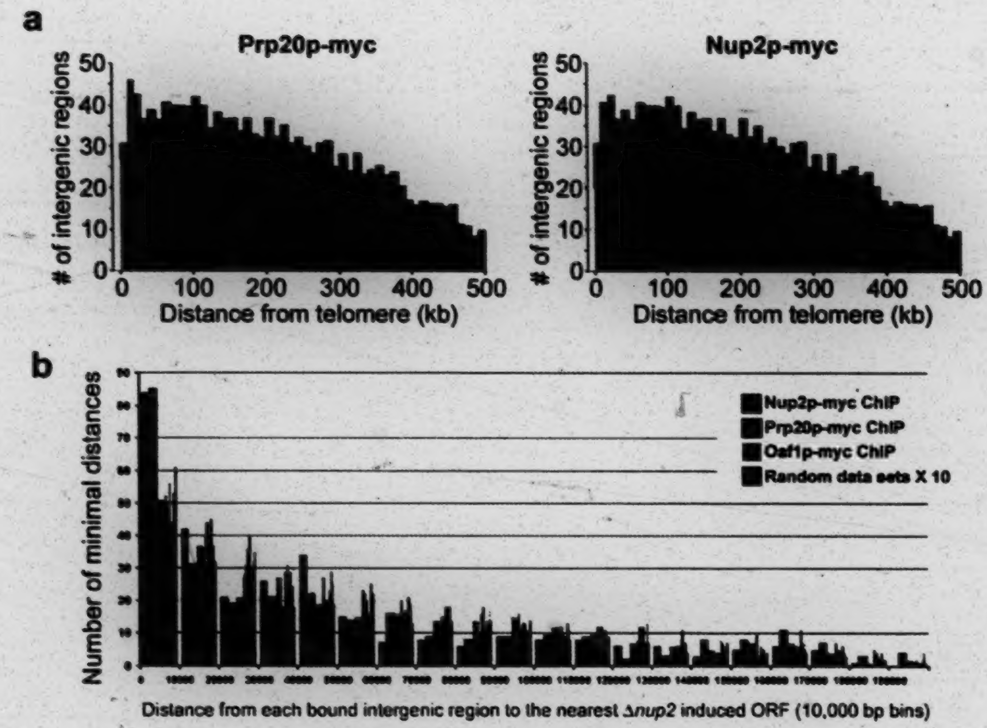

Figure 3-6. Chromatin regions bound by Nup2p and Prp20p are enriched in subtelomeric regions. (a) Histograms of minimal telomeric distance for the top 5 % of significantly enriched intergenic regions bound by myc epitope-tagged fusions to Prp20p and Nup2p reveal a telomeric enrichment similar to that observed for ORFs induced in cells lacking Nup2p (see Fig. 3). The shaded histograms represent the distribution of all intergenic regions shown at 1/4th scale on the y-axis. Using a two-sample Kolmogorov-Smirnov test, the Prp20p and Nup2p profiles are significantly distinct from the distribution of all intergenic regions ($p < 0.000001$ and $p = 0.000367$, respectively). In contrast, the profile of the transcription factor, Oaf1p, displayed no significant enrichment relative to all intergenic regions ($p = 0.368$, data not shown). (b) Chromosomal proximity of transcriptionally induced ORFs in *Δnup2* cells and ChIP-CHIP enriched intergenic regions. The distance between each ChIP-CHIP enriched intergenic region and the nearest *Δnup2*-induced ORF was determined for Nup2p, Prp20p, Oaf1p and 10 randomised ChIP-CHIP data sets. The results, plotted in 10 kb bins, reveal that intergenic regions bound by Nup2p and Prp20p are found much closer to ORFs induced in *Δnup2* cells, relative to the Oaf1p or randomised data sets, as evidenced by the high number of Nup2p and Prp20p enriched intergenic regions found within 10 kb of *Δnup2* ORFs. Indeed, there are significant differences between the Oaf1p profile and those obtained with Prp20p and Nup2p ($p = 0.0282$ and 0.00102, respectively), determined using the Kolmogorov-Smirnov test statistic.

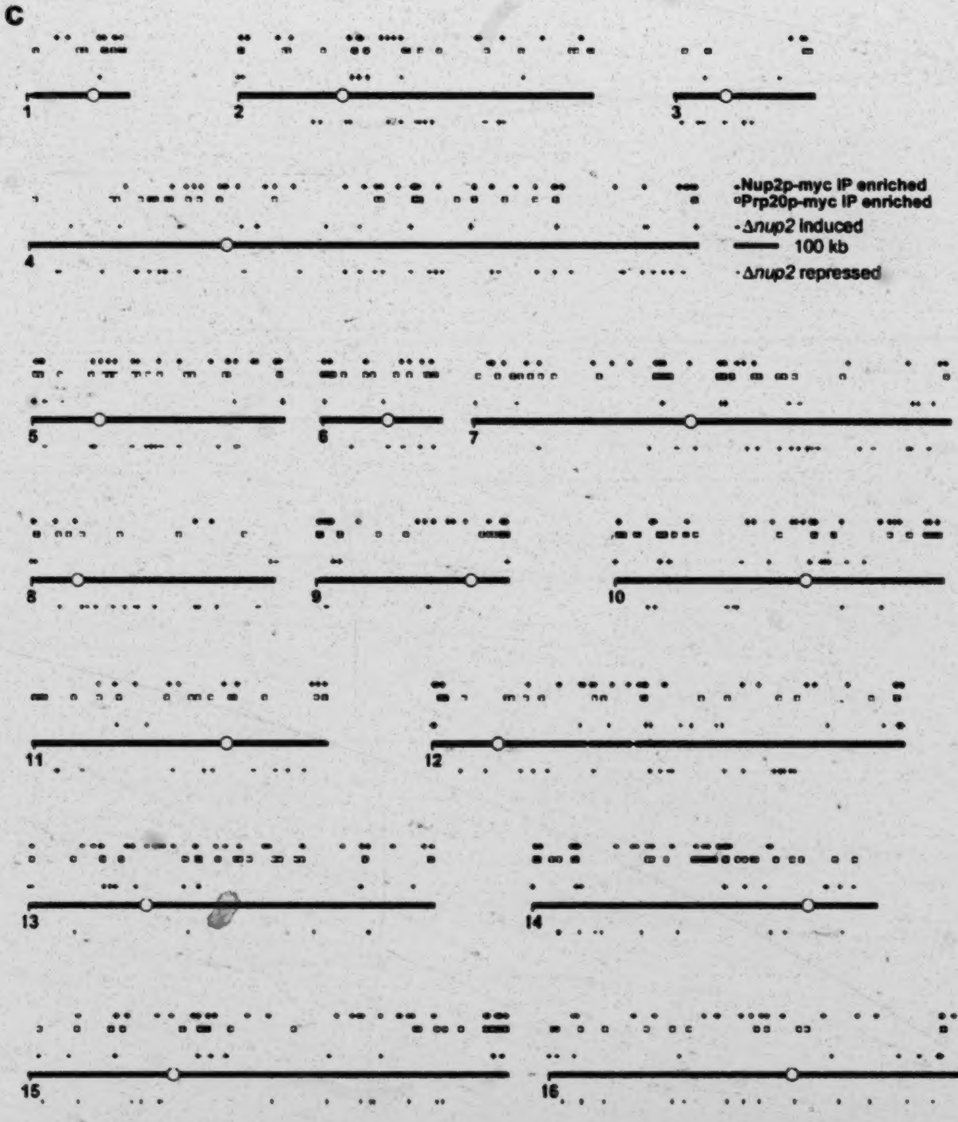

(c) The locations of the DNA regions bound by Nup2p and Prp20p and the *Δnup2* induced and repressed ORFs along the 16 yeast chromosomes are shown (see inset legend). Chromosome lengths are to scale and centromeres are indicated by white circles. Shaded regions exhibit qualitative clustering among the different microarray datasets and are, thus, candidate chromosome regions under the influence of NPC-dependent boundary activity. In particular, the subtelomeric region on the right arm of chromosome 15 warrants further study as it contains two tandemly encoded iron-responsive genes that are induced in cells lacking Nup2p and flanked by intergenic regions bound by Nup2p and Prp20p.

3.2.7. *Δnup2* and *Δnup60* cells exhibit defects in the ability to maintain subtelomerically encoded reporters in the silenced state

The aberrant expression of subtelomeric encoded ORFs in cells lacking Nup2p revealed by mRNA expression microarray studies suggested a role for Nup2p in the maintenance of the transcription states of subtelomeric genes, which have been shown to variegate between ON and OFF states[145]. Given this fact, we suspected that *Δnup2* cells would exhibit defects in subtelomeric expression variegation. Specifically, in cells lacking Nup2p, subtelomerically encoded genes were predicted to be predisposed to the ON state and variegate less efficiently than in wild-type cells. Initial support came from colourimetric analysis of colonies that formed on plates used to assess boundary activity. As discussed previously, the boundary trap strain encodes *ADE2* and *URA3* in *HML*, which is located in the subtelomeric region of the left arm of chromosome III[2]. Growth of these strains on CSM-TRP, to assess viability and ensure equal cell densities, represents a condition in which there is no selective pressure on the expression state of *ADE2* and *URA3*. Given that cells not expressing *ADE2* appear red in colour due to the accumulation of P-ribosylaminoimidazole, while those expressing *ADE2* appear white, the ability of the ON and OFF states to be stably inherited can be analyzed by the red/white sectoring pattern observed for colonies that formed on CSM-TRP media (Figure 3-7a). Similar to the positive control protein BEAF, Nup2p permits stable maintenance of boundaries in *HML* when it is appended to Gbd and expressed in wild-type cells, as evidence by the distinct sectoring of red and white in the colonies. In contrast to BEAF, the sectoring phenotype of Nup2p is lost when *NUP2* or *NUP60* is deleted, as these mutant strains form uniformly red colonies indicating that *ADE2* is predominantly in the OFF state. These results would be expected if competition between endogenous Nup2p and Gbd-Nup2p for Nup60p binding sites on the NPC was required for Nup2p-mediated BA. Interestingly, cells expressing Gbd-Nup60p in a *Δnup2* background form colonies indicative of a stable but modest level of *ADE2* expression. Thus, in unselective conditions stable NPC-association appears to favor gene activation only when Nup2p is absent. In addition to non-selective growth, we also observed defects in subtelomeric silencing under selective pressures, which was determined by two complementary approaches. In the first, we utilised growth on 5-FOA to assess the ability of wild-type and mutant strains to silence *URA3* at the left arm of chromosome VII, which is requisite for growth in the presence of this drug (Figure 3-7b). We observed a modest defect in the ability of strains lacking Nup2p to stably silence the *URA3* gene in this subtelomeric region, but we note that the defect is significantly less severe than that observed in strains lacking *NUP60*, a previously reported phenotype[8,152]. Importantly, the *Δnup2* effect is rescued by introduction of a plasmid encoding *NUP2*, which indicates that it is a specific, albeit weak, defect.

Our second approach was a single cell telomeric silencing assay that analyzes expression variegation in individual cells based on their response to mating pheromone[206]. When grown in the presence of α factor, the vast majority of yeast a-type cells arrest in G1 prior to START and form pseudopod-like projections, termed shmoos. Diploid (**a**/*α*) cells and α cells are insensitive to α factor and therefore continue to divide in its presence. However, if haploid **a** cells express the normally silenced, *α2* gene they act as diploids and are insensitive to α factor. Exploiting this characteristic, Iida *et al.* incorporated a subtelomeric copy of the *α2* gene in **a** cells, which resulted in its variegated expression (Figure 3-7c). Thus, the expression state of the *α2* reporter can be quantified in single cells by analyzing their response to α factor – cells in the ON state are insensitive whereas cells in the OFF state arrest. Consequently, by monitoring the ability of individual cells to maintain the arrested or insensitive phenotype over a time course, the OFF-to-ON switching rate can be determined (Figure 3-7d).

Using this assay, we analyzed strains lacking Nup2p, Nup60p, Htz1p and Gsp2p. The latter two proteins were included because they were identified as Prp20p-associated proteins (Figure 3-1c) and because both have been implicated in boundary function[2,200]. We found that cells lacking either Nup2p or Gsp2p exhibited a modest increase in the initial proportion of cells exhibiting the OFF state relative to wild-type cells. *Δhtz1* and *Δnup60* cells showed significantly increased and decreased rates (respectively) in the initial OFF state (Figure 3-7e, y-axis). These data support the

Figure 3-7. ΔNUP2 *and* ΔNUP60 *cells exhibit defects in the maintenance of expression states of subtelomerically encoded reporters.* (a) Colorimetric analysis of *ADE2* expression under nonselective conditions in wild-type, *Δnup2* and *Δnup60* boundary trap strains. Expression of Gbd-Nup2p allowed wild-type cells to stably inherit the ON and OFF expression states of the subtelomerically encoded copy of *ADE2* resulting in red/white (OFF/ON) sectoring colonies. Deletion of *NUP2* or *NUP60* resulted in loss of sectoring and a shift towards the red (*ADE2* OFF) phenotype for cells expressing Gbd-Nup2p but not those expressing the control protein, Gbd-BEAF, which formed sectoring colonies in all strains tested. Relative to wild-type counterparts, *Δnup2* cells expressing Gbd-Nup60p exhibited a shift towards the white (*ADE2 ON*) phenotype, indicating that the presence of Nup2p at the NPC promotes gene repression. (b) The stable maintenance of the OFF expression state of a subtelomerically encoded copy of *URA3* was assayed in wild-type, *Δnup2* and *Δnup60* cells. The decrease in the ability of *Δnup2* cells to form colonies on media containing 5-FOA indicates that the *URA3* gene could not be maintained in the OFF state. An even more severe defect was observed in cells lacking Nup60p, as would be predicted given previous findings[7,8]. Although relatively weak, the *Δnup2* defect was rescued by plasmid-based expression of *NUP2*, indicating specificity. (c) The expression status of a telomerically encoded *α2* reporter gene was assayed in single cells by monitoring the response of cells to the α factor mating pheromone. Cells that did not express *α2* (OFF) responded to α factor, evidenced by their arrest in G1 and the development of shmoos, while cells expressing *α2* (ON) continued through the cell cycle. The initial 'OFF' proportion was determined by scoring cells after a 4 hr treatment with α factor. (d) Determination of 'OFF' maintenance ratio. The ability of cells to maintain *α2* in the 'OFF' state was assayed by monitoring α factor arrested cells over time. Those cells that switched to the 'ON' state overcame the arrest and gave rise to microcolonies, whereas stably arrested cells did not divide during this period. (e) The wild-type normalised initial 'OFF' ratios (y-axis) and 'OFF' maintenance ratios (x-axis) were plotted for each strain (error bars indicate the standard deviation for 3 independent experiments). Strains lacking Nup2p or Gsp2p exhibited very similar phenotypes as both showed marginally increased initial 'OFF' ratios ($y \geq 1$), while arrested cells from each were unable to efficiently maintain the 'OFF' state ($x < 1$). Cells lacking Nup60p exhibited a steady-state defect in the establishment of the 'OFF' state in addition to an inability to maintain the 'OFF' state in arrested cells (x and $y < 1$), while cells lacking Htz1p showed the opposite phenotype (x and $y > 1$).

proposed functions of Nup60p and Htz1p in establishing silenced and active states, respectively[8,152,200,212]. Furthermore, these data suggest that Gsp2p and Nup2p are not involved in variegation or affect both activation and repression, as would be expected for proteins that confer BA. With respect to the ability to maintain the OFF state *Δnup2, Δnup60* and *Δgsp2* cells were twice as likely to overcome the arrest compared to wild-type cells, while *Δhtz1* cells exhibited a 50 % increase in the ability to maintain the OFF state (Figure 3-7e, x-axis). In summary, these experiments indicate that Nup2p and Gsp2p are required for the stable maintenance, but not the

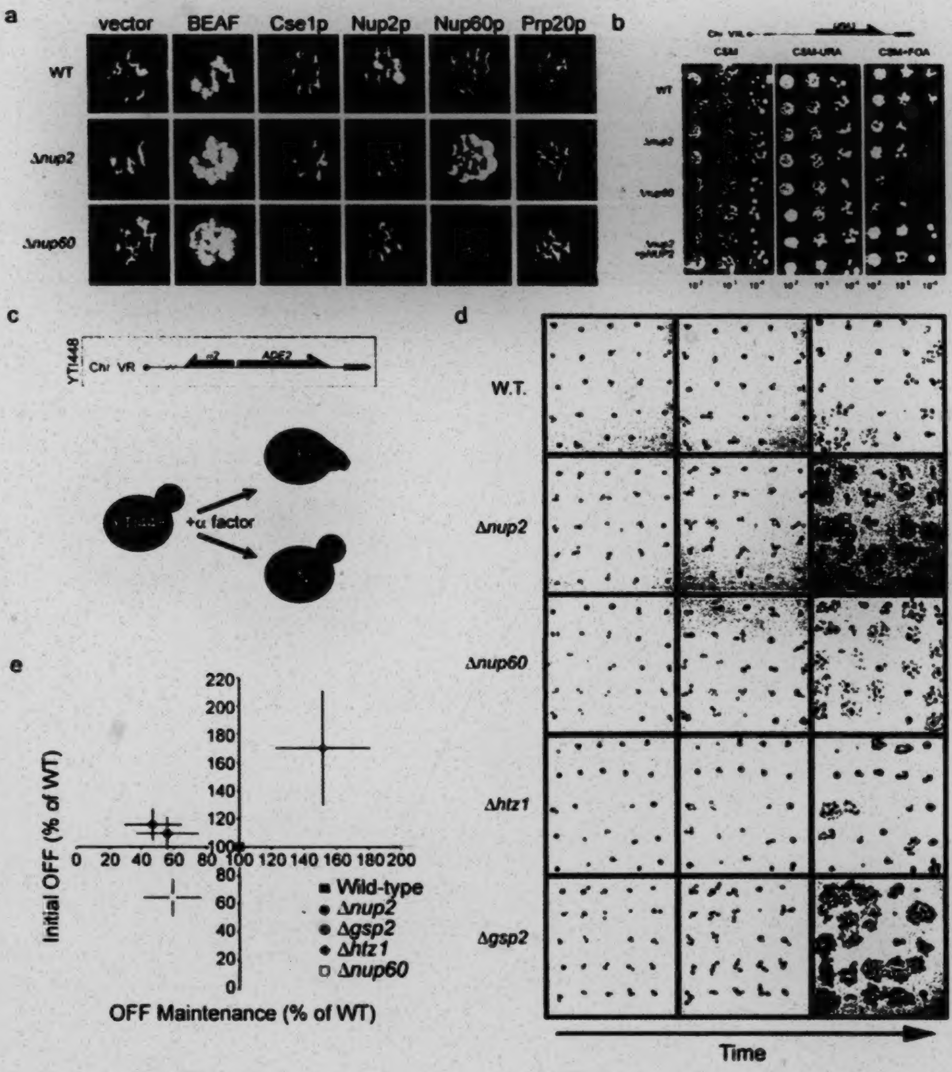

establishment, of a silenced domain. In contrast, Nup60p and Htz1p are involved in both processes, but while Nup60p promotes silencing, Htz1p promotes activation. Given that Nup2p and Gsp2p harbour BA, but Htz1p and Nup60p do not, these results suggest a balance between repression and activation is required for BA. Together with the expression array data, these results strongly support the existence of endogenous Nup2p-mediated boundary activity, and furthermore suggest that this function is linked with the peripheral silencing apparatus through Nup60p.

3.3. Discussion

3.3.1. The convergence of nuclear functions at the NPC

Given that the NPC is one of a limited number of positional markers in the nucleus, it is no surprise that cells have taken advantage of this structure to organise nuclear events. Indeed, yeast nups have been linked to Mlp-dependent gene silencing[8,152], boundary activity[2], ribosome maturation[214], unspliced mRNA retention[7] and *de novo* formation of NPCs and the NE[132]. Lying at the crossroads between the nuclear interior and the nuclear periphery, the NPC has long been suggested, but only recently shown, to interact with actively transcribed genes, enabling ready access of transcription factors to specific sites of the genome and, likewise, newly transcribed mRNA to the cytoplasm, a function termed 'gene gating'[215,216] By doing so, the NPC co-ordinates these cellular events allowing them to proceed more efficiently. Beyond these interpretations, we further propose that the NPC plays an active role in chromatin organisation, by facilitating the transition of chromatin between activity states, which as previously proposed, are partially imposed by three dimensional position of a gene within the nucleus[152,217]. This function may be related to the specific local deposition of import (or removal of export) cargo which could control the access of the transcriptional machinery to chromatin and/or the localised concentration of factors that function in maintaining the silenced or active states. In other words, by providing a mechanism to target the initiation of export and termination of import to specific chromatin regions, the nucleocytoplasmic transport machinery can play an active role in controlling gene expression, intimately linking nuclear transport and chromatin organization.

3.3.2. Endogenous Nup2p-mediated boundary function

In developing a model of endogenous NPC-mediated BA, we must consider the high molecular burden placed on NPCs. Our earlier work, presented in Chapter 2, led us to propose that Nup2p provides a soluble scaffold to decrease the residence time of transport complexes at the NPC, thereby facilitating transport and relieving congestion at NPCs. Extending this paradigm to Nup2p-mediated boundary activity, we propose that DNA boundaries utilise NPCs as waypoints, not stable anchors, *en route* to subnuclear compartments that promote different transcriptional states. Once associated with the nuclear face of the NPC, chromatin can enter the peripheral silencing apparatus, a process proposed to involve the Mlp proteins[8,152], be selectively activated at the periphery[216,218] or be released to freely diffuse to the nuclear interior. The ability of chromatin to transit between active and silent domains by gating through NPCs would provide an epigenetic mechanism for a cell to 'sample' possible transcriptional states. We propose that the mobility of Nup2p is the key to this BA, as no other nups harbour this activity, including Nup60p and Nup1p, which are in very close proximity to NPC-bound Nup2p and share many protein binding partners[4,190]. Moreover, like Nup2p, all the transport factors that exhibit BA transiently associate with NPCs[2]. Thus, we envision Nup2p promotes transcriptional plasticity by effectively 'greasing the wheels' of DNA movement to NPCs. We would further predict that cells lacking Nup2p would fail to efficiently move chromatin to and from NPCs, a defect that would result in the aberrant expression of normally silent subtelomeric ORFs, a prediction that is supported by our microarray analysis and single cell silencing studies.

Previous models of NPC-mediated BA incorporated a static mechanism involving the stable anchoring of chromatin to the nuclear basket of the NPC; however, several observations argue against this model. For example, the static model predicts that nucleoporins associate with both active and silenced ORFs on either side of a chromosomal boundary; yet, they are found to enrich specifically with active ORFs[216]. Also, a static mechanism would predict that multiple nups would possess BA, but in fact this activity appears to be specific to Nup2p. Thus, a dynamic model of NPC-mediated BA explains why Nup2p is unique – it is not stably associated with the NPC – and might also provide an explanation for the lack of correlation between our ChIP-CHIP data sets and those put forth by Caolari *et al.*[216]. That is, differences in the rates of association, or residence times, of coding and non-coding regions of chromatin with NPCs could give rise to unique association patterns when utilising ORFs or intergenic microarrays. In other words, if actively transcribed chromatin associates more avidly with NPCs than inactive chromatin, then highly transcribed ORFs would be more likely to cross-link to this structure during the ChIP-CHIP procedure, which employs overnight cross-linking.

Endogenous NPC-mediated BA also requires a mechanism for chromatin to associate with the NPC, and we have presented several lines of evidence suggesting that the interaction between Prp20p and Nup2p provides this critical link. While the *in vitro* binding data reveal a robust interaction between Prp20p and Nup2p, immunopurification and localisation data suggest that the interaction is transient. Thus we suggest that chromosomal regions interacting with Prp20p attain an equilibrium distribution between subnuclear regions that promote active and silent states and that these transitions are facilitated through Nup2p-dependent associations with the NPC (Figure 3-8). An alternative, but not mutually exclusive, interpretation of the data is that, rather than recruit chromatin to the NPC, Nup2p targets factors important for boundary function from the NPC to specific chromatin sites, thus contributing to boundary maintenance without the requirement of NPC association. The correlation of the loss of Cse1p boundary activity in cells lacking Nup2p with the inability of Cse1p to localise tethered chromatin to the nuclear periphery[2] suggests that, regardless of the mechanism, the result is an accumulation of boundary chromatin at the nuclear periphery.

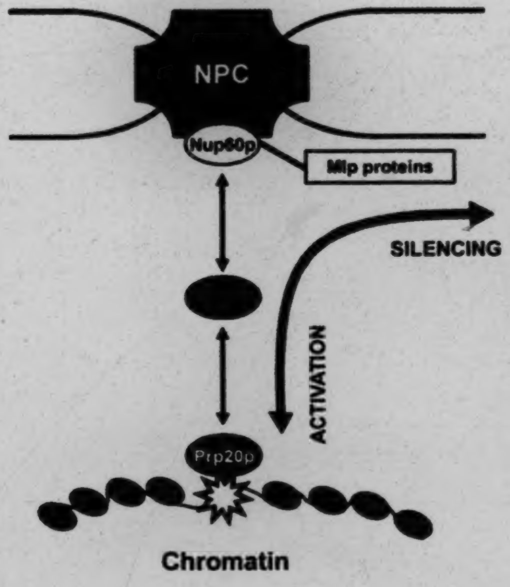

Figure 3-8. Dynamic model of Nup2p-dependent boundary function. Boundaries (star), marked by Prp20p, are proposed to be mobile but spatially restricted within the nucleus due to their transient Nup2p-dependent association with NPCs. The complexation of DNA with the NPC represents an unstable reaction intermediate from which the DNA can either enter the perinuclear silencing region through Nup60p or detach from the NPC, free to enter the nuclear interior.

With respect to the boundary trap assay, the requirement for Nup2p in the BA of other transport factors likely arises from their ability to bind to Nup2p. Thus, when tethered to DNA artificially, Nup2p could catalyze the movement of these proteins and associated DNA to the NPC, in essence mimicking the endogenous function. By linking the functions of the NPC in boundary activity with their role in Mlp dependent silencing, this model also explains the defect in BA that we observed in cells lacking the Mlp proteins, as without them, regions marked for silencing are unable to efficiently enter the peripheral silencing matrix, which is proposed to be established through an interaction between the Mlp proteins and the NPC (in particular Nup60p)[8,152]. It also agrees with the observation by Laemmli's group that simply tethering DNA to the nuclear periphery is not sufficient to establish boundaries in the boundary trap assay[2]. Adjacent regions can become selectively activated or repressed by looping mechanisms[219]. This dynamic aspect of chromatin also agrees with observations by Heun *et al.* that telomeric chromatin is predominantly constrained to perinuclear regions, yet is still subject to occasional large movements into the nuclear interior[220].

Interestingly, Prp20p was originally identified as *SRM1*, a suppressor of the mating defect in *MATα* cells that lack *STE3*, which encodes the **a** factor receptor[221]. The authors identified a temperature-sensitive allele of *PRP20* (*srm1-1*) that partially restored the ability of *MATα Δste3* cells to mate with cells of the opposite mating type, indicating that these double mutants underwent the mating response despite their insensitivity to *α* factor. In light of our data implicating Prp20p in chromatin organisation, it is possible that the inability of strains harbouring *srm1-1* to efficiently maintain chromosome boundaries results in the aberrant expression of normally silenced genes involved in the mating response, thereby allowing cells to mate in the absence of the pheromone receptor.

3.3.3. The chromatin connection

A major unanswered question is how transport complexes are specifically targeted to regions of DNA and how this might be related to chromatin organisation. ChIP-CHIP experiments performed by Casolari *et al.* revealed that Prp20p binds to a broad proportion of the genome (~25 % of all ORFs)[216] and, in light of our data, it is possible that Prp20p interacts both with active and silenced DNA. Perhaps, the GEF activity of Prp20p or the stability of its association with nucleosomes is modulated dependent on its heterochromatic or euchromatic localisation, thereby providing a function in both gene activation and silencing. This potential for modulation of the activity of Prp20p by the local chromatin to which it is bound could provide a direct link between nuclear transport and chromatin organisation, a knowledge of which is required if we are to fully understand the function of Nup2p in these processes.

4. CONCLUSIONS AND PERSPECTIVES

Eukaryotic cells employ a variety of mechanisms to epigenetically regulate gene expression, including the exploitation of the three-dimensional architecture of the nucleus. The ideas presented in this thesis, that the NPC can aid in transcriptional regulation not only through its role in nucleocytoplasmic transport but also through direct interactions with chromatin, open several new avenues for future studies that will likely lead to a more comprehensive understanding of NPC function and, more specifically, the function of Nup2p in these processes. It is possible that the function of the NPC in chromatin organisation is not limited to interphase - it may also be involved in maintaining chromosome fidelity during mitosis. With respect to Nup2p, the major goals of future lines of experimentation would be to more clearly define how Nup2p and Prp20p link nuclear transport and chromatin organisation. Thus, it is necessary to focus on revealing the factors that regulate the interaction between Nup2p and Prp20p and elucidating the dynamics of the association of chromatin with the NPC, discussed in sections 4.1 and 4.2, respectively. Another important line of experimentation, discussed in more detail in section 4.3, is the investigation of whether or not NPC-mediated chromatin organisation exists in metazoans, as these studies could yield important information regarding the role of the NPC in human development and disease.

4.1. Integrating the roles of Nup2p in nuclear transport and BA

It is clear that understanding the means by which the NPC, its associated factors and nuclear transport contribute to chromatin organisation is fundamental to a comprehensive view of how cells express their genome; however, any novel insights must be compatible with the previously established functions of these proteins in nucleocytoplasmic transport. Thus, with respect to integrating the functions of Nup2p in transport and chromatin organisation, the most attractive scenario is that these functions are linked at the stage of import complex dissociation and/or export complex formation, because these are nucleocytoplasmic exchange reactions that involve both Nup2p and Prp20p, which we have shown are key players in NPC-mediated BA. One possible mechanism linking this chromatin organisation to these nuclear transport reactions is that Prp20p-dependent deposition of Htz1p as the terminal step of Htz1p import provides a mechanism of targeting Htz1p-mediated transcriptional activation to specific chromatin regions. Alternatively, enhancement of the GEF activity of Prp20p at Htz1p-associated chromatin could increase nucleocytoplasmic exchange reactions in these regions. Another scenario involves the non-essential Ran paralogue Gsp2p, which, although greater than 95% similar to Gsp1p, was specifically identified in the boundary trap assay[2]. Although both Gsp1p and Gsp2p have been shown to act as multicopy suppressors of a temperature-sensitive *PRP20* allele, very little biochemical characterisation of Gsp2p has been performed[222]. If the biochemical properties of Gsp2p are distinct form those of Gsp1p then modulating the localisation of these two Ran species along chromatin could result in the local production of Ran-GTP at specific chromosomal locations. At this point, the mechanisms discussed above remain highly speculative due to the lack of supporting experimental data; however, they merit consideration for future research.

4.2. Formal proof for a dynamic model - chromosome tattooing

Formal distinction between the static and dynamic models of Nup2p-mediated BA may be attained by monitoring the movement of chromatin regions destined for silencing *in vivo* using chromosome visualisation techniques[8,220,223] to determine whether these regions associate stably with NPCs or are subject to a dynamic equilibrium. Recent observations showing that genes involved in galactose utilisation associate to a higher extent with NPCs and move to the nuclear periphery upon shift into media containing galactose are not inconsistent with our model[216]. In the dynamic model, chromatin is in equilibrium between different nuclear subcompartments, and NPCs serve as gateways for the passage between these distinct nuclear domains. Thus, this model predicts that the *GAL* genes are maintained in a silencing nuclear subcompartment under normal, non-inducing growth conditions (glucose carbon source) but, in conditions that induce *GAL* genes (galactose carbon source), Nup2p continually brings these chromatin regions to NPCs to ensure that they are no longer fixed in the silenced state and possibly promote mRNA export. The link between transcriptional activation and peripheral localisation does not seem to agree with previous links between silencing and the nuclear periphery; however, this apparent discrepancy can be resolved if regions of the nuclear periphery devoid of NPCs are transcriptionally distinct from regions containing NPCs, which evidence suggests is the case[2]. A *caveat* of the *GAL* data described above is that, because they were performed using fixed cells and analysed in two dimensions, the real-time movement of the *GAL* genes in the three-dimensional nucleus could not be determined, and the distinction between NPC-versus non-NPC-mediated peripheral association could not be made, which makes it impossible to distinguish between the static and dynamic models given these data alone.

4.3. Extrapolation to higher eukaryotes

Does endogenous NPC-mediated BA exist beyond yeast? While presently unknown, microarray and proteomic technologies similar to those employed in the yeast model could rapidly address this question. Given the high degree of structural and functional similarity between the yeast and mammalian forms of Nup2p, Prp20p and the Mlp proteins (Nup50, RCC1 and Tpr in humans, respectively)[35,153,186,198,224], the likely answer is, yes. If indeed this mechanism of BA extends to higher eukaryotes, it likely plays an important role in the plasticity and regulation of gene expression. This could be relevant to development, through the temporal coordination of gene expression, and to the progression from normal to cancerous states, through the dysregulation of gene expression. One potential avenue of exploration is the study of spermatogenesis, because it is thought to be regulated at least in part by nucleocytoplasmic transport[225] and previous studies have shown that the subcellular localisation of Nup50 is altered during this process[186]. Together these data suggest that the regulation of genome expression during gametogenesis in males could operate via a Nup50-dependent mechanism.

NO TEXT

5. MATERIALS AND METHODS

5.1. Stocks and growth conditions

5.1.1. Yeast strains

All yeast strains used are listed in Table 5-1 and, for strains whose constructions have not been previously described in detail, their derivations are outlined below.

Protein A tagged strains. Haploid strains expressing chromosomal fusions of the gene encoding *Staphylococcus aureus* Protein A (PrA) to *NUP1*, NUP2, *NUP49*, *NUP60*, *NUP159*, *KAP95*, *KAP104*, *KAP121*, *KAP123*, *PRP20* and *HTZ1* were obtained as previously described[4,51,131,226] using either pPrA/HIS5[4], which utilises the *HIS5* gene from *S. pombe* to complement *his3* in *S. cerevisiae*, or pPrA/HIS3URA3[131], which utilises a double cassette encoding *S. cerevisiae* *HIS3* and *URA3* for selection. The tagging method is explained in more detail in section 5.2.8. A Nup60p-PrA strain lacking Nup2p was derived by crossing the Nup60p-PrA strain to a *Δnup2* strain, LDY627 (*nup2::TRP1*)[162], and subsequent isolation of Nup60p-PrA *Δnup2* spores. Similarly, a *Δnup60* strain, JAY1331[193], generated by deletion/disruption with a *TRP1* cassette, was used to generate a Nup2p-PrA strain lacking Nup60p.

GFP tagged strains. Chromosomal GFP fusions to *NUP2*, *NUP49*, *NSP1*, *NUP159*, *NUP60*, *CSE1*, *KAP60* and *KAP95* were constructed in an identical manner to the PrA-tagged strains, except that the region encoding *S. aureus* PrA downstream of amino acid 54 was replaced with *Aequoria victoria* green fluorescent protein (GFP) using either the pGFP/HIS5 or the pGFP/HIS5U tagging vector[193]. The latter was constructed to allow GFP tagging where the oligonucleotides were originally designed for the pPrA/HIS3URA3 tagging vector[131]. The pGFP/HIS5U plasmid contains the pPrA/HIS3URA3 reverse oligonucleotide annealing site downstream of the *HIS5* marker. A Nup2p-GFP mutant lacking the Ran-binding domain (RBD) was generated using oligonucleotides designed to eliminate amino acids 606 through 720 of Nup2p upon integration of the GFP tag to generate Nup2ΔRBDp-GFP. The Nup2p-GFP strain was crossed to a *Δnup120* strain[131] (*nup120::URA3*) and cells were sporulated to generate Nup2p-GFP *Δnup120* haploid cells. To derive a Nup2p-GFP *Δnup1* strain, the Nup2p-GFP strain was crossed to a

NUP1 null strain, KBY52[167] (*nup1-2::LEU2*) containing the pLDB73 covering plasmid (*CEN URA3 ADE3 NUP1*)[167], sporulated and appropriate haploid strains were grown on 5-FOA to eliminate the covering plasmid. JAY1331 was used to generate Nup2p-GFP, Nup49p-GFP and Nsp1p-GFP strains in a *Δnup60* background. Strains Kap60p-GFP *Δnup2*, Kap60p-GFP *Δnup60* and Kap60p-GFP *Δnup100* were made by crossing strains LDY627, JAY1331 and SWY1031[140] (*nup100::HIS3*) to JBY1[162] (*KAP60-GFP(LEU2)*. The *prp20-7* temperature-sensitive allele was introduced into GFP-tagged strains by crossing Nup2p-GFP, Nup2p-GFP *Δnup60*, Nup49p-GFP and Kap60p-GFP strains to strain prp20-7 and isolation of relevant spores (strain prp20-7 is a *MATα* derivative of M$_3$16/1A[113] generated by crossing to DF5 *MATα* and isolating a *MATα* spore),. Heterokaryon shuttling assays were performed using a *kar1-1* karyogamy mutant strain, MS739[172,173].

Strains used to study genetic interactions. Cells used to analyze genetic interactions between *NUP2* and *NUP60* were derived by crossing JAY1331 to LDY680[162] (*nup2::KAN*^{R}) with covering plasmids pLDB60[162] (encoding full length Nup2p) or pLDB690[162] (Nup2p[1-546]) and isolation of WT, single and double mutant spores. Genetic interactions between *NUP60* and *KAP60/SRP1* were analyzed by crossing JAY1331 cells to strain NOY612[227], which harbours the *srp1-31* temperature-sensitive mutation, and isolation of relevant spores. Genetic interaction studies involving *NUP2, NUP60, NUP53, HTZ1* and *PRP20* were performed using crosses involving the kanamycin-selective RG*Δnup2,* RG*Δnup60,* RG*Δnup53* and RG*Δhtz1* null mutant strains in the BY4742 *MATα* background, all contained within the *S. cerevisiae* Deletion Project library (Invitrogen), the temperature-sensitive *prp20-7* strain, M$_3$16/1A[113], and a nourseothricin-selectable RG*Δhtz1*NAT strain (*MATa htz1::kan*^{R}*::NAT*^{R}) , derived by replacing the kanamycin cassette in the *S. cerevisiae* Deletion Project *HTZ1/htz1::kanMX4* diploid strain with a nourseothricin cassette using the *KAN*^{R} → *NAT*^{R} switch plasmid, p4339[228], and then sporulating this diploid and isolating a *MATa htz1::natMX4* haploid.

Boundary Trap Strains. Boundary trap strains were generated in the KIY54 background which has been previously described, along with a *nup2:: KAN*^{R}

derivative (YGA2)[2]. Other single deletion mutants of KIY54 were generated by homologous recombination using kanamycin or nourseothricin selectable deletion cassette PCR products generated from genomic DNA of corresponding mutants in the *S. cerevisiae* Deletion Project library or nourseothricin-switched derivatives thereof. In a like manner, two independent *Δmlp1/Δmlp2* double mutants were generated by sequential integration of *mlp1::KAN*^{R} followed by *mlp2::NAT*^{R} or *mlp1::NAT*^{R} then *mlp2:: KAN*^{R}. All deletions were confirmed by gene specific PCR.

Single cell silencing assay. Strains lacking Nup2p, Nup60p, Gsp2p or Htz1p were generated in the YTI448 parental background[2] by homologous recombination as described above for boundary trap strains.

ChIP-CHIP strains. For chromatin localisation studies, myc-tagged versions of Prp20p and Nup2p were constructed in the BY4742 background by homologous recombination using gene specific PCR products encoding 13 repeats of the c-myc epitope and a selectable *KAN*^{R} marker that were generated using the plasmid pFA6a-13Myc-KAN^{R} as template and gene specific oligonucleotides as described[229]. Myc-tagged versions of Mlp1p and Mlp2p were generated using the same technique but using the plasmid pMYC/KAN^{R} as template, which was designed for use with JA universal tagging oligonucleotides.

Table 5-1 **Yeast strains**

Name	Genotype	Ref
	Stock strains	
DF5	*MATa/MATα ura3-52/ura3-52 his3Δ200/his3Δ200 trp1-1/trp1-1 leu2-3,112/leu2-3,112 lys2-801/lys2-801*	230
W303	*MATa/MATα ade2-1/ade2-1 his3-11/his3-11 leu2-3,112/leu2-3,112 trp1-1/trp1-1 ura3-1/ura3-1*	231
M316/1A	*MATa prp20-7 ade2-101 his3 Δ 200 tyr1 ura3-52*	113
LDY627	W303 *MATα nup2::*TRP1	162
NOY612	W303 *MATa srp1-31*	227
JAY1331	W303 *MATα nup60::*TRP1	193
Δnup120	DF5 *MATα nup120::*URA3	131
KBY52	*MATα nup1-2::*LEU2 *ade3 ade2-101 lys2-801 trp1Δ1 ura3-52*	167

SWY1031	W303 *MATα nup100::HIS3*	140
LDY680	W303 *MATa nup2::KAN*^{R}	162
prp20-7	*MATα prp20-7* ♦spore from M$_3$16/1A X DF5*α*	193
MS739	*MATα kar1-1 ura3-52 leu2-3 leu2-112 ade2-101*	172,173
	PrA tags	
Nup1p-PrA	DF5 *MATa NUP1-PrA(HIS3-URA3)*	4
Nup2p-PrA	DF5 *MATa NUP2-PrA(HIS5)*	4
Nup2p-PrA *Δnup60*	*MATa NUP2-PrA(HIS5) nup60::TRP1* ♦spore from Nup2p-PrA X JAY1331	193
Nup49p-PrA	DF5 *MATa NUP49-PrA(HIS5)*	4
Nup60p-PrA	DF5 *MATa NUP60-PrA(HIS5)*	4
Nup60p-PrA *Δnup2*	*MATa NUP60-PrA(HIS5) nup2::TRP1* ♦spore from Nup60p-PrA X LDY627	193
Nup159p-PrA	DF5 *MATa NUP159-PrA(HIS5)*	4
Kap95p-PrA	DF5 *MATa KAP95-PrA(HIS3-URA3)*	51
Kap104p-PrA	DF5 *MATa KAP104-PrA(HIS3-URA3)*	51
Kap121p-PrA	DF5 *MATa KAP121-PrA(HIS3-URA3)*	56
Kap123p-PrA	DF5 *MATa KAP1234-PrA(HIS3-URA3)*	56
Prp20p-PrA	BY4742 *MATα PRP20-PrA(HIS5)*	232
Htz1p-PrA	BY4742 *MATα HTZ1-PrA(HIS5)*	232
	GFP tags	
Nup2p-GFP	DF5 *MATa NUP2-GFP(HIS5)*	193
Nup2p-GFP *Δnup120*	DF5 *MATa NUP2-GFP(HIS5) nup120::URA3* ♦spore from Nup2p-GFP X *Δnup120*	193
Nup2p-GFP *Δnup60*	*MATa NUP2-GFP(HIS5) nup60::TRP1* ♦spore from Nup2p-GFP X JAY1331	193
Nup2p-GFP *Δnup1*	*MATa NUP2-GFP(HIS5) nup1-2::LEU2* ♦spore from Nup2p-GFP X KBY52	193
Nup2ΔRBDp-GFP	DF5 *MATa NUP2ΔRBD-GFP(HIS5)*	193
Nup49p-GFP	DF5 *MATa NUP49-GFP(HIS5)*	193
Nup49p-GFP *Δnup60*	*MATa NUP49-GFP(HIS5) nup60::TRP1* ♦spore from Nup49p-GFP X JAY1331	193
Nup60p-GFP	DF5 *MATa NUP60-GFP(HIS5)*	193
Nup159p-GFP	DF5 *MATa NUP159-GFP(HIS5)*	193
Nsp1p- GFP	DF5 *MATa Nsp1-GFP(HIS5)*	193

Nsp1p-GFP *Δnup60*	*MATa NSP1-GFP(HIS5) nup60::TRP1* †spore from Nsp1p-GFP X JAY1331	193
Cse1p-GFP	DF5 *MATa CSE1-GFP(HIS5)*	193
Kap95p-GFP	DF5 *MATa KAP95-GFP(HIS5)*	193
Kap60p-GFP	DF5 *MATa KAP60-GFP(HIS5)*	193
JBY1	W303 *MATa KAP60-GFP(LEU2)*	162
Kap60p-GFP *Δnup2*	*KAP60-GFP(LEU2) nup2::TRP1* †spore from JBY1 X LDY627	193
Kap60p-GFP *Δnup60*	*KAP60-GFP(LEU2) nup60::TRP1* †spore from JBY1 X JAY1331	193
Kap60p-GFP *Δnup100*	*KAP60-GFP(LEU2) nup100::HIS3* †spore from JBY1 X SWY1031	193
Prp20p-GFP	DF5 *MATa PRP20-GFP(HIS5)*	232
Yeast deletion library strains		
BY4741	*MATa ura3Δ0 his3Δ0 leu2Δ0 met5Δ0*	233,234
BY4742	*MATα ura3Δ0 his3Δ0 leu2Δ0 lys2Δ0*	233,234
BY4743	BY4741 X BY4742, 2n	233,234
RG*Δnup2*	BY4742 *MATα nup2::KAN*^{R}	233
RG*Δnup53*	BY4742 *MATα nup53::KAN*^{R}	233
RG*Δnup60*	BY4742 *MATα nup60::KAN*^{R}	233
RG*Δhtz1*	BY4742 *MATα htz1::KAN*^{R}	233
RG*Δhtz1*-2n	BY4743 *MATa/MATα htz1::KAN*^{R}*/HTZ1*	233
RG*Δhtz1NAT*	*MATa htz1::kan*^{R}*::NAT*^{R} (spore from *KAN*^{R}→*NAT*^{R} switched RG*Δhtz1*-2n)	232
Boundary activity strains		
KIY54	*MATa leu2-3,112 his3-11,15 ura3-1 ade2-1 trp1-1 can1-100 hml-EΔi-UASg-ADE2-UASg-URA3*	2
YGA2	KIY54 *nup2::KAN*^{R}	2
BA*Δnup60*	KIY54 *nup60::NAT*^{R}	232
BA*Δgsp2*	KIY54 *gsp2::KAN*^{R}	232
BA*Δmlp1*	KIY54 *mlp1::KAN*^{R}	232
BA*Δmlp2*	KIY54 *mlp2::KAN*^{R}	232
BA*Δmlp1KΔmlp2N*	KIY54 *mlp1::KAN*^{R} *mlp2::NAT*^{R}	232
BA*Δmlp1NΔmlp2K*	KIY54 *mlp1::NAT*^{R} *mlp2::KAN*^{R}	232

	Colony telomeric silencing assay strains	
YTI249	*MATa ade2-1 can1-100 his3-11,15 leu2-3 trp1-1 ura3-1* *VIIL-adh4::URA3-TEL VR::ADE2-TEL*	2
CTSΔ*nup2*	YTI249 *nup2::KAN*^{R}	232
CTSΔ*nup60*	YTI249 *nup60::KAN*^{R}	232
CTSΔ*gsp2*	YTI249 *gsp2::KAN*^{R}	232
CTSΔ*htz1*	YTI249 *htz1::KAN*^{R}	232
	Single cell silencing assay strains	
YTI448	*MATa bar1Δ::hisG ade2Δ::hisG can1-100 his3-11,15 leu2-3 trp1-1* *ura3-1 VR:: α2ADE2-TEL*	2
SCSΔ*nup2*	YTI448 *nup2::KAN*^{R}	232
SCSΔ*nup60*	YTI448 *nup60::KAN*^{R}	232
SCSΔ*gsp2*	YTI448 *gsp2::KAN*^{R}	232
SCSΔ*htz1*	YTI448 *htz1::KAN*^{R}	232
	ChIP-CHIP strains	
Prp20p-myc	BY4742 *PRP20-13XMYC::KAN*^{R}	232
Nup2p-myc	BY4742 *NUP2-13XMYC::KAN*^{R}	232
Mlp1p-myc	BY4742 *MLP1-13XMYC::KAN*^{R}	232
Mlp2p-myc	BY4742 *MLP2-13XMYC::KAN*^{R}	232
Oaf1p-myc	BY4742 *OAF1-13XMYC::KAN*^{R}	232

† indicates the haploid strain was derived by dissection of tetrads from sporulated diploid cultures of the indicated crosses. Note that only known markers are listed; refer to parental strain genotypes for other markers possibly present in these strains.

5.1.2. Bacterial strains

Routine plasmid maintenance, purifications and ligations were performed in the *E. coli* DH5α strain [genotype: F$^-$ ϕ80d*lac*ZΔM15Δ(*lac*ZYAargF)U169 *end*A1 *rec*A1 *hsd*R17 ($r_K^- m_K^+$) *deo*R *thi*-1 *sup*E44 λ$^-$ *gyr*A96 *rel*A1] (Invitrogen) using 100 μg/mL AMP (ampicillin, sodium salt, Sigma-Aldrich) for plasmid maintenance using the *Amp*^{R} selectable marker. GST fusion protein expressions were performed using the BL21(DE3) pLysS strain [genotype: F- *ompT* *hsdS*$_B$ ($r_b^- m_b^-$) *gal* *dcm* (DE3) pLysS/*Cam*^{R}] (Novagen) in which case the media contained 20 μg/mL CAM (chloramphenicol, Sigma-Aldrich) to maintain the *Cam*^{R} selectable marker on the pLysS plasmid and 100 μg/mL ampicillin for maintenance of *Amp*^{R} containing plasmids encoding GST fusions.

5.1.3. Plasmids

A list of all plasmids used can be found in Table 5-2, along with their yeast selectable markers, if any, and information about their cloning if this information has not yet been described in detail elsewhere. With the exception of the pLysS plasmid, all plasmids encoded *AMP*^{R} for selection in bacteria.

Table 5-2 **Plasmids**

Name	Info	Ref
pBxA/HIS5	Parent vector used to construct pPrA/HIS5 and pGFP/HIS5.	4
pPrA/HIS3URA3	First generation PrA tagging plasmid used with 'JA' universal oligonucleotides to make PrA-HIS3URA3 PCR products for tagging by homologous recombination.	131
pPrA/HIS5	As above, but contains *S. pombe HIS5* in place of *HIS3* and *URA3* and encoding a reverse 'JA' oligonucleotide annealing site different from that in pPrA/HIS3URA3.	4
pGFP/HIS5	GFP tagging derivative of pPrA/HIS5 that generates a GFP-HIS5 PCR product. Made by PCR amplification of GFP from pKW430[63] using oligonucleotides oGFP/HIS5-5' and oGFP/HIS5-3' and subsequent cloning into the EcoRI site in pBxA/HIS5.	193
pGFP/HIS5U	GFP tagging derivative for use with pPrA/HIS3URA3 based oligonucleotides. Contains the reverse oligonucleotide annealing site from pPrA/HIS3URA3 downstream of the HIS5 gene. Cloned by PCR amplification of GFP-HIS5 from pGFP/HIS5 using oGFP/HIS5U-5' and oGFP/HIS5U-3' and ligation into the pGem-T vector (Promega).	193
pMYC/KAN^R	MYC tagging derivative of pPrA/HIS5 that was made by PCR amplification of 13XMYC-KAN^R from pFA6-13Myc-kanMX6[229] using oMYC/KAN^R-5' and oMYC/KAN^R-3' and subsequent cloning into NotI/XhoI digested pGFP/HIS5.	232
pGAL-NUP60	Plasmid for galactose inducible production of Nup60p in yeast. Made by PCR amplification of the *NUP60* gene from *S. cerevisiae* genomic DNA with oGAL-NUP60-5' and oGAL-NUP60-3' and cloning into the BamHI site in pYES2 (Clonetech).	193
pLDB73	*nup1* mutant covering plasmid. A kind gift of L. Davis (NUP1-URA3ADE3-CEN).	162
pLDB60	Plasmid expressing a Nup2-myc fusion protein. A kind gift of L. Davis (pRS316-Nup2myc-URA3-CEN).	162
pLDB652	Plasmid (pRS304-Nup2[aa1–174]-TRP1) for expression of a truncated myc-tagged mutant of Nup2p. A kind gift of L. Davis.	162
pLDB690	Plasmid (pRS304-Nup2[aa1–546]-TRP1) for expression of a truncated mutant of Nup2p that lacks its Ran binding domain (RBD). A kind gift of L. Davis.	162
p4339	KAN^R–NAT^R switching plasmid (pCRII-TOPO::MX4-NAT^R) that generates nourseothricin selectable marker from kanamycin markers. A kind gift of C. Boone.	228
pGST-PRP20	Plasmid used for bacterial expression of a GST-PRP20 fusion protein. A kind gift of M. Rexach.	14
pGST-NUP2	Plasmid used for bacterial expression of a GST-NUP2 fusion protein made by cloning a PCR product encoding *NUP2* that was generated from yeast genomic DNA using the oGST-NUP2-5' and oGST-NUP2-3' oligonucleotides and cloned in-frame with GST into the BamHI and EcoRI restriction sites in pGEX-2TK (Amersham).	193

pGST[-1]CFP	Constructed by ligating the SalI-NotI fragment containing the *ECFP* gene from pECFP (BD Biosciences) into pGEX-4T1, resulting in a plasmid in which the ECFP gene is frame-shifted -1 relative to the GST reading frame; therefore, CFP is not expressed.	232
pGST-CFP	The pGST[-1]CFP plasmid was linearised and blunted at the site XbaI and relegated to generate a plasmid that expresses a GST-CFP fusion.	232
pGST-NUP2-CFP	To generate pGST-NUP2-CFP, the NUP2 gene was PCR amplified from genomic DNA using oligonucleotides oGSTNUP2CFP-5' and oGSTNUP2CFP-3' and cloned into EcoRI digested pGST[-1]CFP. Clones ligated in the correct orientation were frame shifted +1 to allow expression of full-length GST-NUP2-CFP.	232
pGBC12	One of two parental plasmids (the other being pGBC11) that was used in the boundary trap assay. Encodes *TRP1* for selection in yeast and the DNA binding domain of Gal4 (Gbd). Kindly provided by U. Laemmli.	2
pGbd-BEAF	Encodes a Gbd-fusion to the C-terminal region of the *Drosophila* protein BEAF. Used as a positive control in the boundary trap assay and kindly provided by U. Laemmli (pGBC11-BEAF-C).	2
pGbd-CSE1	Encodes a Gbd-fusion to the C-terminal region of Cse1p followed by GFP. Used in the boundary trap assay and kindly provided by U. Laemmli (pGBC11-Cse1[474-960]-GFP).	2
pGbd-NUP2	Encodes a Gbd-fusion to Nup2p. Used in the boundary trap assay and kindly provided by U. Laemmli (pGBC12-NUP2[1-720])	2
pGbd-PRP20	Boundary trap plasmid encoding a Gbd-fusion to Prp20p-GFP. *PRP20-GFP* was amplified by PCR from genomic DNA derived from the PRP20-GFP strain using oGBD-PRP20-5'and oGBD-GFP-3' and cloned into SmaI/SalI digested pGBC12.	2
pGbd-NUP60	Boundary trap plasmid encoding a Gbd-fusion to Nup60p-GFP. *NUP60-GFP* was amplified by PCR from genomic DNA derived from the NUP60-GFP strain using oGBD-NUP60-5'and oGBD-GFP-3' and cloned into SmaI/SalI digested pGBC12.	2
pGbd-HTZ1	Boundary trap plasmid encoding a Gbd-fusion to Htz1p. *HTZ1* was amplified by PCR from wild-type genomic DNA using oGBD-HTZ1-5'and oGBD-HTZ1-3' and cloned into SmaI/SalI digested pGBC12.	2
pFA6a-13Myc-KAN^{R}	Plasmid used for C-terminally tagging endogenous genes with 13 repeats of the c-myc epitope. Kindly provided by R. Young. Also used to generate pMYC/KAN^{R}	229
pLysS	Plasmid containing the T7 lysozyme gene cloned into pACYC184 using a Cam^{R} marker for selection with chloramphenicol. Present in the BL21(DE3) *E. coli* strain.	235

5.1.4. Oligonucleotides

With few exceptions oligonucleotides listed in Table 5-3 were synthesised by IDT and standard stock concentration is 100 μM in water. Oligonucleotides of < 40 bases were purified by standard desalting, whereas longer oligonucleotides were subjected to PAGE purification.

Table 5-3 **Oligonucleotides**

Name	Sequence (5'→3')
JA universal tagging oligonucleotides – first generation (HIS3URA3 marker)	
oJA-NUP1-5'	[4]
oJA-NUP1-3'	[4]
oJA-NUP60a-5'	[4]

oJA-NUP60a-3'	[4]
oJA-KAP95-5'	[51]
oJA-KAP95-3'	[51]
oJA-KAP104-5'	[51]
oJA-KAP104-3'	[51]
oJA-KAP121-5'	[56]
oJA-KAP121-3'	[51]
oJA-KAP123-5'	[51]
oJA-KAP123-3'	[51]

JA universal tagging oligonucleotides – second generation (*S. pombe* HIS5 marker)

oJA-NUP2-5'	[4]
oJA-NUP2-3'	[4]
oJA-NUP2ΔRBD-5'	AAAGTAGATGCTACCCCAGAATCAAAGCCAATAAACTTGCAAAACGGTGAGGAAGACGGTGAAGCTCAAAAACTTAAT
oJA-NUP49-5'	[4]
oJA-NUP49-3'	[4]
oJA-NUP60b-5'	AGGAAATGGCTTGGTTGATGAAAATAAAGTTGAGGCTTTCAAGTCCCTATATACCTTTGGCGGTGGCGGTGAAGCTCAAAAACTTAAT
oJA-NUP60b-3'	TCTTTTTGAGAAAGTGGAAAAAAAATGACTAAATAATATCATCTTGGAATGGTATTTTAGCTGACGGTATCGATAAGCTT
oJA-NUP159-5'	[4]
oJA-NUP159-3'	[4]
oJA-NSP1-5'	[4]
oJA-NSP1-3'	[4]
oJA-KAP60-5'	CAAAATGCCGGTAATACTTTCGGCTTTGGTTCTAATGTCAACCAACAATTCAATTTTAACGGTGAAGCTCAAAAACTTAAT
oJA-KAP60-3'	GAATACTGTACGAACTAGTACATGAAAATACTATTGTGCGAATTAAAAGATTAGAATTTCGCTGACGGTATCGATAAGCT
oJA-CSE1-5'	AATTTGCCTCAATTGACCCAAGAAAATCAAGTAAAATTAAATCAATTATTAGTTGGTAATGGTGAAGCTCAAAAACTTAAT
oJA-CSE1-3'	ACAGACCTATGTACTCCGCTGGAAAAGAAACCATATTGCGATCGT---ATTTACGTGCTGACGGTATCGATAAGCT
oJA-PRP20-5'	TCTGGTGGTGTTAAGCTGTCTGATGAGGACGCAGAAAAGAGAGCGGATGAAATGGATGATGGTGAAGCTCAAAAACTTAAT
oJA-PRP20-3'	GAGAATTTGTCGGTATCGGATAATCATATCGTTTTCTCGTTTTTCTTTGATTTATGTTATGCTGACGGTATCGATAAGCTT
oJA-HTZ1-5'	ATATAAATAAAGCATTATTATTGAAAGTGGAAAAAAAGGGAAGTAAGAAAGGCGGTGGCGGTGAAGCTCAAAAACTTAAT
oJA-HTZ1-3'	AAGGAACCAACAAATCGGTAGAAAGTCGACAGTATAACTAGTGGTGAAGCGCTGACGGTATCGATAAGCTT

Oligonucleotides used to generate universal tagging vectors

oGFP/HIS5-5'	GGCGAATTCGGTGAAGCTCAAAAACTTAATGGTGGTATGTCTAAAGGTGAAGAATTATTC
oGFP/HIS5-3'	GCCGAATTCTTATTTGTACAATTCATCCATAC
oGFP/HIS5U-5'	GGCGAATTCGGTGAAGCTC

oGFP/HIS5U-3'	ACTTATAATACAGTTTTTTAGGCTGACGGTATCGATAAGCTT
oMYC/KAN^R-5'	AGCTGCGGCGCGGCCGCGGTGAAGCTCAAAAACTTAATGGTGGTGGTCGGATCCCCGGGTTAATTAA
oMYC/KAN^R-3'	GCCCTCGAGGCTGACGGTATCGATAAGCTTATCGATGAATTCGAGCTCG

Oligonucleotides used to generate GST fusion proteins

oGST-NUP2-5'	GCCGGATCCGGAGGAGGAATGGCCAAAAGAGTTGCCGAT
oGST-NUP2-5'	GCCGAATTCTTATTTCATTTCTTTTTTAGCATC
oGSTNUP2CFP-5'	GGAATTCGGAATGGCCAAAAGAGTTGCCGATG
oGSTNUP2CFP-3'	GGAATTCGTTTCATTTCTTTTTTAGCATCTTC

Oligonucleotides used gene specific knock outs with KAN^R or NAT^R

oΔnup2-5'	GCATCGTGTGGTAAACAAGC
oΔnup2-3'	ATCTATTATAGACAAAGAACTGG
oΔnup2check-5'	GCCGAATTCTGTAAGAAGATAACATAAAG
oΔnup60-5'	ACCTTATTAGCTCAATCTTGAG
oΔnup60-3'	TGAATTCCAAGTGGGCTCTG
oΔnup60check-5'	TTTCGCGACTGAAAGCGCC
oΔgsp2-5'	CTTGTCAATTAGAGAAGTAAGG
oΔgsp2-3'	CATAATTGGGAATACTTTCCTC
oΔgsp2check-5'	TCTGTTACGTAGTATTTGAGAG
oΔmlp1-5'	ATATCTCAAGCAATGAATTCAAG
oΔmlp1-3'	GTCTTCCCATTGAAAAACTGC
oΔmlp1check-5'	TTGCTCTTATTTGTGTATTTGAG
oΔmlp2-5'	GTCCTGAGGCCGGAAACC
oΔmlp2-3'	AGATTGAGGTACCTCGATGG
oΔmlp2check-5'	GGAAGAAGACAAAATTTTAAACG
oΔhtz1-5'	TCGTCTGTATTCTCTGAAGTG
oΔhtz1-3'	TCGACAGTATAACTAGTGGTG
oΔhtz1check-5'	TGGAAGTTCTATGGGGCGT
oKANcheck-3'	TCAGCCAGTTTAGTCTGACC
oNATcheck-3'	GCCGTCCCCGGTGGCGTC

Oligonucleotides used to generate MYC-tags using pFA6a-13Myc-KAN^R

oPRP20-MYC-5'	TGGTGGTGTTAAGCTGTCTGATGAGGACGCAGAAAAGAGAGCGGATGAAATGGATGAT*GGTGGTGGT*CGGATCCCCGGGTTAATTAA
oPRP20-MYC-3'	ATTTGTCGGTATCGGATAATCATATCGTTTTCTCGTTTTTCTTTGATTTATGTTATATTGAATTCGAGCTCGTTTAAAC
oNUP2-MYC-5'	GAAGGAAGAAGGCCGCTCATTTACGAAAGCTATTGAAGATGCTAAAAAAGAAATGAAAGGTGGTGGTCGGATCCCCGGGTTAATTAA

oNUP2-MYC-3'	AAATATAGATTCGTAGTGTTTTTTGGAATAAATTTTGTATTCTTTATTTGCTC AACTATGAATTCGAGCTCGTTTAAAC
oOAF1-MYC-5'	GGTTATTTTGGAGGTTTGGATTTATTTGATTATGACTTTTTGTTTGGCAATG ACTTTGCTGGCGGCGGCGGCCGGATCCCCGGGTTAATTAA
oOAF1-MYC-3'	TTCGAATGTTTAAGAGGGAAGAGCTCTTCTTACGTTAACCGTTATATACATA TATAGAATTCGAGCTCGTTTAAAC

Oligonucleotides used to generate pGAL-NUP60

oGAL-NUP60-5'	GGGCCCGGATCCATGCATCGTA AATCATTGAG
oGAL-NUP60-3'	GGGCCCGGATCCTCAAAAGGTATATAGGGACT

Oligonucleotides used to generate Gbd fusions for use in the boundary trap assay

oGBD-PRP20-5'	ACGCCCCGGGCGGCGGCGTCAAAAGAACAGTCGCCAC
oGBD-NUP60-5'	ACGCCCCGGGCGGCGGCCATCGTAAATCATTGAGGAGGGCTAGCGCTACT
oGBD-GFP-3'	ACGCGTCGACTTATTTGTACAATTCATCCATAC
oGBD-HTZ1-5'	ACGCCCCGGGCGGGATGTCAGGAAAAGCTCATGG
oGBD-HTZ1-3'	ACGCGTCGACTTATTTCTTACTTCCCTTTTTTTC

Oligonucleotides used for chromatin localisation studies (ChIP-CHIP)

oJW102	GCGGTGACCCGGGAGATCTGAATTC
oJW103	GAATTCAGATC

5.1.5. Growth media

Unless otherwise specified, all liquid media contained 2 % w/v glucose [D-glucose/dextrose] (Fisher) and all solid media contained 2 % w/v glucose and 2 % w/v agar (Difco). Standard rich media 1 % yeast extract, 2 % peptone with one of the following carbon sources: YPD: 2 % glucose), YPA: 2 % potassium acetate (Amresco) or YPG: 2 % galactose (Acros). Standard minimal media (CSM) contained 0.17 % YNB-aa-N [yeast nitrogen base lacking amino acids and ammonium sulfate] (Difco), 0.5 % ammonium sulfate (Fisher) and CSM [complete supplement mixture] (Qbiogene), or derivatives that lack adenine, histidine, leucine, lysine, tryptophan or uracil in any combination as required for auxotrophic marker selection at manufacturer's specified concentrations (~0.1 %). Sporulation media containing 1 % potassium acetate, 0.1 % yeast extract and only 0.05 % glucose was used for all strain sporulations except those involving BY4743a/α (and its derivatives) or diploids resulting from crosses involving BY4741a or BY4742α (and their derivatives), in which case sporulation media consisted of 1 % potassium acetate , 0.005 % zinc acetate (Fisher), 0.006 % adenine (Acros), 0.002 % L-histidine (Sigma-Aldrich), 0.006 % L-leucine (Fisher), 0.005 % L-lysine (Sigma-Aldrich), 0.002% L-methionine (Sigma-Aldrich) and 0.002 % uracil (Acros). In addition to auxotrophy markers, selectable *KAN*^{R} and *NAT*^{R} markers were utilised, conferring resistance to 200 μg/mL G418 sulfate (Fisher) or 100 μg/mL cloneNAT/nourseothricin (Werner BioAgents), respectively. To select against expression of *URA3* the toxic uracil analog 5-FOA was added to CSM media at a concentration of 0.1 % once the media cooled to 55 °C after autoclaving (CSM+FOA).

Bacterial strains were cultured in 2XYT (1.6 % tryptone (Difco), 1 % yeast extract and 0.5 % NaCl (Fisher) and containing 100 μg/mL ampicillin/AMP (Fisher) for selection plasmids encoding *AMP*^{R} and 20 μg/mL chloramphenicol/CAM (Sigma-Aldrich) for selection of *Cam*^{R} encoding plasmids (eg. pLysS).

5.2. General laboratory procedures

5.2.1. Mating, sporulation and tetrad dissection

Yeast of opposite mating types were mated to form diploid strains by either of two methods. In cases where the desired diploid strain could be selected from non-mated haploids using auxotrophic markers or drug selection, the haploid strains were patched onto YPD plates as shown in Figure 5-1a, grown O/N and then re-patched onto media selective for the diploid strain. Mating was confirmed by the ability of the 'mixed' cell patch to grow on the diploid selective plate and the inability of either haploid strain to grow on this media. The second method of diploid generation, manual mating or "pulling zygotes", was used when marker based selection of diploids was not possible (Figure 5-1b). Haploid strains grown O/N on YPD plates were mixed and patched on the same plate and incubated at 30 °C for 4 hours at which point a small portion of the mixed cell patch was streaked to single cell density onto a fresh area of the YPD plate. Several (3-5) post-cytoduction mating cells (barbell shaped and often possessing a small bud representing the first generation diploid daughter) were moved to a fresh area of the YPD plate using an Eclipse

E400 microscope fitted with microdissecting stage (Nikon) and grown at 30 °C to allow well isolated diploid colonies to form. Ploidy was confirmed visually by observing the budding pattern of the putative diploid cells: bi-polar if diploid and axial if haploid.

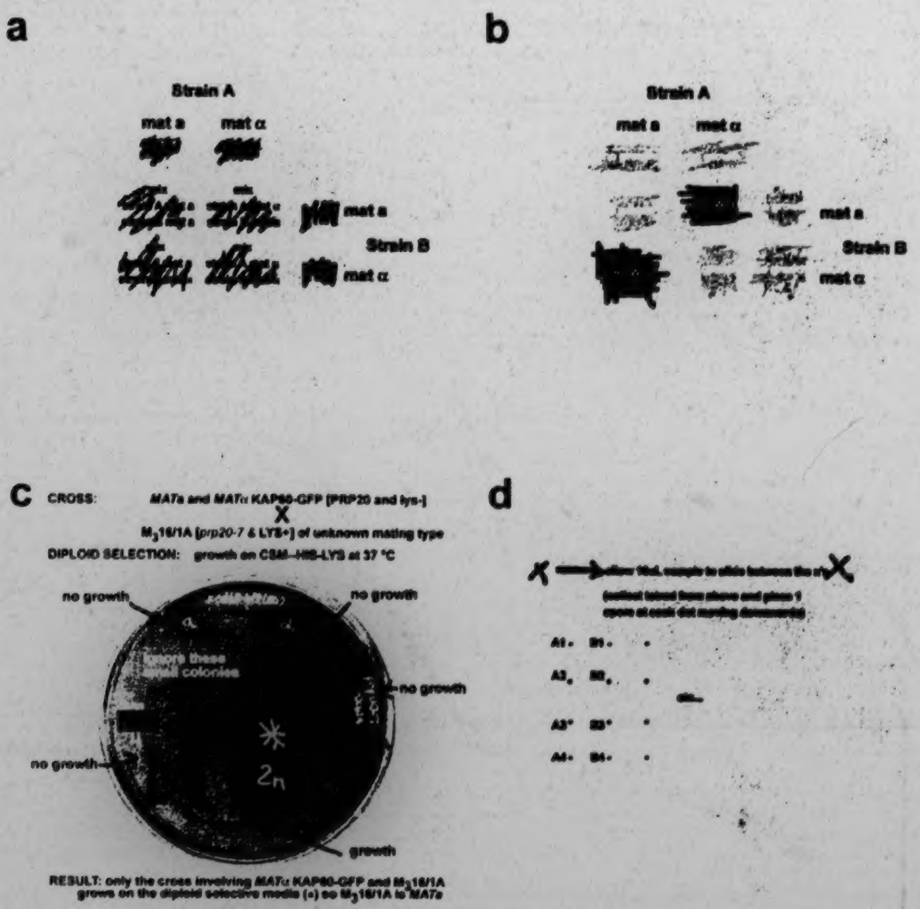
a
Strain A
mat a
mat α
mat a
Strain B
mat α
b
Strain A
mat a
mat α
mat a
Strain B
mat α
c
CROSS:
MATa and MATα KAP60-GFP [PRP20 and lys-]
X
$M_3$16/1A [prp20-7 & LYS+] of unknown mating type
DIPLOID SELECTION: growth on CSM–HIS-LYS at 37 °C
no growth
no growth
ignore these
small colonies
no growth
no growth
2n
growth
RESULT: only the cross involving MATα KAP60-GFP and $M_3$16/1A grows on the diploid selective media (+) so $M_3$16/1A is MATa
d
A1
B1
A2
B2
A3
B3
A4
B4

Figure 5-1. Strain generation by mating, sporulation and tetrad dissection. (a) Strains to be mated are arrayed in a controlled fashion onto rich non-selective media, grown overnight and then replica plated onto media selective for diploids, giving rise to the expected growth pattern shown in (b). (c) A typical cross result. (d) For tetrad microdissection, a small amount of zymolyase-treated sporulated culture was spread onto a YPD plate, such that individual well isolated tetrads could be identified. Tetrads (typically 8-12) were transferred to a fresh region of agar and the spores from each were separated and arrayed linearly, as diagramed.

Diploid strains were grown O/N in selective media at RT, centrifuged at 1,000*g* for 5 min to pellet cells, washed once with water, and then resuspended in a volume of selective media containing 2 % acetate in place of glucose to a final volume resulting in a cell dilution of 1:10. Diluted cells were grown at RT for 8 hrs, centrifuged and washed as above, resuspended in sporulation media to OD_{600} ~ 0.1 and grown at RT until spores formed (usually 4 – 6 days). Tetrads were prepared for dissection by digesting asci with zymolyase 100T (MP Biomedicals) as follows: 50 µL of the sporulated cell culture was added to 500 µL water, cells were pelleted by centrifugation at 10,000*g* for 1 min and washed with an additional 500 µL of water and then resuspended to 500µL with water. 50 µL of this diluted cell suspension was further diluted into 250 µL water and 3 µL of 2 µg/µL zymolyase 100T was added making the total sample volume 300 µL and a final concentration of zymolyase 100T of 20 ng/µL). This mixture was incubated at RT for 20 – 30 min without agitation and after digestion, 10 µL of the cell mixture was carefully spotted onto a YPD plate, allowed to air-dry for 5 min and then between 6 and 12 tetrads were located and microarrayed as diagrammed in Figure 5-1c using an Eclipse E400 microscope fitted with microdissecting stage (Nikon). Spores were allowed to germinate and form colonies by incubation at RT for 3 - 5 days after which they were restreaked onto selective media to determine each spore's genotype. Only spores from tetrads that exhibited the expected pattern of marker segregation were selected for further experiments.

5.2.2. Agarose gel electrophoresis

Running buffer and agarose gels contained 1XTAE buffer [40 mM unbuffered (dissolved in water, pH unadjusted) Tris base (Fisher), 20 mM sodium acetate (Fisher), 1 mM EDTA (Fisher), final unadjusted pH 7.6 - 7.8)]. For optimal resolution of DNA species, agarose gel concentrations were DNA < 2 kb → 1.5 % agarose; 2 kb < DNA < 6 kb → 1.0 %; DNA > 6 kb → 0.8 %. Samples were loaded in 1X DNA loading dye [1.7 mM TrisHCl (pH 7.6); 0.005 % bromophenol blue (Sigma-Aldrich); 0.005 % xylene cyanol FF (Sigma-Aldrich); 10 % glycerol (Fisher); 10 mM EDTA] and ran at 80 V for at least 1 hr. Gels contained 0.4 µg/mL of the intercalating agent, ethidium bromide (Fisher), to allow DNA visualisation under UV light.

5.2.3. SDS-polyacrylamide gel electrophoresis

Proteins, dissolved in 1X SDS-PAGE sample buffer [10 % v/v glycerol, 62.5 mM TrisHCl (pH 6.8), 2 % w/v SDS (Fisher), 5 % v/v βMe (MP Biomedicals), 0.025 % w/v bromophenol blue] or Magic A/B [500 mM unbuffered Tris base, 6.5 % w/v SDS, 15 % v/v glycerol, 100 mM DTT (Fisher), 0.025 % w/v bromophenol blue] were heated to 65 °C for 15 min prior to being resolved over 4-15 % acrylamide gradients using pre-cast TrisHCl ReadyGels in the mini-PROTEAN 3 apparatus (Bio-Rad) in running buffer [25 mM unbuffered Tris base, 192 mM glycine (Fisher), 0.1 % SDS, final unadjusted pH ~ 8.3]. Loading volumes ranged between 2 and 30 μL. Gels were run at a constant voltage of 222 V for 30 min, at which point the bromophenol blue dye front reached the bottom of the gel. With the exception of gels destined for immunoblot analysis (Section 5.2.10), proteins were visualised by incubation with Coomassie blue stain solution [10 % v/v acetic acid (Fisher), 45 % v/v methanol (Fisher), 0.1 % w/v Coomassie brilliant blue R-250 (Fisher)] for ≥ 2 hrs followed by incubation in destain solution [10 % v/v acetic acid, 45 % v/v methanol] for ≥ 2 hrs or, in cases where proteins were present at very low abundance, gels were silver stained as follows: Gels were dehydrated in 50 % v/v methanol with gentle mixing for ≥ 1 hr, rehydrated for 15 min by mixing in silver stain solution [20 mM NaOH (Fisher), 110 mM NH_4OH (Electron Microscopy Sciences), 0.8 % $AgNO_3$ (Electron Microscopy Sciences)], washed 3 times with gentle agitation in water for 5 min each time, incubated in developer [0.0185 % w/w formaldehyde (Fisher), 0.005 % w/v citric acid (Fisher)] with mixing until proteins became visible (usually 10 min), after which the developing reaction was stopped with destain solution (above).

5.2.4. PCR amplification of DNA

Polymerase chain reaction amplification of target DNAs were achieved using the Expand High Fidelity PCR System (Roche). Reactions mixtures contained 0.04 U/ μL enzyme, ~10 ng/μL template, 0.2 mM each dNTP (10 mM stock from Fermentas), 1.5 mM $MgCl_2$ and 1 μM each oligonucleotide. Standard melting, annealing and elongation temperatures and times were, respectively, 95 °C for 45 sec, 50 °C for 45 sec and 69 °C for X sec, where X is calculated based on a 1 kb/min polymerase processivity using the formula: $\text{time}_{\text{elongation}}$ = **[target length in kb • 60** sec/min]/[1 kb/min]. PCR reactions typically consisted an initial 95 °C melting period of 5 min, followed by 30 cycles at the conditions given above and, lastly, a 5 min elongation at 69 °C to complete any partial products. In the rare instances where PCR product yield was low or not obtained using the above conditions, the reactions were troubleshot by lowering annealing temperatures, adding additional cycles, increasing the Mg^{2+} ion concentration or adding up to 5 % v/v DMSO (Fisher).

5.2.5. Transformation of DNA into yeast and bacteria.

Bacterial transformations were performed using commercially available heat-shock competent cells using manufacturer's suggested protocols. Subcloning efficiency DH5α competent cells (Invitrogen) were used for routine work (ligations, plasmid maintenance and DNA preparations), whereas BL21(DE3) pLysS competent cells (Novagen) were employed for expression and purification of GST fusions.

Yeast transformations were performed by either of two established methods, electroporation[236] or lithium acetate (LiAc) transformation[237]. For electroporation, O/N yeast cultures were grown in selective liquid media for null strains and strains already harbouring plasmids or unselective media (YPD) where no selectable markers were available or required. These cultures were diluted 1:100 into liquid YPD and grown to OD_{600} ~ 1.0 (~ 2 X 10^7 cells/mL) at which point they were centrifuged at 1,000*g* for 5 min at 4 °C, washed twice with water, resuspended in a 100 mM LiAc (Sigma-Aldrich)/10 mM TrisHCl (pH 7.4)/1 mM EDTA solution and incubated for 15 – 30 min at RT with gentle rotation. After this initial incubation, DTT was added to a final concentration of 20 mM and the cells were incubated for an additional 15 – 30 min under the same conditions. Cells were pelleted, as above, and kept on ice for the remainder of the procedure. Cells were washed twice with pre-chilled water, twice with 1 M sorbitol (Acros) and then resuspended in 1 M sorbitol to a final volume equal to twice the packed cell volume. For each transformation, 50uL of this cell solution was mixed with ~ 1 μg of purified, salt-free DNA (plasmid or PCR product) and transferred to a Gene Pulser 2 mm gap-width electroporation cuvette (Bio-Rad). Electroporation was performed with a MicroPulser (Bio-Rad) using the Fungi:Sc2 setting (1.5 keV, usually resulting in a time constant of 4 ms). The cells were then plated on selective media allowing only the growth of transformed cells and incubated until colonies have formed (usually 72 hrs), except for transformations involving *KAN*^{R} or *NAT*^{R} selectable markers, in which case cells were recovered O/N on YPD followed by replica plating onto media containing G418 or cloneNAT, respectively, to allow growth of only transformed cells.

For LiAc transformations, cells were prepared as above up to and including the initial washes with water. Cells were then washed twice with 100 mM LiAc, resuspended in 100 mM LiAc to a total volume equal to five times the packed cell volume and ssDNA (Ambion) was added to a final concentration of 1 μg/μL. For each transformation, 25-50 μL of this cell/ssDNA mixture was incubated with 1 - 5 μg of ≥ 1 μg/μL purified plasmid DNA or PCR product at 30 °C for 15 min. The total volume of this mixture is henceforth referred to as 1 volume. After the initial incubation, 5 volumes of a 100 mM LiAc/40 % PEG-8000 (Fisher) solution was added and the cells were incubated at 30 °C for an additional 30 min. Cells were then heat shocked by the addition of $^2/_3$ volume of DMSO and incubation at 42 °C for 20 min, after which cells were pelleted, resuspended in 75 μL water and plated as described for electroporation transformations.

5.2.6. Yeast protein extract preparation

Whole cell protein extracts destined for immunoblot analysis to confirm tagged-fusions and knock-outs were prepared as follows. Liquid cultures containing cells in the late logarithmic growth phase (~3 X 10^7 cell/mL) were harvested by centrifugation (20,000*g* for 30 sec in a microcentrifuge for volumes < 2 mL or 5,000*g* for 5 min with larger volumes). The cell pellet was fully resuspended in 1/10th volume in cracking buffer [1.85 M NaOH (Fisher), 7.4 % v/v βMe] and incubated on ice for 5 min (NOTE: '1 volume' is the volume of liquid culture from which cells were initially harvested; thus, the cell pellet from a 2 mL culture would be resuspended in 200 µL of cracking buffer). Next, 1/10th volume of 50 % TCA (Fisher) was added, the solution was mixed and then spun at 20,000*g* for 10 min at 4 °C to pellet precipitated protein and cellular debris. The pellets were overlaid with ½ volume of water for 2 min to aid in the removal of excess TCA, spun for 1 min at 20,000*g* and then the pellets were resuspended in 1/20th volume of Magic A/B buffer [500 mM unbuffered Tris base, 6.5 % w/v SDS, 15 % v/v glycerol, 100 mM DTT, 0.025 % w/v bromophenol blue] and heated at 65 °C for 15 min to aid protein solubilisation and hydrolysis of disulfide bonds. Since these samples contain a colloidal suspension of cellular debris, the tubes were spun for 30 sec at 20,000*g* just prior to SDS-PAGE analysis. Typically, between 2 and 10 µL of these protein extracts were loaded per lane.

5.2.7. Yeast genomic DNA isolation

Genomic DNA was purified from yeast as described[238]. Saturated 10 mL cell cultures were centrifuged at 2,000*g* for 5 min and the cell pellets were resuspended in 1 mL of water, transferred to 1.6 mL centrifuge tubes, centrifuged at 10,000*g* for 30 sec and resuspended in 200 µL each of breaking buffer [100 mM NaCl, 10 mM TrisHCl (pH 8.0), 1 mM EDTA, 2 % Triton X-100 (MP Biomedicals), 1 % SDS] and buffer-saturated 25:24:1 phenol-chloroform-isoamylalcohol (Sigma-Aldrich) and ~ 300 µL of acid-washed glass beads (Sigma-Aldrich). Tubes were mixed vigorously for 3 min, 200 µL of gTE [100 mM TrisHCl (pH 8.0), 20 mM EDTA] was then added and the tubes were mixed briefly and spun at 20,000*g* for 5 min. The aqueous upper layer was transferred to a fresh tube containing 1 mL of 100 % ethanol (Aaper Alcohol), mixed briefly and centrifuged at 20,000*g* for 5 min to pellet nucleic acids. The pellets were resuspended in 400 µL of TE [10 mM TrisHCl (pH 8.0), 1 mM EDTA] containing 3 µL of 10 mg/mL RNAse A (Sigma-Aldrich) and incubated at 37 °C for 5 min to digest RNA. After this incubation, 10 µL of 4 M ammonium acetate (Fisher) was added, the solution was mixed, 1 mL of 100 % ethanol was added, the solution was mixed again and finally spun at 20,000*g* for 5 min to pellet the DNA. The pellets were air dried for 5 min at RT and then resuspended in 100 µL TE, of which 1 µL was used for PCR amplifications.

5.2.8. Gene tagging, deletion and marker swapping

Genes were knocked out in various strain backgrounds or tagged endogenously with PrA, GFP or MYC by PCR-based long flanking homology integrations, as depicted in Figure 5-2. For transferring *KAN*^{R} or *NAT*^{R} based null mutations, the *geneX::KAN*^{R} or *geneX::NAT*^{R} cassettes were PCR amplified out of gDNA prepared from corresponding yeast deletion library null mutant strains using short oligonucleotide pairs (~ 20 bases, T_m ~ 60 °C) that anneal 500 bp upstream and downstream of the gene of interest's translational start and stop sites, respectively. The ~ 3 kb PCR products were purified, resuspended in 15 µL water and 2 – 5 µL was transformed into the desired strain background. Colonies that developed on selective media were restreaked onto selective media and then correct integration was confirmed by PCR from gDNA using gene specific oligonucleotides and/or immunoblotting of WCLs (when possible). In cases involving transferal of *geneX::NAT*^{R} cassettes, the corresponding *geneX::KAN*^{R} null mutant strain was first switched to *NAT*^{R} by transforming cells with EcoRI digested p4339[228] (a previously described *KAN*^{R} → *NAT*^{R} switch plasmid) and confirming gain of resistance to nourseothricin and loss of resistance to G418.

To facilitate C-terminal fusions of proteins of interest to PrA, GFP or MYC, we constructed a family of plasmids that use common oligonucleotide sequences for generating any of the above tags. These plasmids, described in detail in section 5.1.3, are pPrA/HIS5 or pPrAHIS3URA3 for PrA fusions, pGFP/HIS5 or pGFP/HIS5U for GFP fusions to GFP and pMYC/HIS5 for fusions to 13 repeats of the c-myc epitope. Forward oligonucleotides (5' → 3') consisted of 40 – 60 bases of homology to the extreme 3' coding region of the gene of interest, up to but not including the stop codon, followed by a common plasmid annealing forward sequence (CGGTGAAGCTCAAAAACTTAAT), while reverse oligonucleotides (5' → 3') were comprised of 40 – 60 bp encoding homology to the reverse complemented sequence from ~ 100 bp downstream of the translational stop site of the gene of interest followed by a common plasmid annealing reverse sequence

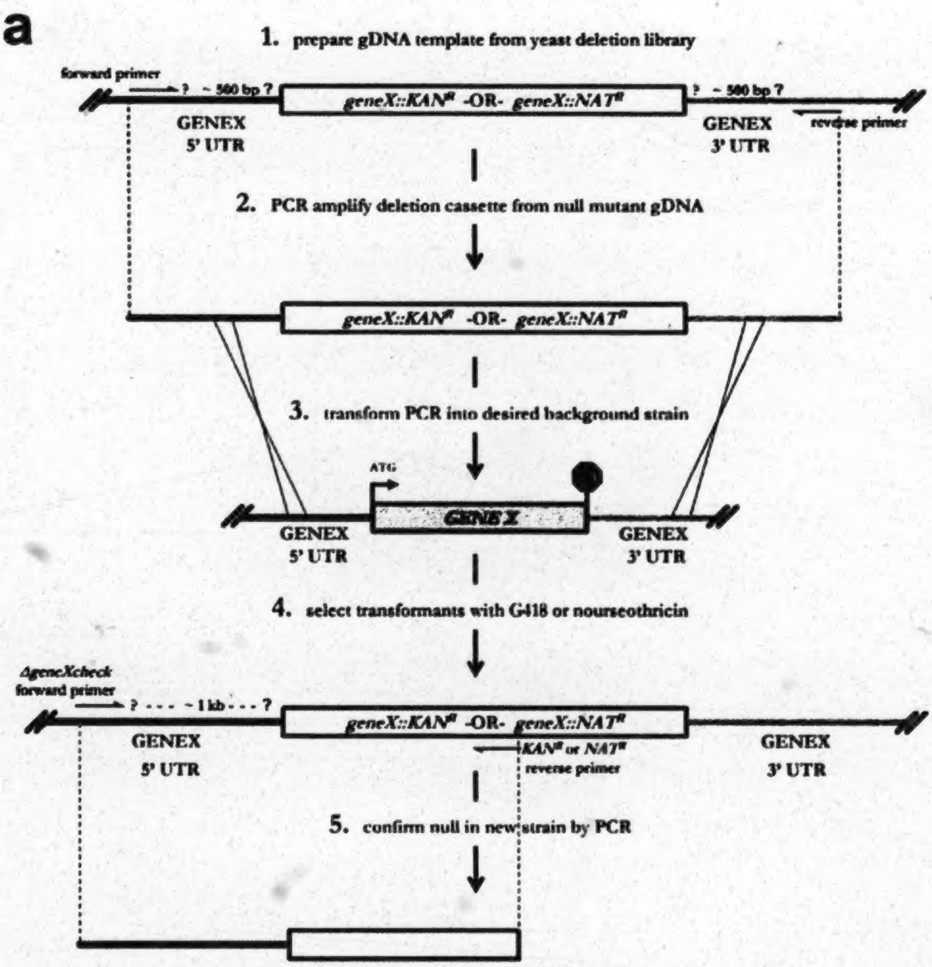
a
1. prepare gDNA template from yeast deletion library
forward primer
? ~ 500 bp ?
geneX::KAN^R -OR- geneX::NAT^R
? ~ 500 bp ?
GENEX 5' UTR
GENEX 3' UTR
reverse primer
2. PCR amplify deletion cassette from null mutant gDNA
geneX::KAN^R -OR- geneX::NAT^R
3. transform PCR into desired background strain
ATG
GENE X
GENEX 5' UTR
GENEX 3' UTR
4. select transformants with G418 or nourseothricin
ΔgeneXcheck forward primer
? - - - ~1 kb - - - ?
geneX::KAN^R -OR- geneX::NAT^R
GENEX 5' UTR
KAN^R or NAT^R reverse primer
GENEX 3' UTR
5. confirm null in new strain by PCR

Figure 5-2. Generation of null strains and strains expressing endogenously encoded fusion proteins. Schematic of the PCR based strategies used to achieve (a) gene deletion (this page) and (b) C-terminal tagging (facing page). See text for details.

(GCTGACGGTATCGATAAGCTT). Together these primers allow amplification of the TAG-HIS5 cassette from the plasmids described above with 5' and 3' extensions that direct site specific integration. PCR reactions were performed, purified and transformed into relevant strains as described above for gene deletion cassette transfers. Correct in-frame integrations and production of full-length fusions were confirmed by western blotting against PrA, GFP or c-myc as required.

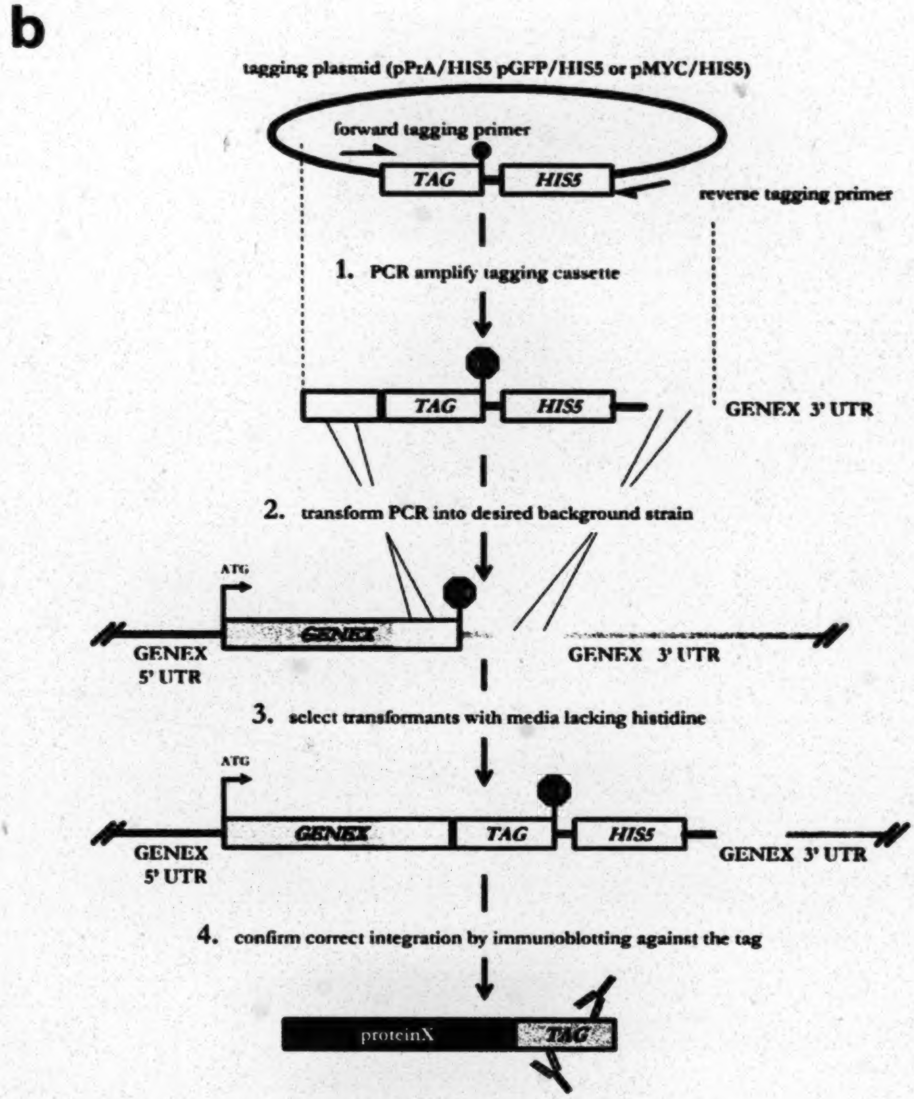
b
tagging plasmid (pPrA/HIS5 pGFP/HIS5 or pMYC/HIS5)
forward tagging primer
TAG
HIS5
reverse tagging primer
1. PCR amplify tagging cassette
TAG
HIS5
GENEX 3' UTR
2. transform PCR into desired background strain
ATG
GENEX
GENEX 5' UTR
GENEX 3' UTR
3. select transformants with media lacking histidine
ATG
GENEX
TAG
HIS5
GENEX 5' UTR
GENEX 3' UTR
4. confirm correct integration by immunoblotting against the tag
proteinX
TAG

5.2.9. Immunoblotting and antibodies

Proteins resolved by SDS-PAGE were transferred to nitrocellulose (Amersham) in modified Towbin transfer buffer [25 mM unbuffered Tris base, 192 mM glycine, 20 % methanol, 0.01 % SDS, unadjusted pH ~8.2][239] using the Mini Trans-Blot Electrophoretic Transfer Cell (BioRad) running at a constant voltage of 100 V for 2 hrs on ice or O/N at a constant current of 100 mA. All subsequent steps were performed at RT. To confirm efficient transfer, immobilised proteins were visualised by immersing in Ponceau stain solution [0.2 % Ponceau S (Fisher), 3 % TCA] for 10 sec and then washing the membrane under running distilled water for ~ 1 min. Residual Ponceau stain was removed by incubation in TBS-T [TBS + Tween-20 = 20 mM TrisHCl, (pH 7.5), 137 mM NaCl, 0.1 % Tween-20 (Fisher)] for 5 min. Nitrocellulose membranes were then blocked in TBS-TM [TBS-T with 5 % skim milk powder (Safeway)] for 30 min, incubated for 2 hrs with TBS-TM containing the primary antibody at the specified dilution (see Table 5-4), washed 3 times for 5 min with TBS-T, incubated with the secondary antibody in TBS-TM at the specified dilution for 1 hr, washed 3 times with TBS-T and immunoreactive bands were visualised with the SuperSignal West Pico ECL kit (Pierce) and either a Fluorchem 8000 digital imager (Alpha Innotech) or autoradiography film (Kodak).

Table 5-4 **Primary and secondary antibodies.**

Name	**Details**	**Source**
αNup2p	Rabbit polyclonal 1° antibody L189 raised against GST Nup2p, used for immunoblotting at 1:1000	[193]
αKap60	Rabbit polyclonal 1° antibody 2652 raised against His$_6$-Srp1, used for immunoblotting at 1:1000	[162]
αGFP	Rabbit polyclonal 1° antibody raised against GFP, used for immunoblotting at 1:5000	[240]
αPrA	Whole rabbit IgG 1° antibody raised against mouse, used for immunoblotting at 1:1000	MP Biomedicals
αMYC$_{western}$	Rabbit polyclonal 1° antibody raised against c-myc, used for immunoblotting at 1:1000	Covance
αMYC$_{ChIP}$	Mouse monoclonal antibody (9E10) raised against c-myc, used in ChIP studies at 1 μg IgG per 10^7 beads	Covance
αGST	Mouse monoclonal antibody raised against *Shistosoma japonicum* glutathione S-transferase, used at 1:2000	Sigma-Aldrich
αrabbit-HRP	Donkey antibody against mouse IgG, conjugated to horseradish peroxidase, 2° antibody used at 1:5000	Amersham
αmouse-HRP	Sheep antibody against mouse IgG, conjugated to horseradish peroxidase, 2° antibody used at 1:5000	Amersham

5.3. Protein interaction studies

5.3.1. GST fusion protein expression and purification

Expression and purification of GST fusion proteins and *in vitro* binding experiments were performed essentially as described[96]. Plasmids encoding GST fusions to Prp20p (pGST-PRP20, Nup2p (pGST-NUP2), cyan fluorescent protein (pGST-CFP) and a NUP2-CFP chimera (pGST-NUP2-CFP) were transformed into the BL21(DE3) pLysS expression strain. Overnight cultures grown at 37 °C in 2XYT+AMP+CAM were diluted 1:100 into 100 mL of 2XYT+AMP+CAM and grown for 4 hours at 37 °C after which isopropyl-1-thio-β-D-galactopyranoside (IPTG) was added to a final concentration of 2 mM and grown for an additional 3 hrs at 23 °C to induce GST protein expression. Cells were harvested by centrifugation at 10,000*g* for 10 min at 4 °C in JA-14 rotor (Beckman), washed once with 100 mL of water and the pellet was snap-frozen in $N_{2(l)}$ and resuspended in 30 mL of ice-cold transport buffer [20 mM HEPES-KOH (pH 7.4) (Fisher), 110 mM potassium acetate, 2 mM $MgCl_2$ (Fisher), 1 µM $CaCl_2$ (Sigma-Aldrich), 1 µM $ZnCl_2$ (Fisher), 1 mM EDTA, 1 mM DTT, 0.1 % w/v Tween-20 and 1:100 solutionP[51] (protease inhibitor stock 0.4 mg/mL pepstatin A (Fisher), 18 mg/mL phenylmethylsulfonyl fluoride/PMSF (Boehringer Mannheim)]. Once thawed, complete lysis was achieved by sonication on ice with a Sonifier 250 (Branson) equipped with the standard probe (not microtip) using 50 % duty at a power setting of 6 for a total of 2 min. The lysate was clarified by centrifugation first at 2,500*g* for 15 min at 4 °C in 50 mL Falcon tubes then at 17,000*g* for 20 min at 4 °C using a JA-17 rotor (Beckman). The supernatants were divided into 5 mL aliquots, snap-frozen in $N_{2(l)}$ and stored at -80 °C until use.

To purify GST fusions from clarified bacterial lysates, 50 µL of glutathione Sepharose (GT-Sepharose) was washed 3 times with 1 mL of transport buffer, resuspended in 100 µL transport buffer and added to bacterial lysates that were thawed on ice. The beads were incubated with the lysates for 1 hr at 4 °C with rotation, centrifuged at 4 °C for 1 min at 3000*g*, the supernatant was removed and the beads were washed 8 times with 1 mL transport buffer to remove any unbound proteins. Proteins bound to the GT-Sepharose were then treated in one of three ways: (1) GST fusions were eluted from the beads by incubation in 100 μL of glutathione elution buffer [10 mM reduced glutathione (Fisher) in 50 mM TrisHCl (pH 8.0)] for 10 minutes, followed by centrifugation through a Micro Bio-Spin chromatography column (Bio-Rad) to remove the Sepharose beads; (2) proteins fused to GST were eluted by cleavage at the thrombin site, achieved by incubation with 1 U of thrombin (Sigma-Aldrich) for 30 min at RT, followed by the addition of 3 U of hirudin (Sigma-Aldrich) to inactivate the thrombin protease, which releases the protein of interest from the Sepharose resin, but not the GST moiety. Again the eluted proteins were removed from the resin by centrifugation through a Micro Bio-Spin chromatography column; (3) GST-fusion proteins were left bound to the GT-Sepharose when they were to be used as bead-bound baits in binding experiments (see below). In all cases, full-length production of fusion proteins and purity were assessed by SDS-PAGE and Coomassie blue staining.

5.3.2. *In vitro* GST binding studies

The ability of bacterially expressed and purified Prp20p to associate directly with Nup2p was assessed as follows. GST, GST-Nup2p and GST-Prp20p were purified from bacterial lysates. Prp20p was cleaved from the beads by thrombin cleavage while the GST and GST-Nup2p fusions were left bound to the GT beads after the wash stages, as described above. Approximately 4 μg of resin-immobilised GST or GST-Nup2p was incubated with 4 μg of purified Prp20p in a total volume of 50 μL of transport buffer for 30 min. The unbound supernatant (~50 μL) was removed and added to 17 μL of 4X SDS-PAGE sample buffer (UNBOUND fraction), the beads were then washed 4 times with 1 mL of transport buffer and proteins still bound to the beads were eluted by the addition of 50 μL of transport buffer and 17 μL of 4X SDS-PAGE sample buffer (BOUND fraction). The BOUND and UNBOUND fractions were heated at 65 °C for 15 min, centrifuged through Micro Bio-Spin chromatography columns and 20 μL was resolved by SDS-PAGE and visualised by Coomassie blue staining.

5.3.3. Yeast whole cell lysate immunopurifications

The development of robust immunopurification procedures was an ongoing process during the course of these studies; therefore, the following describes the various methods employed at each stage the immunopurification process, which essentially consists of seven stages outlined sequentially below: (1) cell growth and harvesting, (2) cell lysis, (3) whole cell extract clarification, (4) binding of PrA fusions to IgG beads, (5) bead washing and elution of bound proteins, (6) precipitation of eluted proteins and (7) mass spectrometric identification of proteins present in eluates.

CELL GROWTH AND HARVESTING. PrA-tagged strains were grown to late log phase (~5 X 10^7 cells/mL) in 2 L cultures and cells were harvested by centrifugation at 5,000*g* for 5 min at 4 °C using a JLA-10-500 rotor (Beckman), the pellets were brought up to a total volume of 50 mL with water, transferred to a 50 mL Falcon tube and spun at 3,000*g* for 5 min at 4 °C in a JS-4.2 rotor (Beckman). Based on the volume of the cell pellet, IP lysis buffer [20 mM Na_2HPO_4 (pH 7.5), 150 mM NaCl, 0.1 mM $MgCl_2$ and 1:200 soultionP] was added to 15 % v/v final cell density.

CELL LYSIS. Efficient cell lysis was achieved by passing the mixture either three times through a French pressure cell (Thermo Electron) at a setting of 1000 (20,000 Ψ) or passed 7 times through a model M-110S microfluidiser (Microfluidics) at an input pressure of 115 Ψ (output = 20,000 Ψ), both of which routinely achieved > 90 % lysis.

WHOLE CELL EXTRACT CLARIFICATION. Lysates were brought up to 20 % v/v DMSO and 5 % v/v Triton X-100 in lysis buffer from pure DMSO, 20 % v/v Triton X-100 and 10X IP lysis buffer stocks using the following equations:

$$V_{20\%\ \text{Triton X-100}} = {}^{9}/_{130}\bullet V_{\text{post}} \qquad V_{100\%\ \text{DMSO}} = {}^{18}/_{65}\bullet V_{\text{post}}$$

$$V_{10\text{X IP LB}} = {}^{1}/_{26}\bullet V_{\text{post}} \qquad V_{\text{post}} = \text{post lysis volume}$$

The solution was next mixed vigorously for 30 sec and clarified by one of two methods: a two step procedure of centrifugation at 15,000 rpm for 15 min at 4 °C in a JA25.50 rotor (Beckman) followed by further clarification at 45,000 rpm for 90 min in a Type70 Ti rotor (Beckman) or, alternatively, a single step procedure of 3,000*g* for 30 min at 4 °C in a JS-4.2 rotor.

BINDING OF PrA FUSIONS TO IgG BEADS. PrA chimeras were immunopurified from clarified supernatants by incubation for 4 to 16 hrs at 4 °C with rotation with either a 50 μL bed-volume of IgG-Sepharose (Amersham) or 5 X 10^7 IgG-coated Dynabeads. IgG Sepharose was prepared for use by washing 3 times with IP lysis buffer (without DMSO and Triton X-100) and M-280 Tosylactivated Dynabeads (Dynal) were coupled to rabbit, affinity-purified antibody to mouse IgG (MP Biomedical) by manufacturer's supplied protocols.

BEAD WASHING AND ELUTION OF BOUND PROTEINS. After binding O/N, the Sepharose or magnetic beads were pelleted by centrifugation at 3,000*g* for 5 min at 4 °C and washed and eluted by one of two methods. Regardless of the method used, immunopurifications involving Sepharose beads utilised centrifugation at 3,000*g* for 30 sec at 4 °C to pellet beads between washes, whereas those involving Dynabeads utilised a magnetic apparatus to separate beads from the wash fractions. In the first wash/elution procedure, the beads were washed in 8-fold with 1 mL of M50 IP wash buffer [20 mM Na_2HPO_4 (pH 7.5), 150 mM NaCl, 50 mM $MgCl_2$, 0.1% v/v Tween-20, 2 μg/mL pepstatin A and 90 μg/mL PMSF] and then all remaining proteins were eluted by incubation in 100 μL of 0.2 % w/v SDS for 5 min at 45 °C. Alternatively, bound proteins were eluted over a Mg^{2+} gradient by washing the beads 3 times with 0.5 mL of M25 IP wash buffer (identical to M50 IP wash buffer, except containing 25 mM $MgCl_2$ instead of 50 mM), then 3 times with 0.5 mL of M50 IP wash buffer, then sequentially with 0.5 mL each of M100, M200, M500 and M1000 IP wash buffers, 0.2 mL of M2000 IP wash buffer and finally with 0.1 mL of M4000 IP wash buffer.

PRECIPITATION OF ELUTED PROTEINS. In all cases, eluate fractions were brought to 1 mL with ice cold water and TCA precipitated by adding 100 μL of 1.5 % sodium deoxycholate (Fisher), mixing, adding 200 μL of 50 % TCA, mixing, incubating the samples on ice for 1 hr after which proteins were pelleted by centrifugation at 20,000*g* for 30 min at 4 °C. The pellets were washed by colloidal resuspension of the pellet in 100 μL ice cold water and the addition of 900 μL of ice-cold, neat acetone. The solution was mixed, incubated at -20 °C for 2 hrs and then centrifuged at 20,000*g* for 30 min at 4 °C. The resulting pellets were air dried for 20 min at RT or dried in a vacuum centrifuge for 5 min.

MASS SPECTROMETRIC IDENTIFICATION OF PROTEINS PRESENT IN ELUATES. Proteins present in eluates were resolved by SDS-PAGE and Coomassie blue visible bands were excised, subjected to in-gel digestion and prepared for LC-MS/MS or MALDI-TOF MS identification using previously described methods[4,241,242]. Briefly, gel slices were washed 3 times for 5 min in distilled water to remove soluble ions and the gel slices were dried to completion with a vacuum centrifuge. Each dried gel slice was rehydrated in ice for 30 min with 100 μL of 50 mM ammonium bicarbonate (AMBIC), pH 9, containing 1 μg of porcine sequencing grade trypsin (Promega), after which the supernatant was removed, 100 μL of fresh 50 mM AMBIC was added and the samples were incubated overnight at 37 °C. The following morning, the supernatant was collected and peptides were further extracted by 4 successive incubations in 100 μL 50 % acetonitrile in water. These liquid fractions were pooled and vacuum centrifuged to dryness at which point the samples were ready for MS/MS analysis. In cases where protein composition was determined without SDS-PAGE, protein pellets were resuspended in 100 μL 50 mM ammonium bicarbonate, pH 9, containing 2 ng/μL porcine sequencing grade trypsin (Promega), incubated at 37 °C O/N, dried in a vacuum centrifuge at which point peptides were identified by LC-MS/MS. Samples were analyzed either by members of the Chait laboratory at the Rockefeller University or by the Proteomics facility at the Institute for Systems Biology.

5.3.4. Prp20p-nucleosome complex formation with Nup2p

The ability of bacterially expressed and purified fusions to associate with the Prp20p-nucleosome complex was determined by two complementary methods. First, Prp20p-PrA was immunopurified from yeast whole cell lysates using the microfluidiser/single-step clarification/Dynabead method described above, but the complex was not eluted from the Dynabeads after washing; rather, the beads were washed additionally twice with transport buffer[96] (see also section 5.3.1 and 5.3.2), divided into equal fractions and incubated for 30 min at RT with the indicated GST-fusion proteins in transport buffer at a total volume of 50 μL. The unbound fraction was collected and mixed with 17 μL 1X SDS-PAGE sample buffer. The beads were washed 4 times with transport buffer and then eluted with 67 μL 1X SDS-PAGE sample buffer to obtain the bound fraction. Samples were heated to 65 °C for 15 min and then resolved by SDS-PAGE, transferred to nitrocellulose and GST-containing proteins and Prp20p-PrA were identified by immunoblotting using a monoclonal mouse antibody directed against GST (Sigma-Aldrich). In the second experiment, performed by Richard Rogers at the Institute for Systems Biology, GST-CFP and GST-Nup2p-CFP were immobilised on glutathione-Sepharose beads and incubated with yeast lysates prepared by the microfluidisation/single-step clarification procedure described above using cells expressing Prp20p-PrA. The presence of Prp20p-PrA in the bound and unbound fractions was determined by immunoblotting with rabbit affinity purified antibody to mouse IgG (Cappel).

5.3.5. Prp20p-nucleosome complex histone modification analysis

Histone acetylation and methylation levels were determined as part of a collaboration with Alan Tackett at the Rockefeller University as described[202,204,205].

5.4. Genetic interaction studies

5.4.1. *NUP2-NUP60* interactions

NUP2-NUP60 genetic interactions were analyzed by testing for dependency on a *URA3* based plasmid encoding full-length Nup2p (pLDB60). WT, *Δnup2*, *Δnup60* and *Δnup2*/*Δnup60* spores harbouring pLDB60 were obtained by sporulation and tetrad dissection of the diploid resulting from a LDY627 X JAY1331 cross (*Δnup2* X *Δnup60*) that was transformed with pLDB60 prior to sporulation. Strains of each genotype were spotted at hundred-fold serial dilutions onto YPD, to ensure viability, and CSM+FOA, to test for the ability to grow without plasmid-encoded *NUP2* on pLDB60. Cells that cannot lose the plasmid (i.e. cells that are dependent on *NUP2* expression from this plasmid) will also maintain plasmid-based expression of *URA3* and therefore will not grow on media containing the toxic uracil analog 5-FOA. In contrast, strains whose viabilities are not dependent on production of Nup2p grow on CSM+FOA.

Similarly, we generated WT, *Δnup2*, *Δnup60* and *Δnup2*/*Δnup60* strains expressing a truncated version of Nup2p that lacks its RBD, Nup2p[aa1-546] from the *TRP1*-based plasmid, pLDB690 and tested the viability of each strain at different growth temperatures (23 °C, 30 °C and 37 °C). The specific inability of *Δnup2*/*Δnup60* double mutants expressing Nup2p[1-542] to grow at 37 °C indicates that this fragment of Nup2p can partially overcome the synthetic lethality between *NUP2* and *NUP60* as these cells are viable at 23 °C and 30 °C.

5.4.2. ***NUP60-KAP60*** **interactions**

To assess *NUP60-KAP60* genetic interactions, we crossed JAY1331 (*Δnup60*) to NOY612 (*srp1-1*, at temperature-sensitive allele of *KAP60*), sporulated this diploid and analyzed the viability of WT, *Δnup60, srp1-1 and Δnup60*/*srp1-1* spores at 23 °C, 30 °C and 37 °C. The *srp1-1* allele alone is inviable at 37 °C but viable at 23 °C and 30 °C; in contrast, when combined with deletion of *NUP60*, the *srp1-1* allele is inviable at 30 °C as well as 37 °C indicating a genetic interaction between these genes.

5.4.3. ***NUP2-NUP60-PRP20-HTZ1*** **interactions**

We tested for genetic interactions between *NUP2, NUP60, PRP20, HTZ1* and the negative control, *NUP53*, by observing the growth rates of strains harbouring single and double mutant combinations these genes at various temperatures (23 °C, 30 °C and 37 °C). A genetic interaction is indicated by decreased growth of double mutant combinations at any of the temperatures tested., relative to the relevant single mutant strains with the exception of those involving *prp20*-7, as this mutation alone confers inviability at 37 °C; thus, only growth differences at 23 °C and 30 °C were analyzed.

5.5. Fluorescence microscopy

5.5.1. Microscope and growth conditions

Unless otherwise indicated, strains harbouring genomically tagged GFP-chimeras were grown at 23 °C in selective media to the mid-logarithmic phase of growth. GFP fluorescence was visualised by confocal microscopy using a Zeiss LSM 510 NLO confocal microscope (Carl Zeiss Microscopy). GFP was excited at a wavelength of 488 nm and emitted light >505 nm was collected using a long-pass filter. Images were compiled and prepared for figures using Photoshop (Adobe).

5.5.2. Heterokaryon mobility assay

Equal volumes of mid-logarithmic growth phase *kar1-1* (*MAT*α) cells and genomically integrated NUP-GFP strains (*MATa*) grown in CSM at 23 °C were mixed and pelleted by brief centrifugation. The cell pellets were resuspended in 200 μL of CSM and incubated for 30 min at RT without agitation to allow mating. Samples were then mixed gently and prepared for confocal microscopy by placing 50 μL on a microscope slide coated with 200 μL of CSM containing 2 % agarose. Coverslips were placed over the samples and sealed to prevent drying. Slides were incubated at RT for an additional 3 hrs to allow mating followed by simultaneous acquisition of GFP fluorescence and bright-field signals for 30 min. Mating cells were scored as shuttling if GFP signal was detected in two well-separated nuclei, non-shuttling if GFP signal was only detected in one nucleus or inconclusive when the nuclei displaying GFP fluorescence were not clearly separated and thus could be confused with the onset of nuclear fission. For time-course shuttling experiments, z-stacks of approximately 5 μm slices were acquired at 20 min intervals (usually 10 slices per time point stack). Analysis was performed using the public domain NIH Image program v1.62 (developed at the U.S. National Institutes of Health and available on at http://rsb.info.nih.gov/nih-image/) essentially as described[173] with the exception that mean nuclear signal measurements were normalised for image acquisition bleaching as determined by signal loss in non-zygotic controls. Averages and error estimates of duplicate measurements were determined with Excel (Microsoft) using the AVERAGE and STDEV functions.

5.5.3. Photobleach-recovery protein turnover assay

Nup2p-GFP (*MATa*) and Nup49p-GFP (*MATa*) cells were grown to the mid-logarithmic phase of growth at 23 °C in CSM-HIS media. Slides were prepared as described in 'Heterokaryon Shuttling Assay'. Cells in a single field of view were photobleached with 30 iterations of the 488 nm wavelength at 40 % power in an area encompassing only the nucleus or the entire cell. Z-stacks, typically 10 slices at 0.5 μm/slice, were acquired pre-bleach, post-bleach and 20, 40 and 60 minutes following bleaching. Data were analyzed with NIH image as for heterokaryon experiments, with the exception that the mean fluorescence of bleached cells was normalised for sample acquisition bleaching by the rate of signal loss in unbleached controls over the course of the experiment.

5.5.4. Galactose induction of Nup60p

The pGAL-NUP60 plasmid was transformed into Nup2p-GFP cells lacking Nup60p and these cells were grown to the mid-logarithmic phase of growth at 23 °C in CSM-HIS-TRP-URA with 2 % glucose. Initial images of uninduced cells were acquired at this time after which, cells were spun down, washed twice with CSM-HIS-TRP-URA containing 2 % galactose and then resuspended in the same media at the initial cell density. Cells were grown for 5 hrs at 23 °C to allow galactose dependent induction of Nup60p and then visualised again.

5.5.5. Quantitation of fluorescent intensity along nuclear bisects

To determine the relative amount of intranuclear signal in Nup2ΔRBD-GFP compared to Nup2p-GFP in WT and Δ*nup60* strains, cells from single confocal slices were analyzed using the 'Plot Profile' tool in NIH image. Lines (4 pixels wide) were drawn to bisect the nucleus; thus, the profiles obtained are the average fluorescent intensity of four adjacent pixels across the length of the nucleus. Profiles were oriented with the nucleolus to the left in cases where the nucleolus was visible due to the exclusion of GFP signal from this organelle. The numerical data were exported to Excel (Microsoft) and montages for 15 cells were compiled. The average and standard deviation of these data were also determined and plotted as an indication of the variability of the nuclear fluorescence.

5.5.6. Metabolic poisoning

Cells were grown to the mid-logarithmic phase of growth at 23 °C in selective media containing 2 % glucose and visualised. After initial image acquisition, cells were centrifuged, washed once with sterile water, resuspended in sterile water containing 10 mM deoxyglucose and 10 mM sodium azide and incubated at RT without agitation (see also (175)). GFP signal was monitored at 15 min intervals for 45 min. Cells were then spun down and recovered in selective media containing 2 % glucose for 10 minutes and visualised again.

5.5.7. *prp20-7* temperature shift

Strains were grown to the mid-logarithmic phase of growth at 23 °C in CSM and slides were prepared for confocal microscopy as described under 'heterokaryon shuttling assay'. Zero time point images were acquired, after which slides were incubated at 37 °C for 90 min and observed. After the temperature shift, cells were recovered at 23 °C for 1 hr and visualised again.

5.6. DNA microarray experiments

5.6.1. mRNA expression microarrays

Expression microarray analyses were performed essentially as described[211,243]. Total RNA was prepared by the hot acid phenol method[238]. Logarithmically growing cells in 50 mL liquid YPD were harvested at an OD_{600} between 0.8 and 1.0 by centrifugation at 1,500*g* for 5 min at 4 °C. Cell pellets were resuspended in 2 mL TES buffer [10 mM TrisHCl (pH 7.5), 10 mM EDTA, 0.5 % SDS], transferred to 14 mL polypropylene snap-cap tubes (Becton Dickinson) containing 2 mL of water-saturated phenol (Fisher) pre-warmed to 65 °C, mixed for 10 sec and incubated at 65 °C for 1 hr with mixing every 10 min. Tubes were incubated on ice for 5 min and centrifuged at 15,000*g* for 5 min at 4 °C. The aqueous (upper) layer was transferred to a new snap-cap tube containing 2 mL fresh water-saturated phenol, mixed and centrifuged as above and this phenol extraction was repeated once more. For each sample, the aqueous layer (~2 mL) was transferred into a clean 14 mL snap-cap tube containing 200 µL (1/10th sample volume) of 3 M sodium acetate (pH 5.2), tubes were mixed and 5 mL (2.5X sample volume) of 100 % ethanol was added. The samples were again mixed and then incubated for 1 hr at -80 °C to facilitate RNA precipitation. Precipitated RNA was pelleted by centrifugation at 15,000*g* for 5 min at 4 °C, mixed in 6 mL ice-cold 70 % ethanol, centrifuged at 15,000*g* for 5 min at 4 °C. The pellets were allowed to air dry for 15 min after which time they were resuspended in 400 µL of DEPC-treated water (Fisher). Quality and yield of total RNA were determined by spectrophotometry and/or formaldehyde-agarose gel electrophoresis. Typical yields were 5 - 10 mg of total RNA with A_{260}/A_{280} ratios of 1.6 – 1.8 when analyzed in DEPC-treated water.

Poly(A)+ RNA was enriched from total RNA with the Poly(A)Pure mRNA purification kit (Ambion) at RT unless otherwise specified using provided protocols and proprietary reagents. Briefly, 2 µg of total RNA was adjusted to a final NaCl concentration of 0.45 M by adding 1/10th volume of a 5 M NaCl solution and then brought up to a final volume of 4 mL with 'Binding Buffer' in a 15 mL Falcon tube (Fisher), mixed and heated for 5 min at 65 °C. One vial of oligo(dT) cellulose was added and the slurry was incubated with rotation for 60 min. After the incubation period the oligo(dT) cellulose was pelleted by centrifugation at 4,000*g* for 3 min at and washed three times with 10 mL of 'Binding Buffer', three times with 10 mL 'Wash Buffer'. After the final wash, the oligo(dT) cellulose pellet was resuspended in 0.6 mL 'Wash Buffer', transferred to a supplied 2 mL microcentrifuge spin column and spun at 5,000*g* for 30 sec to force the 'Wash Buffer' though the column. The oligo(dT) cellulose was washed similarly an additional two times with 0.5 mL 'Wash Buffer' and then eluted twice with 200 µL 'Elution Buffer' [10 mM TrisHCl (pH 7.5), 1 mM EDTA] pre-heated to 65 °C. The enriched mRNA was precipitated by the mixing 0.1 volumes (40 µL) of 5 M ammonium acetate and 1 µL of supplied glycogen with the 400 µL mRNA eluate, the subsequent addition of 1.1 mL of 100 % ethanol, followed by incubation for 30 min at -80 °C and centrifugation for 20,000*g* for 20 min at 4 °C. The pelleted RNA was mixed briefly in 1 mL ice-cold 70 % ethanol, spun at 20,000*g* for 20 min at 4 °C, air-dried for 15 min at RT and finally resuspended in 20 µL of DEPC-treated water. Quality and yield of total RNA were determined by spectrophotometry in DEPC-treated water. Typically, 40 – 80 μg of poly(A)+ enriched RNA with an A_{260}/A_{280} ratio of ~1.8 was obtained.

From enriched mRNA, Cy3 and Cy5 labeled cDNAs were prepared with SuperScript II RNAse H: reverse transcriptase (Invitrogen) by incorporation of Cy-dUTP into reverse transcribed cDNA. Four micrograms of poly(A)+ enriched RNA was mixed with 2 μL of 0.5 μg/μL oligo$(dT)_{12\text{-}18}$ and 2 μL of 3 μg/μL random 6-9mers (Invitrogen) in total reaction volume of 10 μL. This mixture was heated at 70 °C for 10 min, chilled on ice for 30 sec and 9 μL of a premixed solution consisting of 4 μL of 5X Superscript RT reaction buffer, 2 μL of Cy3-dUTP or Cy5-dUTP (Amersham), 2 uL of 0.1 M DTT and 1 μL of lowT-dNTPs [10mM each of dATP, dCTP and dGTP and 1 mM dTTP]. This 19 μL reaction solution was incubated at RT for 10 min, 1 μL of SuperScript II RNAse H: reverse transcriptase was then added and the mixture was incubated for 3 hrs are 42 °C in the dark. The reaction was terminated by the addition of 1 μL 0.5 M EDTA and the mRNA template was hydrolyzed with 1 μL of 5 M NaOH and incubation at 37 °C for 10 min. The reaction mixture was neutralised and buffered by the addition of 1 μL of 5 M HCl followed by 5 μL of 1 M TrisHCl (pH 7.0). Labeled cDNA was purified using a QIAquick PCR purification kit (Qiagen), typically yielding 100 – 200 pmol of label quantified by spectrophotometry using the equations: $\text{pmol}_{Cy3} = [A_{550} \bullet v_{probe}(\mu L)]/0.15$ and $\text{pmol}_{Cy5} = [A_{650} \bullet v_{probe}(\mu L)]/0.25$

For mRNA expression microarrays, 40 pmol each of Cy3 and Cy5 labels were mixed and reduced to ~3 μL with a vacuum centrifuge (Savant) and the remaining stages are described in section 5.6.3.

5.6.2. Genome localisation microarrays (ChIP-CHIP)

ChIP-CHIP experiments were performed as described[213] and available at: http://jura.wi.mit.edu/young_public/regulatory_network/Location_analysis_protocol.pdf up to microarray hybridisations. Mid-logarithmic growth phase cells were cultured in 50 mL YPD to OD = 0.8, at which point 1.37 mL of 37 % formaldehyde solution (Fisher) was added to the media (1 % final formaldehyde concentration). The liquid was transferred to a 50 mL Falcon tube and incubated at RT for 20 minutes with rotation followed by O/N at 4 °C with rotation. The following morning cells were pelleted by centrifugation at 2,000*g* for 5 min and the pellets were resuspended in 1 mL TBS, transferred to 1.6 mL microcentrifuge tubes, spun at 20,000*g* for 15 sec and the supernatants were removed. This wash was performed an additional 4 times, after which cells were resuspended in 700 μL ChIP lysis buffer [50 mM HEPES-KOH (pH 7.5), 140 mM NaCl, 1 mM EDTA, 1 % v/v Triton X-100, 0.1 % w/v sodium deoxycholate, and 1:100 of solutionP], ~ 700 μL of acid washed glass beads were added and tubes were mixed for 2 hrs at 4 °C to lyse cells. The base of each tube was punctured with an ~ 18 gauge needle, placed into fresh microcentrifuge tubes and centrifuged at 5,000*g* for 20 sec to collect the cell lysate. DNA was sheared at 4 °C by repeated sonication with a Sonifier 250 (Branson) equipped with a microtip probe and using constant duty at a power setting of 1.5 for 20 sec for a total of 4 cycles, with incubation on ice for at least 30 sec between cycles. The lysates were clarified by centrifugation at 20,000*g* for 5 min at 4 °C and the supernatant was transferred to a fresh microcentrifuge tube. Of this, 20 μL was placed in a separate tube and stored at -20 °C until the following day to be used as the 'WCL' control sample and 30 μL of magnetic beads were added to the remaining liquid (~ 700 μL) and incubated O/N at 4 °C with rotation.

Beads were prepared as follows: On the day of cell harvesting, 50 μL (2 X 10^7 beads) of pan-mouse IgG coupled M-450 Dynabeads (Dynal) were washed twice with 3 mL PBS-BSA [137 mM NaCl, 2.7 mM KCl, 10 mM Na_2HPO_4, 2 mM KH_2PO_4, 5 mg/mL BSA] using a magnetic apparatus, resuspended in PBS-BSA (250 μL per sample) containing 2 μg of mouse anti-c-myc 9E11 antibody (Covance) and incubated O/N at 4 °C with rotation to allow the anti-myc IgG to bind to the beads. The following morning (i.e. on the day of glass bead lysis), the beads were washed twice with 3 mL of PBS-BSA, resuspended in 30 μL PBS-BSA and added to the 700 μL whole cell lysate samples.

After O/N incubation with the whole cell lysates, Dynabeads were washed sequentially, twice with 1 mL ChIP lysis buffer, twice with 1 mL ChIP high salt lysis buffer [50 mM HEPES-KOH (pH 7.5), 500 mM NaCl, 1 mM EDTA, 1 %

Triton X-100 and 0.1 % w/v sodium deoxycholate], twice with 1 mL ChIP wash buffer [10 mM TrisHCl (pH 8.0), 250 mM LiCl, 0.5 % w/v sodium deoxycholate, 0.5 % v/v Nonidet P40 (USB) and 1 mM EDTA] and finally once with 1 mL TE. Bound proteins and DNA were eluted by the addition of 50 µL of ChIP elution buffer [50 mM TrisHCl (pH 8.0), 1 % w/v SDS and 10 mM EDTA] and incubation at 65 °C for 10 min with mixing every 2 min. The eluate, henceforth referred to as the 'IP' sample was transferred to a fresh tube containing 250 µL of ChIP TES [10 mM TrisHCl (pH 8.0), 1 % w/v SDS and 1 mM EDTA], mixed and incubated O/N at 65 °C to catalyze the destruction of formaldehyde crosslinks. Similarly, a control sample, prepared by diluting 10 µL of the 'WCL' sample (stored at -20 °C from the previous day) into 40 µL ChIP elution buffer and 250 µL ChIP TES, was incubated O/N at 65 °C.

Proteins in the sample were digested by the addition of 230 µL of TE, 5 µL of 20 mg/mL glycogen (Fermentas) and 15 µL of proteinase K (Fermentas) and incubation at 37 °C for 2 hrs. Peptides were removed by extraction once with buffer saturated phenol (Sigma-Aldrich) and then once with 24:1 chloroform:isoamyalcohol (Sigma-Aldrich) each time with centrifugation for 5 min at RT to collect protein at the organic-aqueous interface and transferal of the aqueous layer to a fresh tube. After the second extraction, nucleic acids were precipitated by bringing the solution to 200 mM NaCl (20 µL of 5 M NaCl if sample is 500 µL) and adding two volumes of 100 % ethanol (1 mL if sample is 500 µL). The solution was mixed, incubated at -20 °C for 15 min, centrifuged at 20,000*g* for 10 min at 4 °C and the pelleted nucleic acids were washed with 1 mL 70 % ethanol, centrifuged at 20,000*g* for 5 min at 4 °C and the pellet was air dried for 10 min after removal of the supernatant. RNA was degraded by resuspension of the nucleic acid pellet in 30 µL TE containing 10 µg of RNAse A (1 µL of 10 µg/µL RNAse A stock in 30 µL TE) and incubation at 37 °C for 1 hr. The DNA was purified from this solution with a QIAquick PCR purification kit, eluted in 40 µL 10 mM TrisHCl (pH 8.0) and processed for linker mediated PCR amplification of DNA as follows: The samples were first normalised to account for different DNA concentrations between the WCL and IP: the entire

40 μL of the IP sample was used but only 2 μL of the WCL sample was used and brought to 40 μL by the addition of 38 μL of 10 mM TrisHCl (pH 8.0). To each 40 μL normalised sample, 57.3 μL water, 11 μL 10X T4 DNA polymerase buffer (NEB), 0.5 μL BSA, 1.0 μL dNTP mix [10 mM each dATP, dCTP, dGTP, dTTP] (Fermentas) and 0.2 μL T4 DNA polymerase (NEB) were added, making the total volume 110 μL, and the samples were incubated at 12 °C for 20 min to make the DNA ends blunt. Afterwards, 11.5 μL of 3 M sodium acetate (pH 5.2) and 0.5 μL of 20 mg/mL glycogen were added and the solution was extracted with 120 μL of buffer saturated 25:24:1 phenol:chloroform:isoamylalcohol, centrifuged at 20,000*g* for 5 min and the aqueous layer was transferred to a fresh tube containing 230 μL of 100 % ethanol. The solution was mixed, incubated at -20 °C for 15 min, centrifuged at 20,000*g* for 10 min at 4 °C, the DNA pellet was washed with 0.5 mL 70 % ethanol, centrifuged at 20,000*g* for 5 min at 4 °C, the liquid was removed, the pellet was air dried for 10 min and finally resuspended in 25 μL water. To this 25 μL sample, 25 μL consisting of 12.8 μL of water, 5 μL of 10X T4 DNA ligase buffer (Fermentas), 6.7 μL of annealed linkers (see below) and 0.5 μL T4 DNA ligase (Fermentas) was added and the mixture was ligated O/N at 16 °C. Annealed linkers were prepared as follows from oligonucleotides oJW102 and oJW103, which are described in section 5.1.4. A mixture containing 250 μL of 1 M TrisHCl (pH 7.9) and 375 μL each of 40 μM oJW102 and oJW103 stocks was prepared, heated to 95 °C for 5 min, heated at 70 °C for 5 min, allowed to slowly cool to RT over 10 min, then incubated O/N at 4 °C and stored at -20 °C until use.

After ligation of unidirectional linkers, the DNA was precipitated by addition of 6 μL of 3 M sodium acetate (pH 5.2) and 130 μL of 100 % ethanol. The mixture was mixed, incubated at -20 °C for 15 min, centrifuged at 20,000*g* for 10 min at 4 °C, the DNA pellet was washed with 0.5 mL 70 % ethanol, centrifuged at 20,000*g* for 5 min at 4 °C, the liquid was removed, the pellet was air dried for 10 min and finally resuspended in 25 μL water. PCR amplification of ligated DNA and simultaneous incorporation of fluorescent Cy3 and Cy5 labels was achieved by adding 15 μL of a pre-made mix consisting of 5.75 µL of water, 4 µL of 10X ThermoPol reaction buffer (NEB), 2 µL of lowT dNTP mix (2 mM dTTP and 5 mM each of dATP, dCTP and dGTP), 2 µL of Cy3-dUTP or Cy5-dUTP (Cy3 was used for WCL and Cy5 was used for IP) and 1.25 µL of 40 µM oJW102 oligonucleotide. A PCR cycle [(55 °C for 2 min, 72 °C for 5 min, 95 °C for 2 min) X 1; (95 °C for 30 sec, 55 °C for 30 sec, 72 °C for 60 sec) X 35; (72 °C for 4 min, hold @ 4 °C) X 1] was initiated and during the initial 2 min incubation at 55 °C 10 µL of polymerase solution, consisting of 7.99 µL water, 1 µL 10X ThermoPol reaction buffer, 1 µL Taq DNA polymerase (Roche) and 0.01 µL PFU Turbo DNA polymerase (Stratagene), was added. After the PCR reaction was complete, samples were purified using a QIAquick PCR purification kit, eluted with 50 µL of 10 mM TrisHCl (pH 8.0) and 5 µL of the eluate was resolved on a 1.5 % agarose gel to assess quality (a DNA smear between 200 bp and 600 bp is indicative of successful ligation mediated PCR amplification of IP and WCL DNA). The remaining 45 µL of corresponding Cy3-WCL and Cy5-IP samples were mixed and reduced to ~ 3 µL using a vacuum centrifuge and the remaining stages (hybridisation, washing, scanning and analysis) are described in sections 5.6.3 and 5.6.4. below.

5.6.3. Microarray hybridisation conditions, scanning parameters and data analysis pipeline.

These steps were performed using a protocol modified from[210] with microarrays generated in-house at the Institute for Systems Biology Microarray Facility. Genome localisation and mRNA expression studies employed intergenic PCR spotted microarrays and ORF oligonucleotide spotted microarrays, respectively, and treated identically. Prior to hybridisation, microarrays were incubated at RT for 30 min with gentle rotation in 50 mL Falcon tubes (Fisher) containing 0.1 % SDS and 100 µg/mL ssDNA in 3XSSC [450 mM NaCl, 45 mM sodium citrate (pH 7.0)], then washed by dipping sequentially into 5 containers of water and dried with compressed air. LifterSlip coverslips (Erie) were rinsed twice in water, twice in 100 % ethanol, dried with compressed air and then overlaid onto microarray slides until hybridisation. The hybridisation mixtures were comprised of labeled probes (previously reduced to ~3 μL using a vacuum centrifuge) that were brought up to 55 μL with hybridisation solution [DIG Easy-Hyb (Roche) containing 0.5 mg/mL yeast tRNA (Invitrogen) and 0.5 mg/mL ssDNA (Ambion)]. Immediately prior to their application to microarrays, hybridisation mixtures were heated at 90 °C for 1 min and cooled on ice for 1 min. Microarrays were hybridised O/N (12 – 18 hrs) at 37 °C in sealed chambers and washed with solutions derived from 20XSSC [3 M NaCl, 300 mM sodium citrate (pH 7.9)] and 20 % SDS stock solutions as follows. First, the slides were immersed gently several times into a 55 °C pre-heated solution of 1XSSC with 0.2 % SDS, until the coverslips slid off, and then further incubated in this solution for 5 min with gentle rotation. Next, the microarrays were washed similarly in 0.1XSSC with 0.2 % SDS but at RT, they were then incubated for 5 min in 0.5XSSC at 45 °C with inversion once per min and finally in 0.1XSSC for 2 min at RT without agitation, after which the slides were quickly sequentially dipped into three fresh containers of RT water to remove trace salt and SDS and lastly blow dried with compressed air and stored desiccated at RT in the dark until scanning.

Arrays were scanned with a ScanArray 5000 microarray scanner (PerkinElmer) and ScanArray software (Packard BioChip) and spot finding and quantitation were performed using AnalyzerDG (MolecularWare). Subsequent steps were performed on-line using the SBEAMS (Systems Biology Experiment Analysis Management System) microarray analysis pipeline developed at the Institute for Systems Biology and available at http://www.sbeams.org). This included normalisation of Cy3 and Cy5 data, which resulted in equal median probe intensity values for each microarray and, since all microarray experiments were performed in triplicate or greater, the individual normalised intensity data for replicate arrays were merged and statistically analyzed using VERA and SAM[210,211,244] to calculate overall $\log_{10}$ WT/*Δnup2* ratios for all spotted DNAs and to assign probability scores (λ) to each. High λ values denote high probability that a given spotted DNA is differentially enriched in one sample and its calculation is based on the reproducibility of spots repeated within and between replicate microarrays, proportional to the fold-difference observed between the two hybridised samples and inversely proportion to the spot signal intensity; that is, it becomes increasingly difficult to conclude that a given spot is significantly enriched or depleted in a given sample as the intensity of the spot approaches background and when the spot intensities for the two samples hybridised approach each other. These raw data were further analyzed as described in section 5.6.4.

5.6.4. Post-pipeline analyses.

All post-pipeline analyses were performed using Excel (Microsoft). Raw data contained in output *.clone files were imported into Excel and cropped into significant data by λ thresholding to include only the top 5% most significant data: 313 of 6,271 potential ORFs for mRNA expression microarrays and 304 of 6,081 potential intergenic sequences for genome localisation microarrays. To determine if subtelomeric bias existed in any datasets, the distance to the closest telomere (bp) for each significant ORF or intergenic region was calculated using sequence information available at http://www.yeastgenome.org/. These distances were compiled and binned into 10 kb portions (bin1 = 0 – 10,000 bp; bin2 = 10,001-20,000 bp etc.) and displayed as histograms. A bias to subtelomeric regions is indicated by a high relative abundance of ORFs in the first three bins (i.e. many ORFs are < 30 kb from a telomere).

The proximity between ChIP-CHIP enriched intergenic regions and ORFs induced in cell lacking Nup2p was determined as follows. The distance between each of the 304 significantly enriched ChIP-CHIP intergenic regions and the closest of the 123 *Δnup2*-induced ORFs was calculated for the following ChIP-CHIP datasets: Nup2p, Prp20p, an unrelated transcription factor control, Oaf1p, and 10 datasets containing 304 intergenic regions chosen at random throughout the genome. These minimal distances were compiled, binned and plotted in the same manner as telomeric bias investigations; however, in this case, an enrichment data at short minimal distances (< 30 kb) indicates that the significant data in compared datasets lie in close proximity to one another on chromosomes, but does not *implicitly* denote enrichment at subtelomeric regions.

For all histogram plots, the statistical significance of observed differences were assessed using the two-sample Kolmogorov-Smirnov test, which, with a large enough sample size, is able to detect any differences between two population distributions from which the samples were chosen, based on the maximum vertical distance between the two sample cumulative distribution functions.

Chromosome localisation maps indicating possible regions subject to Nup2p-dependent boundary function were generated by plotting significant data linearly on scatter plots, where the x-axis represent the location on each chromosome. Briefly, each significant ORF or intergenic region was assigned an arbitrary number (chromap) based on the standardised chromosome number of the chromosome on which it is encoded (1 through 16) and its distance from the start of the chromosome (left arm = bp# 1) that was calculated with: chromap = chromosome# + region $bp_{average}/1{,}750{,}000$. This resulted in chromap values > 1 and < 17, where regions on chromosome 1 are > 1 and < 2, those on chromosome 2 are > 2 and < 3 and so on. Note that shaded areas (potential boundary domains) placed arbitrarily.

5.7. Other methods

5.7.1. Immunoelectron microscopic localisation of protein A tags

IEM localisation of PrA-tagged nups was carried at the Rockefeller University Electron Microscopy Facility by Adisetyantari Suprapto and Helen Shio as described for nuclear envelopes[4,31,169] and intact nuclei[153].

5.7.2. Quantitation of nucleoporin expression by flow cytometry

Liquid cultures of Nup-GFP (*MATa*) strains as well as an untagged DF5 (*MATa*) strain were grown in YPD at 23 °C to log-phase, at which time they were diluted 1:100 in PBS and analyzed using a FACSCalibur flow cytometer and CELLQuest software (Beckton-Dickenson). A total of 10^4 events were measured for each acquisition and cells were gated based on the SSC and FSC to limit analysis to cells of uniform size and granularity. Between 5000 and 8000 events remained for analysis after gating. The mean GFP fluorescence (FL1) was calculated for each sample. Each acquisition was repeated in triplicate to ensure run to run consistency and final analysis was performed with Excel (Microsoft). Error in these repeated measurements was never more than 2 %. The mean GFP intensity was normalised by subtraction of the mean intensity of the DF5 control (representing background autofluorescence). Four independent experiments were performed and the average normalised fluorescence and standard deviation of the experiments were calculated for each protein.

5.7.3. Boundary trap assay

These experiments were performed as described[2] Briefly, the wild-type KIY54 boundary trap strain and null mutant derivatives, each harbouring tryptophan selectable Gbd fusion plasmids were grown to log-phase at 30 °C in selective liquid media (CSM-TRP for WT cells and CSM-TRP+G418 for all others, with the exceptions of the *Δnup60* strain, which was grown in CSM-TRP+NAT, and the *Δmlp1/Δmlp2* double null strains, which were grown in CSM-TRP+G418+NAT. Cell density was normalised for each strain to ~1 X 10^7 cells/mL (1000 cells/μL), serially diluted 10-fold to a final density of ~1 X 10^3 cells/mL (1 cell/μL) and then 3 μL of each strain at each dilution was spotted onto CSM-TRP, CSM-TRP-ADE, CSM-TRP+FOA and CSM-TRP-ADE+FOA plates and grown at 30 °C until colonies formed, which ranged from 72 hrs, for plates lacking 5-FOA to ≥ 120 hrs for those that did not. For colourimetric analyses of unselective *ADE2* expression, the CSM-TRP plates were incubated for an additional 5 days at 4 °C to facilitate the build-up of P-ribosylaminoimidazole, a red coloured adenine precursor that accumulates in cells that do not express the *ADE2* gene product.

5.7.4. Single cell telomeric silencing assay

This assay was modified from the procedure described in (206). Wild-type YTI448 null mutant derivatives were grown to log phase at 30 °C in liquid YPD supplemented with 40 mg/L adenine (YPDA) and then treated with 3 μg/mL α factor (Sigma-Aldrich) for 4 hrs to allow shmoo formation. All subsequent procedures were performed at RT (23 °C). The initial proportion of shmooing cells was determined by visual scoring of at least 100 cells using an Eclipse E400 microscope (Nikon). Then, for OFF maintenance studies, these cultures were diluted 1:100 in sterile water, sonicated briefly in an Aquasonic Model 75D water bath sonitçator (VWR) and spotted onto YPDA containing 3 μg/mL α factor (YPDAα). From these spotted cells, grids containing 16 to 30 shmooing cells for each genotype were arrayed on the YPDAα media using an Eclipse E400 microscope fitted with microdissecting stage (Nikon). Grids were periodically visualised over a 20 hr time course using an Eclipse TS100 inverted microscope (Nikon) and digital images were acquired with a Coolpix 990 camera (Nikon). Images were compiled using Photoshop (Adobe) and data were analyzed with Excel (Microsoft). For both 'initial OFF' and 'OFF maintenance' experiments, the data, consisting of three independent experiments, were normalised to WT controls to account for run to run variability and were plotted as percentage of WT activity.

NO TEXT

6. REFERENCES

1. Rout, M.P. & Aitchison, J.D. The nuclear pore complex as a transport machine. *J Biol Chem* **29**, 29 (2001).
2. Ishii, K., Arib, G., Lin, C., Van Houwe, G. & Laemmli, U.K. Chromatin boundaries in budding yeast: the nuclear pore connection. *Cell* **109**, 551-62 (2002).
3. Rout, M.P., Aitchison, J.D., Magnasco, M.O. & Chait, B.T. Virtual gating and nuclear transport: the hole picture. *Trends Cell Biol* **13**, 622-8 (2003).
4. Rout, M.P. et al. The yeast nuclear pore complex: composition, architecture, and transport mechanism. *J Cell Biol* **148**, 635-51 (2000).
5. Ho, Y. et al. Systematic identification of protein complexes in Saccharomyces cerevisiae by mass spectrometry. *Nature* **415**, 180-3 (2002).
6. Ishii, K. & Laemmli, U.K. Structural and dynamic functions establish chromatin domains. *Mol Cell* **11**, 237-48 (2003).
7. Galy, V. et al. Nuclear retention of unspliced mRNAs in yeast is mediated by perinuclear Mlp1. *Cell* **116**, 63-73 (2004).
8. Feuerbach, F. et al. Nuclear architecture and spatial positioning help establish transcriptional states of telomeres in yeast. *Nat Cell Biol* **4**, 214-21 (2002).
9. Quimby, B.B. & Corbett, A.H. Nuclear transport mechanisms. *Cell Mol Life Sci* **58**, 1766-73 (2001).
10. Pemberton, L.F., Blobel, G. & Rosenblum, J.S. Transport routes through the nuclear pore complex. *Curr Opin Cell Biol* **10**, 392-9 (1998).
11. Weis, K. Regulating access to the genome: nucleocytoplasmic transport throughout the cell cycle. *Cell* **112**, 441-51 (2003).
12. Wente, S.R. Gatekeepers of the nucleus. *Science* **288**, 1374-7 (2000).
13. Keminer, O. & Peters, R. Permeability of single nuclear pores. *Biophys J* **77**, 217-28 (1999).
14. Denning, D. et al. The nucleoporin Nup60p functions as a Gsp1p-GTP-sensitive tether for Nup2p at the nuclear pore complex. *J Cell Biol* **154**, 937-50 (2001).
15. Dingwall, C., Kandels-Lewis, S. & Seraphin, B. A family of Ran binding proteins that includes nucleoporins. *Proc Natl Acad Sci U S A* **92**, 7525-9 (1995).
16. Rexach, M. & Blobel, G. Protein import into nuclei: association and dissociation reactions involving transport substrate, transport factors, and nucleoporins. *Cell* **83**, 683-92 (1995).
17. Yang, Q., Rout, M.P. & Akey, C.W. Three-dimensional architecture of the isolated yeast nuclear pore complex: functional and evolutionary implications. *Mol Cell* **1**, 223-34 (1998).
18. Akey, C.W. & Radermacher, M. Architecture of the Xenopus nuclear pore complex revealed by three-dimensional cryo-electron microscopy. *J. Cell Biol.* **122**, 1-19 (1993).
19. Allen, T.D., Cronshaw, J.M., Bagley, S., Kiseleva, E. & Goldberg, M.W. The nuclear pore complex: mediator of translocation between nucleus and cytoplasm. *J Cell Sci* **113**, 1651-9 (2000).
20. Ris, H. High-resolution field-emission scanning electron microscopy of nuclear pore complex. *Scanning* **19**, 368-75 (1997).
21. Cronshaw, J.M., Krutchinsky, A.N., Zhang, W., Chait, B.T. & Matunis, M.J. Proteomic analysis of the mammalian nuclear pore complex. *J Cell Biol* **158**, 915-27 (2002).
22. Rout, M.P. & Blobel, G. Isolation of the yeast nuclear pore complex. *J Cell Biol* **123**, 771-83 (1993).
23. Reichelt, R. et al. Correlation between structure and mass distribution of the nuclear pore complex and of distinct pore complex components. *J Cell Biol* **110**, 883-94 (1990).
24. Stoffler, D., Fahrenkrog, B. & Aebi, U. The nuclear pore complex: from molecular architecture to functional

dynamics. *Curr Opin Cell Biol* **11**, 391-401 (1999).

25. Buss, F., Kent, H., Stewart, M., Bailer, S.M. & Hanover, J.A. Role of different domains in the self-association of rat nucleoporin p62. *J Cell Sci* **107**, 631-8 (1994).

26. Bastos, R., Pante, N. & Burke, B. Nuclear pore complex proteins. *Int Rev Cytol* **162B**, 257-302 (1995).

27. Denning, D.P., Patel, S.S., Uversky, V., Fink, A. & Rexach, M. The "FG" Nucleoporins of S. Cerevisiae Constitute a Family of Natively Unfolded Proteins. *ASCB Annual Conference Proceedings* **Presentation 811**(2002).

28. Denning, D.P., Uversky, V., Patel, S.S., Fink, A.L. & Rexach, M. The Saccharomyces cerevisiae nucleoporin Nup2p is a natively unfolded protein. *J Biol Chem* **277**, 33447-55 (2002).

29. Radu, A., Moore, M.S. & Blobel, G. The peptide repeat domain of nucleoporin Nup98 functions as a docking site in transport across the nuclear pore complex. *Cell* **81**, 215-22 (1995).

30. Bayliss, R., Littlewood, T. & Stewart, M. Structural basis for the interaction between FxFG nucleoporin repeats and importin-beta in nuclear trafficking. *Cell* **102**, 99-108 (2000).

31. Nehrbass, U., Rout, M.P., Maguire, S., Blobel, G. & Wozniak, R.W. The yeast nucleoporin Nup188p interacts genetically and physically with the core structures of the nuclear pore complex. *J Cell Biol* **133**, 1153-62 (1996).

32. Fabre, E. & Hurt, E. Yeast genetics to dissect the nuclear pore complex and nucleocytoplasmic trafficking. *Annu Rev Genet* **31**, 277-313 (1997).

33. Suntharalingam, M. & Wente, S.R. Peering through the pore: nuclear pore complex structure, assembly, and function. *Dev Cell* **4**, 775-89 (2003).

34. Ryan, K.J. & Wente, S.R. The nuclear pore complex: a protein machine bridging the nucleus and cytoplasm. *Curr Opin Cell Biol* **12**, 361-71 (2000).

35. Lindsay, M.E., Plafker, K., Smith, A.E., Clurman, B.E. & Macara, I.G. Npap60/Nup50 is a tri-stable switch that stimulates importin-alpha:beta-mediated nuclear protein import. *Cell* **110**, 349-60 (2002).

36. Kendirgi, F., Barry, D.M., Griffis, E.R., Powers, M.A. & Wente, S.R. An essential role for hGle1 nucleocytoplasmic shuttling in mRNA export. *J Cell Biol* **160**, 1029-40 (2003).

37. Harel, A. et al. Removal of a single pore subcomplex results in vertebrate nuclei devoid of nuclear pores. *Mol Cell* **11**, 853-64 (2003).

38. Vasu, S.K. & Forbes, D.J. Nuclear pores and nuclear assembly. *Curr Opin Cell Biol* **13**, 363-75 (2001).

39. Dingwall, C. & Laskey, R.A. Nuclear targeting sequences-a consensus? *Trends in Biochemical Sciences* **16**, 478-481 (1991).

40. Fischer, U., Michael, M., Luhrmann, R. & Dreyfuss, G. Signal-mediated nuclear export pathways of proteins and RNAs. *Trends Cell Biol.* **6**, 290-293 (1996).

41. Gerace, L. Nuclear export signals and the fast track to the cytoplasm. *Cell* **82**, 341-4 (1995).

42. Yoshida, K. & Blobel, G. The karyopherin Kap142p/Msn5p mediates nuclear import and nuclear export of different cargo proteins. *J Cell Biol* **152**, 729-40 (2001).

43. Kaffman, A., Rank, N.M. & O'Shea, E.K. Phosphorylation regulates association of the transcription factor Pho4 with its import receptor Pse1/Kap121. *Genes Dev* **12**, 2673-83 (1998).

44. Kaffman, A., Rank, N.M., O'Neill, E.M., Huang, L.S. & O'Shea, E.K. The receptor Msn5 exports the phosphorylated transcription factor Pho4 out of the nucleus. *Nature* **396**, 482-6 (1998).

45. Strom, A.C. & Weis, K. Importin-beta-like nuclear transport receptors. *Genome Biol* **2**, REVIEWS3008 (2001).

46. Wozniak, R.W., Rout, M.P. & Aitchison, J.D. Karyopherins and kissing cousins. *Trends Cell Biol* **8**, 184-8 (1998).

47. Gorlich, D. & Mattaj, I.W. Nucleocytoplasmic transport. *Science* **271**, 1513-8 (1996).

48. Nigg, E.A. Nucleocytoplasmic transport: signals, mechanisms and regulation. *Nature* **386**, 779-87 (1997).

49. Fridell, R.A., Truant, R., Thorne, L., Benson, R.E. & Cullen, B.R. Nuclear import of hnRNP A1 is mediated by a novel cellular cofactor related to karyopherin-beta. *J Cell Sci* **110 (Pt 11)**, 1325-31 (1997).

50. Nakielny, S. et al. Transportin: nuclear transport receptor of a novel nuclear protein import pathway. *Exp Cell Res* **229**, 261-6 (1996).

51. Aitchison, J.D., Blobel, G. & Rout, M.P. Kap104p: a karyopherin involved in the nuclear transport of messenger RNA binding proteins. *Science* **274**, 624-7 (1996).

52. Pollard, V.W. et al. A novel receptor-mediated nuclear protein import pathway. *Cell* **86**, 985-94 (1996).

53. Bonifaci, N., Moroianu, J., Radu, A. & Blobel, G. Karyopherin beta2 mediates nuclear import of a mRNA binding protein. *Proc Natl Acad Sci U S A* **94**, 5055-60 (1997).

54. Fornerod, M. et al. The human homologue of yeast CRM1 is in a dynamic subcomplex with CAN/Nup214 and a novel nuclear pore component Nup88. *Embo J* **16**, 807-16 (1997).

55. Izaurralde, E. et al. A role for the M9 transport signal of hnRNP A1 in mRNA nuclear export. *J Cell Biol* **137**, 27-35 (1997).

56. Rout, M.P., Blobel, G. & Aitchison, J.D. A distinct nuclear import pathway used by ribosomal proteins. *Cell* **89**, 715-25 (1997).

57. Gorlich, D. et al. A novel class of RanGTP binding proteins. *J Cell Biol* **138**, 65-80 (1997).

58. Yaseen, N.R. & Blobel, G. Cloning and characterization of human karyopherin beta3. *Proc Natl Acad Sci U S A* **94**, 4451-6 (1997).

59. Schlenstedt, G. et al. Yrb4p, a yeast ran-GTP-binding protein involved in import of ribosomal protein L25 into the nucleus. *Embo J* **16**, 6237-49 (1997).

60. Seedorf, M. & Silver, P.A. Importin/karyopherin protein family members required for mRNA export from the nucleus. *Proc Natl Acad Sci U S A* **94**, 8590-5 (1997).

61. Fornerod, M., Ohno, M., Yoshida, M. & Mattaj, I.W. CRM1 is an export receptor for leucine-rich nuclear export signals [see comments]. *Cell* **90**, 1051-60 (1997).

62. Pemberton, L.F., Rosenblum, J.S. & Blobel, G. A distinct and parallel pathway for the nuclear import of an mRNA-binding protein. *J Cell Biol* **139**, 1645-53 (1997).

63. Stade, K., Ford, C.S., Guthrie, C. & Weis, K. Exportin 1 (Crm1p) is an essential nuclear export factor. *Cell* **90**, 1041-50 (1997).

64. Kutay, U., Bischoff, F.R., Kostka, S., Kraft, R. & Gorlich, D. Export of importin alpha from the nucleus is mediated by a specific nuclear transport factor. *Cell* **90**, 1061-71 (1997).

65. Adachi, Y. & Yanagida, M. Higher order chromosome structure is affected by cold-sensitive mutations in a Schizosaccharomyces pombe gene crm1+ which encodes a 115-kD protein preferentially localized in the nucleus and its periphery. *J Cell Biol* **108**, 1195-207 (1989).

66. Rosenblum, J.S., Pemberton, L.F. & Blobel, G. A nuclear import pathway for a protein involved in tRNA maturation. *J Cell Biol* **139**, 1655-61 (1997).

67. Simos, G. et al. Nuclear pore proteins are involved in the biogenesis of functional tRNA. *Embo J* **15**, 2270-84 (1996).

68. Palacios, I., Hetzer, M., Adam, S.A. & Mattaj, I.W. Nuclear import of U snRNPs requires importin beta. *Embo J* **16**, 6783-92 (1997).

69. Kadowaki, T. et al. Isolation and characterization of Saccharomyces cerevisiae mRNA transport-defective (mtr) mutants. *J Cell Biol* **126**, 649-59 (1994).

70. Ossareh-Nazari, B., Bachelerie, F. & Dargemont, C. Evidence for a role of CRM1 in signal-mediated nuclear protein export. *Science* **278**, 141-4 (1997).

71. Wolff, B., Sanglier, J.J. & Wang, Y. Leptomycin B is an inhibitor of nuclear export: inhibition of nucleo-cytoplasmic translocation of the human immunodeficiency virus type 1 (HIV-1) Rev protein and Rev-dependent mRNA. *Chem Biol* **4**, 139-47 (1997).

72. Chow, T.Y., Ash, J.J., Dignard, D. & Thomas, D.Y. Screening and identification of a gene, PSE-1, that affects protein secretion in Saccharomyces cerevisiae. *J Cell Sci* **101 (Pt 3)**, 709-19 (1992).

73. Brinkmann, U., Brinkmann, E., Gallo, M. & Pastan, I. Cloning and characterization of a cellular apoptosis susceptibility gene, the human homologue to the yeast chromosome segregation gene CSE1. *Proc Natl Acad Sci U S A* **92**, 10427-31 (1995).

74. Irniger, S., Piatti, S., Michaelis, C. & Nasmyth, K. Genes involved in sister chromatid separation are needed for B-type cyclin proteolysis in budding yeast. *Cell* **81**, 269-78 (1995).

75. Xiao, Z., McGrew, J.T., Schroeder, A.J. & Fitzgerald-Hayes, M. CSE1 and CSE2, two new genes required for accurate mitotic chromosome segregation in Saccharomyces cerevisiae. *Mol Cell Biol* **13**, 4691-702 (1993).

76. Shen, W.C., Stanford, D.R. & Hopper, A.K. Los1p, involved in yeast pre-tRNA splicing, positively regulates members of the SOL gene family. *Genetics* **143**, 699-712 (1996).

77. Hurt, D.J., Wang, S.S., Lin, Y.H. & Hopper, A.K. Cloning and characterization of LOS1, a Saccharomyces cerevisiae gene that affects tRNA splicing. *Mol Cell Biol* **7**, 1208-16 (1987).

78. Toda, T. et al. Fission yeast pap1-dependent transcription is negatively regulated by an essential nuclear protein, crm1. *Mol Cell Biol* **12**, 5474-84 (1992).

79. Arts, G.J., Kuersten, S., Romby, P., Ehresmann, B. & Mattaj, I.W. The role of exportin-t in selective nuclear export of mature tRNAs. *Embo J* **17**, 7430-7441 (1998).

80. Arts, G.J., Fornerod, M. & Mattaj, I.W. Identification of a nuclear export receptor for tRNA. *Curr Biol* **8**, 305-14 (1998).

81. Kutay, U. et al. Identification of a tRNA-specific nuclear export receptor. *Mol Cell* **1**, 359-69 (1998).

82. Senger, B. et al. Mtr10p functions as a nuclear import receptor for the mRNA-binding protein Npl3p. *Embo J* **17**, 2196-207 (1998).

83. Pemberton, L.F., Rosenblum, J.S. & Blobel, G. Nuclear import of the TATA-binding protein: mediation by the karyopherin Kap114p and a possible mechanism for intranuclear targeting. *J Cell Biol* **145**, 1407-17 (1999).

84. Ferrigno, P., Posas, F., Koepp, D., Saito, H. & Silver, P.A. Regulated nucleo/cytoplasmic exchange of HOG1 MAPK requires the importin beta homologs NMD5 and XPO1. *Embo J* **17**, 5606-14 (1998).

85. Albertini, M., Pemberton, L.F., Rosenblum, J.S. & Blobel, G. A novel nuclear import pathway for the transcription factor TFIIS. *J Cell Biol* **143**, 1447-55 (1998).

86. Chaves, S.R. & Blobel, G. Nuclear import of Spo12p, a protein essential for meiosis. *J Biol Chem* **276**, 17712-7 (2001).

87. Titov, A.A. & Blobel, G. The karyopherin Kap122p/Pdr6p imports both subunits of the transcription factor IIA into the nucleus. *J Cell Biol* **147**, 235-46 (1999).

88. Shulga, N., James, P., Craig, E.A. & Goldfarb, D.S. A nuclear export signal prevents Saccharomyces cerevisiae Hsp70 Ssb1p from stimulating nuclear localization signal-directed nuclear transport. *J Biol Chem* **274**, 16501-7 (1999).

89. Yan, C., Lee, L.H. & Davis, L.I. Crm1p mediates regulated nuclear export of a yeast AP-1-like transcription factor. *Embo J* **17**, 7416-29 (1998).

90. Jensen, T.H. et al. Identification of novel Saccharomyces cerevisiae proteins with nuclear export activity: cell cycle-regulated transcription factor ace2p shows cell cycle-independent nucleocytoplasmic shuttling. *Mol Cell Biol* **20**, 8047-58 (2000).

91. Fukuda, M. et al. CRM1 is responsible for intracellular transport mediated by the nuclear export signal. *Nature* **390**, 308-11 (1997).

92. Hakata, Y., Umemoto, T., Matsushita, S. & Shida, H. Involvement of human CRM1 (exportin 1) in the export and multimerization of the Rex protein of human T-cell leukemia virus type 1. *J Virol* **72**, 6602-7 (1998).

93. Yang, J. et al. Control of cyclin B1 localization through regulated binding of the nuclear export factor CRM1. *Genes Dev* **12**, 2131-43 (1998).

94. Zhu, J. & McKeon, F. NF-AT activation requires suppression of Crm1-dependent export by calcineurin. *Nature* **398**, 256-60 (1999).

95. Nakielny, S. & Dreyfuss, G. Transport of proteins and RNAs in and out of the nucleus. *Cell* **99**, 677-90 (1999).

96. Lee, D.C. & Aitchison, J.D. Kap104p-mediated nuclear import. Nuclear localization signals in mRNA-binding proteins and the role of Ran and Rna. *J Biol Chem* **274**, 29031-7 (1999).

97. Neville, M., Stutz, F., Lee, L., Davis, L.I. & Rosbash, M. The importin-beta family member Crm1p bridges the interaction between Rev and the nuclear pore complex during nuclear export. *Curr Biol* **7**, 767-75 (1997).

98. Sarkar, S. & Hopper, A.K. tRNA nuclear export in saccharomyces cerevisiae: In situ hybridization analysis. *Mol Biol Cell* **9**, 3041-55 (1998).

99. Hood, J.K. & Silver, P.A. Cse1p is required for export of Srp1p/importin-alpha from the nucleus in Saccharomyces cerevisiae. *J Biol Chem* **273**, 35142-6 (1998).

100. Leslie, D.M. et al. Characterization of karyopherin cargoes reveals unique mechanisms of Kap121p-mediated nuclear import. *Mol Cell Biol* **24**, 8487-503 (2004).

101. Weis, K., Mattaj, I.W. & Lamond, A.I. Identification of hSRP1 alpha as a functional receptor for nuclear localization sequences. *Science* **268**, 1049-53 (1995).

102. Conti, E., Uy, M., Leighton, L., Blobel, G. & Kuriyan, J. Crystallographic analysis of the recognition of a nuclear localization signal by the nuclear import factor karyopherin alpha. *Cell* **94**, 193-204 (1998).

103. Mattaj, I.W. & Englmeier, L. Nucleocytoplasmic transport: the soluble phase. *Annu Rev Biochem* **67**, 265-306 (1998).

104. Marelli, M., Aitchison, J.D. & Wozniak, R.W. Specific binding of the karyopherin Kap121p to a subunit of the nuclear pore complex containing Nup53p, Nup59p, and Nup170p. *J Cell Biol* **143**, 1813-30 (1998).

105. Damelin, M. & Silver, P.A. Mapping interactions between nuclear transport factors in living cells reveals pathways through the nuclear pore complex. *Mol Cell* **5**, 133-40 (2000).

106. Strawn, L.A., Shen, T., Shulga, N., Goldfarb, D.S. & Wente, S.R. Minimal nuclear pore complexes define FG repeat domains essential for transport. *Nat Cell Biol* **6**, 197-206 (2004).

107. Pyhtila, B. & Rexach, M. A gradient of affinity for the karyopherin Kap95p along the yeast nuclear pore complex. *J Biol Chem* **278**, 42699-709 (2003).

108. Ben-Efraim, I. & Gerace, L. Gradient of Increasing Affinity of Importin beta for Nucleoporins along the Pathway of Nuclear Import. *J Cell Biol* **152**, 411-8. (2001).

109. Kehlenbach, R.H., Dickmanns, A., Kehlenbach, A., Guan, T. & Gerace, L. A role for RanBP1 in the release of CRM1 from the nuclear pore complex in a terminal step of nuclear export. *J Cell Biol* **145**, 645-57 (1999).

110. Cole, C.N. & Hammell, C.M. Nucleocytoplasmic transport: driving and

directing transport. *Curr Biol* **8**, R368-72 (1998).

111.Moore, M.S. Ran and nuclear transport. *J Biol Chem* **273**, 22857-60 (1998).

112.Hopper, A.K., Traglia, H.M. & Dunst, R.W. The yeast RNA1 gene product necessary for RNA processing is located in the cytosol and apparently excluded from the nucleus. *J Cell Biol* **111**, 309-21. (1990).

113.Amberg, D.C., Fleischmann, M., Stagljar, I., Cole, C.N. & Aebi, M. Nuclear PRP20 protein is required for mRNA export. *Embo J* **12**, 233-41 (1993).

114.Kalab, P., Weis, K. & Heald, R. Visualization of a Ran-GTP gradient in interphase and mitotic Xenopus egg extracts. *Science* **295**, 2452-6 (2002).

115.Gorlich, D. & Kutay, U. Transport between the cell nucleus and the cytoplasm. *Annu Rev Cell Dev Biol* **15**, 607-60 (1999).

116.Gorlich, D., Pante, N., Kutay, U., Aebi, U. & Bischoff, F.R. Identification of different roles for RanGDP and RanGTP in nuclear protein import. *Embo J* **15**, 5584-94 (1996).

117.Ribbeck, K., Lipowsky, G., Kent, H.M., Stewart, M. & Gorlich, D. NTF2 mediates nuclear import of Ran. *Embo J* **17**, 6587-98 (1998).

118.Smith, A., Brownawell, A. & Macara, I.G. Nuclear import of Ran is mediated by the transport factor NTF2. *Curr Biol* **8**, 1403-6 (1998).

119.Nehrbass, U. & Blobel, G. Role of the nuclear transport factor p10 in nuclear import. *Science* **272**, 120-2 (1996).

120.Bayliss, R. et al. Interaction between NTF2 and xFxFG-containing nucleoporins is required to mediate nuclear import of RanGDP. *J Mol Biol* **293**, 579-93 (1999).

121.Quimby, B.B., Wilson, C.A. & Corbett, A.H. The interaction between Ran and NTF2 is required for cell cycle progression. *Mol Biol Cell* **11**, 2617-29 (2000).

122.Stewart, M., Whytock, S. & Moir, R.D. Nuclear envelope dynamics and nucleocytoplasmic transport. *J Cell Sci Suppl* **14**, 79-82 (1991).

123.Blobel, G. Unidirectional and bidirectional protein traffic across membranes. *Cold Spring Harb Symp Quant Biol* **60**, 1-10 (1995).

124.Pante, N. & Kann, M. Nuclear pore complex is able to transport macromolecules with diameters of about 39 nm. *Mol Biol Cell* **13**, 425-34 (2002).

125.Feldherr, C.M. & Akin, D. The location of the transport gate in the nuclear pore complex. *J. Cell Sci.* **110**, 3065-70 (1997).

126.Feldherr, C.M., Kallenbach, E. & Schultz, N. Movement of a karyophilic protein through the nuclear pores of oocytes. *J Cell Biol* **99**, 2216-22 (1984).

127.Ribbeck, K. & Gorlich, D. Kinetic analysis of translocation through nuclear pore complexes. *Embo J* **20**, 1320-30 (2001).

128.Macara, I.G. Transport into and out of the nucleus. *Microbiol Mol Biol Rev* **65**, 570-94, table of contents (2001).

129.Lusk, C.P., Makhnevych, T., Marelli, M., Aitchison, J.D. & Wozniak, R.W. Karyopherins in nuclear pore biogenesis: a role for Kap121p in the assembly of Nup53p into nuclear pore complexes. *J Cell Biol* **159**, 267-78 (2002).

130.Singer, R.H. & Green, M.R. Compartmentalization of eukaryotic gene expression: causes and effects. *Cell* **91**, 291-4 (1997).

131.Aitchison, J.D., Blobel, G. & Rout, M.P. Nup120p: a yeast nucleoporin required for NPC distribution and mRNA transport. *J Cell Biol* **131**, 1659-75 (1995).

132.Marelli, M., Lusk, C.P., Chan, H., Aitchison, J.D. & Wozniak, R.W. A link between the synthesis of nucleoporins and the biogenesis of the nuclear envelope. *J Cell Biol* **153**, 709-24 (2001).

133.Doye, V., Wepf, R. & Hurt, E.C. A novel nuclear pore protein Nup133p with distinct roles in poly(A)+ RNA transport and nuclear pore distribution. *Embo J* **13**, 6062-75 (1994).

134.Wente, S.R. & Blobel, G. NUP145 encodes a novel yeast glycine-leucine-phenylalanine-glycine (GLFG) nucleoporin required for nuclear envelope structure. *J Cell Biol* **125**, 955-69 (1994).

135. Gorsch, L.C., Dockendorff, T.C. & Cole, C.N. A conditional allele of the novel repeat-containing yeast nucleoporin RAT7/NUP159 causes both rapid cessation of mRNA export and reversible clustering of nuclear pore complexes. *J Cell Biol* **129**, 939-55 (1995).

136. Heath, C.V. et al. Nuclear pore complex clustering and nuclear accumulation of poly(A)+ RNA associated with mutation of the Saccharomyces cerevisiae RAT2/NUP120 gene. *J Cell Biol* **131**, 1677-97 (1995).

137. Li, O. et al. Mutation or deletion of the Saccharomyces cerevisiae RAT3/NUP133 gene causes temperature-dependent nuclear accumulation of poly(A)+ RNA and constitutive clustering of nuclear pore complexes. *Mol Biol Cell* **6**, 401-417 (1995).

138. Pemberton, L.F., Rout, M.P. & Blobel, G. Disruption of the nucleoporin gene NUP133 results in clustering of nuclear pore complexes. *Proc Natl Acad Sci U S A* **92**, 1187-91 (1995).

139. Goldstein, A.L., Snay, C.A., Heath, C.V. & Cole, C.N. Pleiotropic nuclear defects associated with a conditional allele of the novel nucleoporin Rat9p/Nup85p. *Mol Biol Cell* **7**, 917-34 (1996).

140. Murphy, R., Watkins, J.L. & Wente, S.R. GLE2, a Saccharomyces cerevisiae homologue of the Schizosaccharomyces pombe export factor RAE1, is required for nuclear pore complex structure and function. *Mol Biol Cell* **7**, 1921-37 (1996).

141. Siniossoglou, S. et al. A novel complex of nucleoporins, which includes Sec13p and a Sec13p homolog, is essential for normal nuclear pores. *Cell* **84**, 265-75 (1996).

142. Makhnevych, T., Lusk, C.P., Anderson, A.M., Aitchison, J.D. & Wozniak, R.W. Cell cycle regulated transport controlled by alterations in the nuclear pore complex. *Cell* **115**, 813-23 (2003).

143. Cockell, M. & Gasser, S.M. Nuclear compartments and gene regulation. *Curr Opin Genet Dev* **9**, 199-205 (1999).

144. Fawcett, D.W., Bloom, W. & Raviola, E. *A textbook of histology*, xx, 964 (Chapman & Hall, New York, 1994).

145. Gottschling, D.E., Aparicio, O.M., Billington, B.L. & Zakian, V.A. Position effect at S. cerevisiae telomeres: reversible repression of Pol II transcription. *Cell* **63**, 751-62 (1990).

146. Fourel, G., Revardel, E., Koering, C.E. & Gilson, E. Cohabitation of insulators and silencing elements in yeast subtelomeric regions. *Embo J* **18**, 2522-37 (1999).

147. Loo, S. & Rine, J. Silencers and domains of generalized repression. *Science* **264**, 1768-71 (1994).

148. Smith, J.S. & Boeke, J.D. An unusual form of transcriptional silencing in yeast ribosomal DNA. *Genes Dev* **11**, 241-54 (1997).

149. Gotta, M. et al. The clustering of telomeres and colocalization with Rap1, Sir3, and Sir4 proteins in wild-type Saccharomyces cerevisiae. *J Cell Biol* **134**, 1349-63 (1996).

150. Maillet, L. et al. Ku-deficient yeast strains exhibit alternative states of silencing competence. *EMBO Rep* **2**, 203-10 (2001).

151. Andrulis, E.D., Neiman, A.M., Zappulla, D.C. & Sternglanz, R. Perinuclear localization of chromatin facilitates transcriptional silencing. *Nature* **394**, 592-5 (1998).

152. Galy, V. et al. Nuclear pore complexes in the organization of silent telomeric chromatin. *Nature* **403**, 108-12 (2000).

153. Strambio-de-Castillia, C., Blobel, G. & Rout, M.P. Proteins connecting the nuclear pore complex with the nuclear interior. *J Cell Biol* **144**, 839-55 (1999).

154. Hediger, F., Dubrana, K. & Gasser, S.M. Myosin-like proteins 1 and 2 are not required for silencing or telomere anchoring, but act in the Tel1 pathway of telomere length control. *J Struct Biol* **140**, 79-91 (2002).

155. Hediger, F., Neumann, F.R., Van Houwe, G., Dubrana, K. & Gasser, S.M. Live Imaging of Telomeres. yKu and Sir Proteins Define Redundant Telomere-

Anchoring Pathways in Yeast. *Curr Biol* **12**, 2076-89 (2002).

156. Pai, C.Y. & Corces, V.G. The nuclear pore complex and chromatin boundaries. *Trends Cell Biol* **12**, 452-5 (2002).

157. Gerasimova, T.I. & Corces, V.G. Chromatin insulators and boundaries: effects on transcription and nuclear organization. *Annu Rev Genet* **35**, 193-208 (2001).

158. Donze, D. & Kamakaka, R.T. RNA polymerase III and RNA polymerase II promoter complexes are heterochromatin barriers in Saccharomyces cerevisiae. *Embo J* **20**, 520-31 (2001).

159. Donze, D., Adams, C.R., Rine, J. & Kamakaka, R.T. The boundaries of the silenced HMR domain in Saccharomyces cerevisiae. *Genes Dev* **13**, 698-708 (1999).

160. Fourel, G., Magdinier, F. & Gilson, E. Insulator dynamics and the setting of chromatin domains. *Bioessays* **26**, 523-32 (2004).

161. Loeb, J.D., Davis, L.I. & Fink, G.R. NUP2, a novel yeast nucleoporin, has functional overlap with other proteins of the nuclear pore complex. *Mol Biol Cell* **4**, 209-22 (1993).

162. Booth, J.W., Belanger, K.D., Sannella, M.I. & Davis, L.I. The yeast nucleoporin Nup2p is involved in nuclear export of importin alpha/Srp1p. *J Biol Chem* **274**, 32360-7 (1999).

163. Hood, J.K., Casolari, J.M. & Silver, P.A. Nup2p is located on the nuclear side of the nuclear pore complex and coordinates Srp1p/importin-alpha export. *J Cell Sci* **113**, 1471-80 (2000).

164. Hartmann, E. et al. Evolutionary conservation of components of the protein translocation complex [see comments]. *Nature* **367**, 654-7 (1994).

165. Kunzler, M., Gerstberger, T., Stutz, F., Bischoff, F.R. & Hurt, E. Yeast Ran-binding protein 1 (Yrb1) shuttles between the nucleus and cytoplasm and is exported from the nucleus via a CRM1 (XPO1)-dependent pathway. *Mol Cell Biol* **20**, 4295-308 (2000).

166. Wu, J., Matunis, M.J., Kraemer, D., Blobel, G. & Coutavas, E. Nup358, a cytoplasmically exposed nucleoporin with peptide repeats, Ran- GTP binding sites, zinc fingers, a cyclophilin A homologous domain, and a leucine-rich region. *J Biol Chem* **270**, 14209-13 (1995).

167. Belanger, K.D., Kenna, M.A., Wei, S. & Davis, L.I. Genetic and physical interactions between Srp1p and nuclear pore complex proteins Nup1p and Nup2p. *J Cell Biol* **126**, 619-30 (1994).

168. Solsbacher, J., Maurer, P., Vogel, F. & Schlenstedt, G. Nup2p, a yeast nucleoporin, functions in bidirectional transport of importin alpha. *Mol Cell Biol* **20**, 8468-79 (2000).

169. Kraemer, D.M., Strambio-de-Castillia, C., Blobel, G. & Rout, M.P. The essential yeast nucleoporin NUP159 is located on the cytoplasmic side of the nuclear pore complex and serves in karyopherin-mediated binding of transport substrate. *J Biol Chem* **270**, 19017-21 (1995).

170. King, M.G. & Baskin, D.G. Effect of paraformaldehyde fixation on localization and characterization of insulin-like growth factor-I (IGF-I) receptors in the rat brain. *Anat Rec* **231**, 467-72 (1991).

171. Smitherman, M., Lee, K., Swanger, J., Kapur, R. & Clurman, B.E. Characterization and targeted disruption of murine Nup50, a p27(Kip1)-interacting component of the nuclear pore complex. *Mol Cell Biol* **20**, 5631-42 (2000).

172. Vallen, E.A., Hiller, M.A., Scherson, T.Y. & Rose, M.D. Separate domains of KAR1 mediate distinct functions in mitosis and nuclear fusion. *J Cell Biol* **117**, 1277-87 (1992).

173. Bucci, M. & Wente, S.R. In vivo dynamics of nuclear pore complexes in yeast. *J Cell Biol* **136**, 1185-99 (1997).

174. Schwoebel, E.D., Ho, T.H. & Moore, M.S. The mechanism of inhibition of Ran-dependent nuclear transport by cellular ATP depletion. *J Cell Biol* **157**, 963-74 (2002).

175. Shulga, N. et al. In vivo nuclear transport kinetics in Saccharomyces cerevisiae: a

role for heat shock protein 70 during targeting and translocation. *J Cell Biol* **135**, 329-39 (1996).

176.Nesvizhskii, A.I., Keller, A., Kolker, E. & Aebersold, R. A statistical model for identifying proteins by tandem mass spectrometry. *Anal Chem* **75**, 4646-58 (2003).

177.Keller, A., Nesvizhskii, A.I., Kolker, E. & Aebersold, R. Empirical statistical model to estimate the accuracy of peptide identifications made by MS/MS and database search. *Anal Chem* **74**, 5383-92 (2002).

178.Taura, T., Krebber, H. & Silver, P.A. A member of the Ran-binding protein family, Yrb2p, is involved in nuclear protein export. *Proc Natl Acad Sci U S A* **95**, 7427-32 (1998).

179.Taura, T., Schlenstedt, G. & Silver, P.A. Yrb2p is a nuclear protein that interacts with Prp20p, a yeast Rcc1 homologue. *J Biol Chem* **272**, 31877-84 (1997).

180.Del Priore, V. et al. A structure/function analysis of Rat7p/Nup159p, an essential nucleoporin of *Saccharomyces cerevisiae*. *J. Cell Sci* **110**, 2987-99 (1997).

181.Saavedra, C.A., Hammell, C.M., Heath, C.V. & Cole, C.N. Yeast heat shock mRNAs are exported through a distinct pathway defined by Rip1p. *Genes Dev* **11**, 2845-56 (1997).

182.Fontoura, B.M., Blobel, G. & Yaseen, N.R. The nucleoporin nup98 is a site for GDP/GTP exchange on ran and termination of karyopherin beta 2-mediated nuclear import. *J Biol Chem* **275**, 31289-96 (2000).

183.Traglia, H.M. et al. Nucleus-associated pools of Rna1p, the Saccharomyces cerevisiae Ran/TC4 GTPse activating protein involved in nucleus/cytosol transit. *Proc Natl Acad Sci U S A* **93**, 7667-72 (1996).

184.Yaseen, N.R. & Blobel, G. Two distinct classes of Ran-binding sites on the nucleoporin Nup-358. *Proc Natl Acad Sci U S A* **96**, 5516-21 (1999).

185.Yaseen, N.R. & Blobel, G. GTP Hydrolysis Links Initiation and Termination of Nuclear Import on the Nucleoporin Nup358. *J Biol Chem* **274**, 26493-26502 (1999).

186.Fan, F. et al. cDNA cloning and characterization of Npap60: a novel rat nuclear pore- associated protein with an unusual subcellular localization during male germ cell differentiation. *Genomics* **40**, 444-53 (1997).

187.Guan, T. et al. Nup50, a nucleoplasmically oriented nucleoporin with a role in nuclear protein export. *Mol Cell Biol* **20**, 5619-30 (2000).

188.Rabut, G., Doye, V. & Ellenberg, J. Mapping the dynamic organization of the nuclear pore complex inside single living cells. *Nat Cell Biol* **6**, 1114-21 (2004).

189.Allen, N.P. et al. Deciphering networks of protein interactions at the nuclear pore complex. *Mol Cell Proteomics* **1**, 930-46 (2002).

190.Allen, N.P., Huang, L., Burlingame, A. & Rexach, M. Proteomic analysis of nucleoporin interacting proteins. *J Biol Chem* **276**, 29268-74 (2001).

191.Gilchrist, D. & Rexach, M. Molecular basis for the rapid dissociation of nuclear localization signals from karyopherin alpha in the nucleoplasm. *J Biol Chem* **278**, 51937-49 (2003).

192.Gilchrist, D., Mykytka, B. & Rexach, M. Accelerating the rate of disassembly of karyopherin.cargo complexes. *J Biol Chem* **277**, 18161-72 (2002).

193.Dilworth, D.J. et al. Nup2p dynamically associates with the distal regions of the yeast nuclear pore complex. *J Cell Biol* **153**, 1465-78 (2001).

194.Bilbao-Cortes, D., Hetzer, M., Langst, G., Becker, P.B. & Mattaj, I.W. Ran binds to chromatin by two distinct mechanisms. *Curr Biol* **12**, 1151-6 (2002).

195.Cushman, I., Stenoien, D. & Moore, M.S. The dynamic association of RCC1 with chromatin is modulated by Ran-dependent nuclear transport. *Mol Biol Cell* **15**, 245-55 (2004).

196.Li, H.Y., Wirtz, D. & Zheng, Y. A mechanism of coupling RCC1 mobility to RanGTP production on the chromatin in vivo. *J Cell Biol* **160**, 635-44 (2003).

197. Nemergut, M.E., Mizzen, C.A., Stukenberg, T., Allis, C.D. & Macara, I.G. Chromatin docking and exchange activity enhancement of RCC1 by histones H2A and H2B. *Science* **292**, 1540-3 (2001).

198. Aebi, M., Clark, M.W., Vijayraghavan, U. & Abelson, J. A yeast mutant, PRP20, altered in mRNA metabolism and maintenance of the nuclear structure, is defective in a gene homologous to the human gene RCC1 which is involved in the control of chromosome condensation. *Mol Gen Genet* **224**, 72-80 (1990).

199. Krogan, N.J. et al. A Snf2 family ATPase complex required for recruitment of the histone H2A variant Htz1. *Mol Cell* **12**, 1565-76 (2003).

200. Meneghini, M.D., Wu, M. & Madhani, H.D. Conserved histone variant H2A.Z protects euchromatin from the ectopic spread of silent heterochromatin. *Cell* **112**, 725-36 (2003).

201. Adam, M., Robert, F., Larochelle, M. & Gaudreau, L. H2A.Z is required for global chromatin integrity and for recruitment of RNA polymerase II under specific conditions. *Mol Cell Biol* **21**, 6270-9 (2001).

202. Smith, C.M. et al. Mass spectrometric quantification of acetylation at specific lysines within the amino-terminal tail of histone H4. *Anal Biochem* **316**, 23-33 (2003).

203. Kurdistani, S.K., Tavazoie, S. & Grunstein, M. Mapping global histone acetylation patterns to gene expression. *Cell* **117**, 721-33 (2004).

204. van Leeuwen, F., Gafken, P.R. & Gottschling, D.E. Dot1p modulates silencing in yeast by methylation of the nucleosome core. *Cell* **109**, 745-56 (2002).

205. Tackett, A.J. et al. Proteomic and genomic characterization of chromatin complexes at a boundary. *J Cell Biol* **169**, 35-47 (2005).

206. Iida, T. & Araki, H. Noncompetitive counteractions of DNA polymerase epsilon and ISW2/yCHRAC for epigenetic inheritance of telomere position effect in Saccharomyces cerevisiae. *Mol Cell Biol* **24**, 217-27 (2004).

207. Floer, M., Blobel, G. & Rexach, M. Disassembly of RanGTP-karyopherin beta complex, an intermediate in nuclear protein import. *J Biol Chem* **272**, 19538-46 (1997).

208. Akhtar, N., Hagan, H., Lopilato, J.E. & Corbett, A.H. Functional analysis of the yeast Ran exchange factor Prp20p: in vivo evidence for the RanGTP gradient model. *Mol Genet Genomics* **265**, 851-64 (2001).

209. Noguchi, E., Hayashi, N., Nakashima, N. & Nishimoto, T. Yrb2p, a Nup2p-related yeast protein, has a functional overlap with Rna1p, a yeast Ran-GTPase-activating protein. *Mol Cell Biol* **17**, 2235-46 (1997).

210. Smith, J.J. et al. Transcriptome profiling to identify genes involved in peroxisome assembly and function. *J Cell Biol* **158**, 259-71 (2002).

211. Ideker, T. et al. Integrated genomic and proteomic analyses of a systematically perturbed metabolic network. *Science* **292**, 929-34 (2001).

212. Mizuguchi, G. et al. ATP-driven exchange of histone H2AZ variant catalyzed by SWR1 chromatin remodeling complex. *Science* **303**, 343-8 (2004).

213. Ren, B. et al. Genome-wide location and function of DNA binding proteins. *Science* **290**, 2306-9 (2000).

214. Ho, J.H., Kallstrom, G. & Johnson, A.W. Nmd3p is a Crm1p-dependent adapter protein for nuclear export of the large ribosomal subunit. *J Cell Biol* **151**, 1057-66 (2000).

215. Blobel, G. Gene gating: a hypothesis. *Proc Natl Acad Sci U S A* **82**, 8527-9 (1985).

216. Casolari, J.M. et al. Genome-wide localization of the nuclear transport machinery couples transcriptional status and nuclear organization. *Cell* **117**, 427-39 (2004).

217. Gartenberg, M.R., Neumann, F.R., Laroche, T., Blaszczyk, M. & Gasser, S.M. Sir-mediated repression can occur independently of chromosomal and

subnuclear contexts. *Cell* **119**, 955-67 (2004).

218. Brickner, J.H. & Walter, P. Gene recruitment of the activated INO1 locus to the nuclear membrane. *PLoS Biol* **2**, e342 (2004).

219. Marshall, W.F., Dernburg, A.F., Harmon, B., Agard, D.A. & Sedat, J.W. Specific interactions of chromatin with the nuclear envelope: positional determination within the nucleus in Drosophila melanogaster. *Mol Biol Cell* **7**, 825-42 (1996).

220. Heun, P., Laroche, T., Shimada, K., Furrer, P. & Gasser, S.M. Chromosome dynamics in the yeast interphase nucleus. *Science* **294**, 2181-6 (2001).

221. Clark, K.L. & Sprague, G.F., Jr. Yeast pheromone response pathway: characterization of a suppressor that restores mating to receptorless mutants. *Mol Cell Biol* **9**, 2682-94 (1989).

222. Belhumeur, P. et al. GSP1 and GSP2, genetic suppressors of the prp20-1 mutant in Saccharomyces cerevisiae: GTP-binding proteins involved in the maintenance of nuclear organization. *Mol Cell Biol* **13**, 2152-61 (1993).

223. Heun, P., Laroche, T., Raghuraman, M.K. & Gasser, S.M. The positioning and dynamics of origins of replication in the budding yeast nucleus. *J Cell Biol* **152**, 385-400 (2001).

224. Cordes, V.C., Reidenbach, S., Rackwitz, H.R. & Franke, W.W. Identification of protein p270/Tpr as a constitutive component of the nuclear pore complex-attached intranuclear filaments. *J Cell Biol* **136**, 515-29 (1997).

225. Hogarth, C., Itman, C., Jans, D.A. & Loveland, K.L. Regulated nucleocytoplasmic transport in spermatogenesis: a driver of cellular differentiation? *Bioessays* **27**, 1011-25 (2005).

226. Aitchison, J.D., Rout, M.P., Marelli, M., Blobel, G. & Wozniak, R.W. Two novel related yeast nucleoporins Nup170p and Nup157p: complementation with the vertebrate homologue Nup155p and functional interactions with the yeast nuclear pore-membrane protein Pom152p. *J Cell Biol* **131**, 1133-48 (1995).

227. Yano, R., Oakes, M.L., Tabb, M.M. & Nomura, M. Yeast Srp1p has homology to armadillo/plakoglobin/beta-catenin and participates in apparently multiple nuclear functions including the maintenance of the nucleolar structure. *Proc Natl Acad Sci U S A* **91**, 6880-4 (1994).

228. Tong, A.H. et al. Systematic genetic analysis with ordered arrays of yeast deletion mutants. *Science* **294**, 2364-8 (2001).

229. Bahler, J. et al. Heterologous modules for efficient and versatile PCR-based gene targeting in Schizosaccharomyces pombe. *Yeast* **14**, 943-51 (1998).

230. Finley, D., Ozkaynak, E. & Varshavsky, A. The yeast polyubiquitin gene is essential for resistance to high temperatures, starvation, and other stresses. *Cell* **48**, 1035-46 (1987).

231. Thomas, B.J. & Rothstein, R. The genetic control of direct-repeat recombination in Saccharomyces: the effect of rad52 and rad1 on mitotic recombination at GAL10, a transcriptionally regulated gene. *Genetics* **123**, 725-38 (1989).

232. Dilworth, D.J. et al. The mobile nucleoporin Nup2p and chromatin-bound Prp20p function in endogenous NPC-mediated transcriptional control. *J Cell Biol* ***In press*** (2005).

233. Winzeler, E.A. et al. Functional characterization of the S. cerevisiae genome by gene deletion and parallel analysis. *Science* **285**, 901-6 (1999).

234. Brachmann, C.B. et al. Designer deletion strains derived from Saccharomyces cerevisiae S288C: a useful set of strains and plasmids for PCR-mediated gene disruption and other applications. *Yeast* **14**, 115-32 (1998).

235. Studier, F.W. Use of bacteriophage T7 lysozyme to improve an inducible T7 expression system. *J Mol Biol* **219**, 37-44 (1991).

236. Meilhoc, E., Masson, J.M. & Teissie, J. High efficiency transformation of intact

yeast cells by electric field pulses. *Biotechnology (N Y)* **8**, 223-7 (1990).

237. Schiestl, R.H. & Gietz, R.D. High efficiency transformation of intact yeast cells using single stranded nucleic acids as a carrier. *Curr Genet* **16**, 339-46 (1989).

238. Ausubel, F.M. et al. *Current Protocols in Molecular Biology*, (Greene Publishing Associates, New York, NY, 1989).

239. Towbin, H., Staehelin, T. & Gordon, J. Electrophoretic transfer of proteins from polyacrylamide gels to nitrocellulose sheets: procedure and some applications. *Proc Natl Acad Sci U S A* **76**, 4350-4 (1979).

240. Cristea, I.M., Williams, R., Chait, B.T. & Rout, M.P. Fluorescent proteins as proteomic probes. *Mol Cell Proteomics* (2005).

241. Eng JK, M.A., and Yates JR 3rd. An Approach to Correlate Tandem Mass Spectral Data of Peptides with Amino Acid Sequences in a Protein Database. *J Am Soc Mass Spectrom* **5**, 976-989 (1994).

242. Hayashi, F. et al. The innate immune response to bacterial flagellin is mediated by Toll-like receptor 5. *Nature* **410**, 1099-103 (2001).

243. Fisher, A.G. & Merkenschlager, M. Gene silencing, cell fate and nuclear organisation. *Curr Opin Genet Dev* **12**, 193-7 (2002).

244. Ideker, T., Thorsson, V., Siegel, A.F. & Hood, L.E. Testing for differentially-expressed genes by maximum-likelihood analysis of microarray data. *J Comput Biol* **7**, 805-17 (2000).

6

7. APPENDICES

7.1. Digital data available on DVD-ROM

- Laboratory notebook images – JPEG (Adobe)
- Copy of thesis text – Word (Microsoft)
- Copy of thesis figures – JPEG (Adobe)
- Copy of thesis references – EndNote (Thomson ISI)
- Copy of assembled thesis – PDF (Adobe)
- Copy of thesis defense presentation – PowerPoint (Microsoft)
- MIAME compliant array data – TIFF & TXT (Adobe & Microsoft)
- Microarray analysis – Excel (Microsoft)
- LC-MS/MS data from immunopurification eluates – Excel (Microsoft)
- Dilworth *et al.* J. Cell Biol. 2001 in pdf format (Adobe)
- Dilworth *et al.* J. Cell Biol. 2005 *In press* in pdf format (Adobe)

NO TEXT

8. CURRICULUM VITAE

David J. Dilworth, Ph.D.

Institute for Systems Biology
1441 N 34 St
Seattle, WA 98103

cell: (206) 427-5251
lab: (206) 732-1381
fax: (206) 732-1299

E-mail: ddilworth@systemsbiology.net

Research Interests

- the structure and function of the nuclear pore complex
- the dynamics of chromatin in the eukaryotic nucleus and its relation to the epigenetic inheritance of expression states
- the development and application of new technologies to answer fundamental questions in cell biology

Personal Information

Marital Status: Single
Citizenship: Canadian
Birth Date: 08-oct-75

Current Position and Title

Graduate Research Assistant, Institute for Systems Biology, Seattle, WA.
Supervisor: Dr. John Aitchison. (2000 – present)

Education

Ph.D. 2005 Cell Biology	University of Alberta, Edmonton, AB, Canada
M.Sc. 1999 Medical Biophysics	University of Toronto, Toronto, ON, Canada
B.Sc. 1997 Honours Biochemistry	University of Alberta, Edmonton, AB, Canada

Professional Experience

Graduate Student [Ph.D.] – Institute for Systems Biology, Seattle, WA, U.S.A. (November 2000 – present) and Department of Cell Biology, University of Alberta, Edmonton, Alberta, Canada (April 1999 – October 2000).
Investigating the dynamic association of Nup2p with the yeast nuclear pore complex and its relevance to nucleocytoplasmic transport, the organisation of chromatin in the nucleus and the epigenetic maintenance of expression states.
Supervisor: Dr. John Aitchison

Graduate Student [M.Sc.] – Department of Medical Biophysics, University of Toronto, Toronto, Ontario, Canada (September 1997 – March 1999).
Examining the role of germline mutations in the cell cycle regulator, *CDKN2A*, in the predisposition to cancer.
Supervisor: Dr. David Hogg

Undergraduate Research Assistant [B.Sc.] – Department of Physiology, University of Alberta, Edmonton, Alberta, Canada (May 1996 – August 1997).
Initial characterisation of the cytoplasmic domains of the chloride/bicarbonate anion exchange proteins, AE2 and AE3.
Supervisor: Dr. Joseph Casey

Fellowships, Awards, and Honours

Ph.D.

- Alberta Heritage Foundation for Medical Research Studentship *(2000-2004)*
- Canadian Institutes of Health Research Doctoral Research Award *(2000-2002)*
- Walter H. Johns Graduate Fellowship *(1999-2002)*
- Natural Sciences & Engineering Research Council of Canada Post-Graduate Scholarship (PGS-B) *(offered/declined 2000)*

M.Sc.

- Natural Sciences & Engineering Research Council of Canada Post-Graduate Scholarship (PGS-A) *(1998-1999)*
- Ontario Graduate Scholarship *(offered/declined 1998)*

B.Sc.

- Alberta Heritage Foundation for Medical Research Summer Studentship *(1997)*
- Dean's Silver Medal in Science *(1997)*
- Canada Scholarship *(1993-1996)*
- James McCrie Douglas Memorial Scholarship *(1996)*
- University of Alberta Undergraduate Scholarship *(1995)*
- University of Alberta Entrance Scholarship *(1993)*
- Alma Mater Entrance Scholarship *(1993)*
- Alexander Rutherford Scholarship *(1993)*

Professional Activities & Memberships

2003-2004 Member of the American Society for Cell Biology

Peer-Reviewed Publications

Dilworth DJ, Tackett AJ, Rogers RS, Yi EC, Christmas RH, Smith JJ, Chait BT, Wozniak RW, Aitchison JD. (2005). "The mobile nucleoporin Nup2p and chromatin-bound Prp20p function in endogenous NPC-mediated transcriptional control." ***J Cell Biol.*** *In press.*

Scott RJ, Lusk CP, Dilworth DJ, Aitchison JD, Wozniak RW. (2005). "Interactions between Mad1p and the nuclear transport machinery in the yeast *Saccharomyces cerevisiae*." ***Mol Biol Cell.*** 16(9):4362-74.

Tackett AJ, Dilworth DJ, Davey MJ, O'donnell M, Aitchison JD, Rout MP, Chait BT. (2005). "Proteomic and genomic characterisation of chromatin complexes at a boundary." ***J Cell Biol.*** 169(1):35-47.

Sydorskyy Y, Dilworth DJ, Halloran BP, Yi EC, Makhnevych TR, Wozniak RW, Aitchison JD. (2005). "Nop53p is a novel nucleolar 60S ribosomal biogenesis protein." ***Biochem J.*** Epub Feb 2.

Sydorskyy Y, Dilworth DJ, Yi EC, Goodlett DR, Wozniak RW, Aitchison JD. (2003). "Intersection of the Kap123p-mediated nuclear import and ribosome export pathways." ***Mol Cell Biol.*** 23(6):2042-54.

Smith JJ, Marelli M, Christmas RH, Viseacoumar FJ, Dilworth DJ, Ideker T, Galitski T, Dimitrov K, Rachubinski RA, Aitchison JD. (2002). "Transcriptome profiling to identify genes involved in peroxisome assembly and function." ***J Cell Biol.*** 158(2):259-71.

Dilworth DJ, Suprapto A, Padovan JC, Chait BT, Wozniak RW, Rout MP, Aitchison JD. (2001). "Nup2p dynamically associates with the distal regions of the yeast nuclear pore complex." ***J Cell Biol.*** 153(7):1465-78.

Dilworth D, Liu L, Stewart AK, Berenson JR, Lassam N, Hogg D. (2000). "Germline *CDKN2A* mutation implicated in predisposition to multiple myeloma." ***Blood.*** 95(5):1869-71.

Liu L, Dilworth D, Gao L, Monzon J, Summers A, Lassam N, Hogg D. (1999). "Mutation of the *CDKN2A* 5' UTR creates an aberrant initiation codon and predisposes to melanoma." ***Nat Genet.*** 21(1):128-32.

Review Articles

Marelli M, Dilworth DJ, Wozniak RW, Aitchison JD. (2001). "The dynamics of karyopherin-mediated nuclear transport." ***Biochem Cell Biol.*** 79(5):603-12.

Conference Presentations and Abstracts

17-dec-03 Dilworth DJ, Yi E, Goodlett DR, Wozniak RW, Aitchison JD. "Prp20p and Nup2p interact to define chromosomal boundaries in *Saccharomyces cerevisiae*." 43rd Annual American Society for Cell Biology Meeting, San Francisco, CA.

11-dec-00 Dilworth DJ, Suprapto A, Padovan JC, Chait BT, Wozniak RW, Rout MP, Aitchison JD. "The role of the nucleoporin, Nup2p, in nuclear transport." 40th Annual American Society for Cell Biology Meeting, San Francisco, CA.